INSTALLED CAPACITY OPTIMIZATION IN COMBINATION OF DISTRIBUTED ENERGY RESOURCE DEVICES FOR RESIDENTIAL BUILDINGS

高, 翔翔

https://doi.org/10.15017/1398304

出版情報：九州大学, 2013, 博士（工学）, 課程博士
バージョン：

Installed Capacity Optimization in Combination of Distributed Energy Resource Devices for Residential Buildings

A dissertation

submitted to
Kyushu University
in fulfillment of the requirements
for the degree of

Doctor of Engineering

in
Department of Architecture
Graduate School of Human-Environment Studies

by

Xiangxiang Gao

九州大学
KYUSHU UNIVERSITY

大学院人間環境学府
Graduate School of
Human-Environment Studies

June 2013

To

My beloved parents,

Only parents, but you give your all.

Your love & emotional support of my education

Have been a constant

For as long as I can remember.

Only parents, but the best of all.

Contents

Abstract

Rapid depletion of fossil fuels will surely lead to shortage of end-use energy supply if no actions are taken. Energy consumption level of commercial and residential sector is growing larger and larger and increasing at a much faster rate than that of the other sectors. Thus, taking effective actions focusing on the commercial and residential sector brooks no delay.

Accordingly, this research aims for proposing a method to integrate the distributed energy resource (DER) devices and determine the optimal combination with installed capacities of them, and for clarifying the reduction effects of energy consumption and expenses in residential buildings through case studies by numerical simulations.

The dynamic models of photovoltaic (PV) device, solar water heating (SWH) device and solid oxide fuel cell (SOFC) device as three kinds of DER devices are built on the basis of their working principles. And then, the models are integrated as an overall system with the operation strategies for the generation of electric power and hot water. Finally, a genetic algorithm is applied to optimize the installed capacities of these DER devices.

As a result, for the cases selected in this research, the optimum combination of the DER devices for maximum energy reduction includes 30 modules of photovoltaic panel, a fuel cell with the capacity of 740 W and the hot water tank volume of 200 L. In this case, for one year, about 57% of conventional energy consumption can be directly reduced and 7,714 kWh of surplus amount of electric power can be obtained. The optimum combination for maximum cost economization changes to 28 modules of the photovoltaic panel and a solar thermal collector with 8 tubes with the hot water tank volume of 150 L for the initial ten years. In the subsequent ten years, a fuel cell with the capacity of 630 W and the hot water tank volume of 170 L will be additionally installed to the integrated system because the unit price of it would be highly decreased at that time. In this case, as the life time is assumed as 20 years, about 16% of the life cycle cost can be saved.

The methodology proposed in this dissertation is validated to reduce considerable quantity of residential energy consumption and expenses. The results of this research can help residents reform their existing DER devices, assist developers to equip the newly completed buildings with optimal DER devices, and also support designers in designing the hardware of newer types of DER devices.

Acknowledgements

I would like to express my gratitude to all whose help and support have contributed to this dissertation. There are a number of people who deserve special mentions.

For the three years of doctoral study in Graduate School of Human-environment Studies in Kyushu University, I have ever been belonging to two laboratories, and researching under the guidance of two supervisors. Thus, my deepest thanks go first and foremost to the two supervisors.

To my first supervisor, one of the members of my committee, Prof. Yasunori Akashi, who has given me the guidance for the first two and a half years of my research, I wish to express my sincere thanks. During the period that I studied in his laboratory, he has walked me through all the stages of the writing for this dissertation and made it a very rewarding and enjoyable experience. Although he has been in the University of Tokyo, he still contacted me very often by e-mails to discuss the writing for this dissertation and came back frequently for the various affairs on this dissertation. His constant guidance, expertise and support were of tremendous help to me. Especially, the trust from him was the best incentive to me.

To my second supervisor, my committee chairman, Prof. Kazutoshi Fujimoto, who has given me the guidance for the last half a year of my research, I would like to express my sincere gratitude. I can never forget his acceptance of me as a member in his laboratory for my last half a year in Kyushu University, after the transfer of Prof. Yasunori Akashi. His academic rigor was of great help to this dissertation, and his approachable attitude made me always feel comfortable in his laboratory.

In addition, I am especially thankful for the other members of my committee, Associate Profs. Yasuko Koga and Shichen Zhao who has taken much time to review my dissertation and advised me a lot in writing dissertation in a scientific way.

During the three years of my doctoral study, Assistant Prof. Daisuke Sumiyoshi has been always giving me useful suggestions for my research, to whom I also wish to express my sincere thanks. His devotion to the science encouraged me a lot, which has indeed facilitated me to work harder and harder so as to graduate on time in three years.

I would like to express my heartfelt gratitude to Prof. Jiaping Liu of Xi'an University of Architecture and Technology, who has ever been the supervisor of me for my master's thesis. It is he that introduced me to Prof. Yasunori Akashi, and facilitated my studying abroad in Kyushu University. The personal charisma of him has always been the inspiration for me to do research constantly with a scientific attitude.

I am also greatly indebted to my uncle, Senior Engineer Jun Ren of Shenzhen Institute of Building Research. He led me into the academic world of building science and technology. Without his introduction and encouragement, I might not enter this field.

To all the members of formal Akashi Laboratory, with whom I shared my first two and a half years, I have to express my thanks. And also, I would like to thank the members in Fujimoto Laboratory, with whom I shared my last half a year. It is a fortune for me to get to know and share my time with all the people here.

I would also like to acknowledge Fukuoka International Association (FIA) and Japan Student Services Organization (JASSO) as the scholarship sponsors for me.

To my dearest friends, I also wish to express my sincere thanks. Without the support and companionship of them, I would not complete this dissertation in such a short time.

In particular, I would like to thank my girlfriend Xinyu Zhuang for making the periods of my staying in Japan an enjoyable and interesting time, whose endless encouragement was of immense help to me.

Lastly, enormous thanks go to my beloved parents whose emotional support of my education and endeavors has been a constant for as long as I can remember.

Xiangxiang Gao
May 30, 2013
Fukuoka, Japan

Publications Arising

Journal Publications:

1. Gao, X., Liu, J., Hu, R., Akashi, Y. & Sumiyoshi, D. (2011). Numerical calculation method for indoor thermal environment of the Kang-heating room in north China. *Journal of Habitat Engineering, 3(2),* 163-176.
2. Gao, X., Akashi, Y. & Sumiyoshi, D. (2013). Energy conservation effect analysis on combination of household energy supplying systems. *Journal of Habitat Engineering and Design, Selected papers from ISHED conference 2012, Shanghai,* 57-64.
3. Gao, X., Akashi, Y. & Sumiyoshi, D. Installed capacity optimization of distributed energy resource systems for residential buildings. *Energy and Buildings*. (Under review)

Conference Publications:

1. Gao, X., Akashi, Y. & Sumiyoshi, D. (2012). Energy conservation effect of energy supplying systems used in residential houses: A case study of Fukuoka city. *First International Conference on Habitat Engineering and Design,* Shanghai.

Nomenclature

I. Nomenclature for Chapter 2

F	area, m^2
K	heat transfer coefficient of the lightweight building envelope, $J/(m^2 \cdot K \cdot h)$
Q_F	heat gain from indoor anthropogenic sensible heat and the lighting, J/h
Q_G	heat exchange by natural convection between the indoor and outdoor air, J/h
Q_V	heat exchange by infiltration between the indoor and outdoor air, J/h
Q_c	convective heat exchange between the interior surfaces of the building envelope and the indoor air, J/h
Q_{kc}	convective heat exchange between the interior surfaces of the kang and the air inside the kang, J/h
Q_{kG}	instantaneous heat gain from the heat medium inside the kang, J/h
Q_{kr}	radiative heat exchange between the interior surfaces of the kang and other interior surfaces, J/h
$Q_{k\lambda}$	heat exchange between the interior surfaces of the kang and the indoor air through envelopes of the kang, J/h

Q_r	radiative heat exchange between the interior surfaces of the building envelope and the other interior surfaces, J/h
Q_s	heat gain from the interior surfaces of the building envelopes by solar radiation, J/h
Q_λ	heat exchange between the exterior surfaces of the building envelope and the outdoor ambient through building envelopes, J/h
V	volume, m^3
Y	reaction coefficient of heat transfer, J/(m²·K·h)
Z	reaction coefficient of heat absorption of the interior surface, J/(m²·K·h)
c	constant pressure specific heat, J/(kg·K)
c_p	specific heat of the air, J/(kg·K)
t	instantaneous temperature, °C
t_a	temperature of the air inside the kang, °C
t_e	outdoor aimbient temperature, °C
t_{ej}	temperature of the exterior surface of the jth envelope, °C
t_i	indoor air temperature, °C
t_j	temperature of the interior surface of the jth envelope, °C
t_n	temperature of the nth exterior surface of the kang's plate, °C
t_z	outdoor sol-air temperature, °C
t_∞	temperature of infinite depth in the shallow ground, °C
u	a period of time, h
x	distance, m
α_{ec}	convective heat transfer coefficient of the exterior surface of the envelope, J/(m²·K·h)
λ	thermal conductivity coefficient, J/(m·K·h)

ρ	density, kg/m^3
τ	instant time, h

Subscripts

a	air inside the kang
i	indoor air
j	jth building envelope
n	nth plate of the kang
k	kang
w	building envelope

Organization Acronyms

BERC	Building Energy Research Center, Tsinghua University, China
EEGNRA	Energy and Environment Group of Northern Rural Areas, Tsinghua University, China
GAQSIQ	General Administration of Quality Supervision, Inspection and Quarantine of the People's Republic of China
MEP	Ministry of Environmental Protection of the People's Republic of China
MOH	Ministry of Health of the People's Republic of China

II. Nomenclature for Chapters 3-5

A	area, m^2
A_{in}	total area for installing PV modules and SWH tubes, m^2
C_T	temperature coefficient
C_m	monthly costs of electric power and gas, JPY
C_p	water specific heat at a constant pressure, 4.2×10^3 J/(kg·K)
C_r	replacement cost, JPY
C_i	initial capital cost, JPY
F_R	collector heat removal factor
$F^{'}$	collector efficiency factor
G	incident solar radiation, J/(s·m^2)
I	current, A
I_{ph}	photogenerated current, A
I_0	diode p-n junction reverse saturation current, A
$\dot{L}_s$	removal rates of energy to the load, J/s
N	number
P	electric power, W
P_r	rated electric power of fuel cell, W
P_m	monthly profit by selling excess electricity, JPY
$\dot{Q}_{gas}$	gas consumption of fuel cell evaluated in heat, J/s;
$\dot{Q}_r$	rates of addition of recovered exhausted heat from generation unit, J/s
$\dot{Q}_u$	rates of addition of energy from solar collector, J/s
R	resistance, Ω

T	temperature, K
T_a	ambient temperature for the outside, K
$T_a^{'}$	ambient temperature for the water tank, K
T_i	water inlet temperature of fluid circulating tube, K
T_m	municipal water temperature, K
T_s	hot water temperature in water tank, K
U	collector heat loss coefficient, W/(m^2·K)
V	voltage, V
V_t	diode emission factor
V_{tank}	volume of water tank, L
X	matrix enumerating the decision variables for energy conservation analysis
$X^{'}$	matrix enumerating the decision variables for cost economization analysis
k	Boltzmann constant, 1.38×10^{-23} J/K
$r^{\cdot}$	mass flow rate of hot water to the load, kg/s
n	diode emission factor
q	charge of electron, 1.602×10^{-19} C
t	time instant, s
α	absorptance
ε	emissivity
η	thermal efficiency
η_e	electric power generating efficiency of generation unit of the fuel cell
η_h	exhausted heat recovery ratio of generation unit of the fuel cell
η_{mppt}	maximum power point tracking efficiency
ρ	density of water, 1 kg/L
σ	Stefan-Boltzmann constant, 5.6697×10^{-8} W/(m^2·K^4)

τ	transmittance
LCC	life cycle cost, JPY
$ACEC$	annual conventional energy consumption, J

Subscripts

L	load
P	parallel
S	series
b	insulation box
d	diode
du	directly used within the buildings
ex	export to the grid
fc	fuel cell device
g	glass pipe
m	month
min	minute
mo	photovoltaic module
mp	maximum power
oc	open circuit
p	absorbed plate
pp	power plant
pv	photovoltaic device
ref	reference condition
rep	replacement
s	surface

sb sub-boiler

sc short current

sky background sky

sw solar water heating device

t/tu evacuated tube

tank tank

ub upper bound

Technical Acronyms

DER Distributed Energy Resource

PV Photovoltaic device

S. Switch

SOFC Solid Oxide Fuel Cell device

SWH Solar Water Heating device

V. Valve

Organization Acronyms

AIJ Architectural Institute of Japan

ANRE Agency for Natural Resources and Energy, Japan

SHASC.CESR Committee of Energy Simulation for Residence, Society of Heating, Air-conditioning and Sanitary Corporation, Japan.

DECEE Department of Electrical, Computer, & Energy Engineering, University of Colorado, US

DOE Department of Energy, US

EIA	Energy Information Administration, US
IBEC	Institute of Building Environment & Energy Conservation, Japan.
KEP	Kyushu Electric Power Co. Ltd., Japan
NHK	NHK Broadcasting Culture Research Institute, Japan
NI	National Instruments Corporation, US
SG	Saibu Gas Co. Ltd., Japan
FCWB.WPD	Water Purification Department, Fukuoka City Waterworks Bureau, Japan

List of Figures

List of Tables

Chapter 1

Introduction

With today's rapid economic development, increases in the pursuit of comfort have caused the energy demands of humans to grow higher and higher. However, we are fast approaching the peak of our consumption of fossil fuel and are faced with dwindling fossil fuel resources, particularly oil and gas (EIA, 2011). The rapid depletion of fossil fuels and the growing criticisms of nuclear energy will surely lead to shortages of end-use energy supplies if no actions are taken.

Among three main energy consumption sectors in Japan, energy consumption level of commercial and residential sector is growing larger and larger, increasing at a much faster rate than that of the other sectors, which are also increasing very quickly (ANRE, 2010). In order to meet these continuously increasing energy demands of humans, effective actions should be taken. Thus, taking effective actions focusing on the commercial and residential sector brooks no delay, which can be operated by two manners as

- using alternative sources of energy;
- increasing efficiency in both the conversion and transport of energy.

1.1 Background

Regarding the use of alternative sources of energy, instead of additional conventional power plants, increasing numbers of central power plants utilizing renewable energy should be established, including solar energy, wind energy, geothermal energy, etc. As for using conventional energy more efficiently, growing numbers of polygeneration plants should be built, since they can attain higher overall efficiencies than traditional plants. As the above mentioned types of technologies are very diverse, it is important to be able to accurately determine their capacities, in order to efficiently integrate them. In this pursuit, many researchers have targeted the determination of the optimum capacity, according to the energy demands of consumers, to facilitate more economical and efficient power plant operations (Ashok, 2007; Carvalho, Lozano, & Serra, 2012; H. C. Chen, 2013; Ekren & Ekren, 2010; Groscurth, Bruckner, & Kümmel, 1993; Rubio-Maya, Uche-Marcuello, Martínez-Gracia, & Bayod-Rújula, 2011; H. Yang, Zhou, Lu, & Fang, 2008).

However, construction of these plants usually takes many years, and also improvements of energy efficiency in both the conversion and transportation are considered, thus distributed energy resource (DER) devices for residential use, that can be easily installed and quickly implemented merit promotion. DER devices are defined as small-scale electric power and hot water generation devices used to provide alternative to or enhancement of the traditional power station and hot water boiler in this research.

Therefore, a number of research tasks had been done in dealing with DER devices (Andreadis, Roaf, & Mallick, 2012; Ganguly, Misra, & Ghosh, 2010; Ren & Gao, 2010a, 2010b; Yamaguchi et al., 2012). Since a single DER device is very unlikely to provide enough electric power and heat in a highly-efficient manner, many researchers have done the tasks in determining the optimum installed capacities of DER devices (Khatib, Mohamed, & Sopian, 2012; Khatib, Mohamed, Sopian, & Mahmoud, 2011; C.-H. Li, Zhu, Cao, Sui, & Hu, 2009; Ren, Gao, & Ruan, 2008; Taghipour Rezvan, Shams Gharneh, & Gharenpetian, 2013), and furthermore, finding solutions for the operations of them (Y.-H. Chen, Lu, Chang, Lee, & Hu, 2012; Hamdy, Hasan, & Siren, 2012; Kayo & Ooka, 2010; H. Li, Nalim, & Haldi, 2006; Lozano, Ramos, Carvalho, & Serra, 2009; Ren, Zhou, Nakagami, Gao, & Wu, 2010).

It can be seen that existing papers have mainly referred to the analysis and optimization of electric power and heat generation, rarely any directly involves hot water demand. However, at the present time, the small-scale photovoltaic (PV) and solar water heating (SWH) devices, which use solar as their energy source, have received plenty of attention in residential use. Additionally, the small-scale solid oxide fuel cell (SOFC) device turns out to be a good choice for residential energy conservation, since it can generate electric power in a highly-efficient manner, and meanwhile supply hot water for residential use. It is well known that a single PV or SWH device is very unlikely to provide a stable electrical or hot water supply, due to the low energy density and high randomness of solar energy. A single SOFC device is unlikely to provide enough end-use energy in a highly-efficient manner, due to its working principles that the generation efficiency diminishes as the load drops, and in this situation the electrical load fluctuates considerably. Thus, there remains significant work to be done, in order to make optimal use of DER devices that would supply not only electric power, but also hot water directly, while additionally reducing conventional energy and life cycle costs. We believe it will be a great benefit for the residents and the society to find an effective way to reduce conventional energy consumption levels, which will result in greater cost efficiencies.

1.2 Objectives

Accordingly, this study aims to present an integration and optimization methodology for the optimum capacities determination of DER devices, which include a PV device, an SWH device and an SOFC device.

Initially, the dynamic models of the DER devices are aimed to be built in this research. Appropriate operation strategies for the integration of the electric power and hot water are determined based on the dynamic mathematical models. With the operation strategies determined, combinations of the devices are selected. Energy conservation effect of each combination of the DER devices is analyzed and evaluated.

Followed, a genetic algorithm is tend to be used to determine the optimum capacities of the devices with consideration for their multi-period operations for an entire year, as the optimization in this research is highly complicated due to the uncertainty of solar radiation together with the load demand variability and the nonlinearity of heat loss from the exhausted hot water. The decision variables that need to be optimized include the quantities of the PV module and the SWH collector, the volumes of the SWH tank and SOFC tank, as well as the capacity of the generation unit of the SOFC. The conventional energy consumption and life cycle costs are treated as the optimization objectives in this research, while limitations of decision variables are chosen as constrained conditions.

At last, a case study of a typical residential building located in Fukuoka City in Japan is aimed to be carried out to clarify the simulation process by utilizing specifications of the systems provided by the manufacturers, as well as available weather data, municipal water data, and energy load data calculated by a life style calculation program, and a thermal environment simulation program.

1.3 Organization

As Figure 1-1 shows, overall, this dissertation consists of six chapters, excluding Chapter 1 presents the background and the objectives of this research, and Chapter 6 proposes the synopsis and the prospects, the remaining chapters are mainly written in two main parts. Chapter 2 focuses on the traditional Chinese kang, which takes efficient utilization of energy resource, is the prelude of the subsequent part, and is an inspiration for us to make optimal use of energy in researching on modern energy devices. Chapters 3 to 5 constitute the core of the dissertation, which focus on the DER devices used in residential buildings, and they are progressively related:

- Modeling of three selected DER devices, including PV, SWH, and SOFC;
- Integration of the models of the selected DER devices using proper operation strategies of electrical and hot water;
- Installed capacity optimization of the DER system integrated by the selected DER devices.

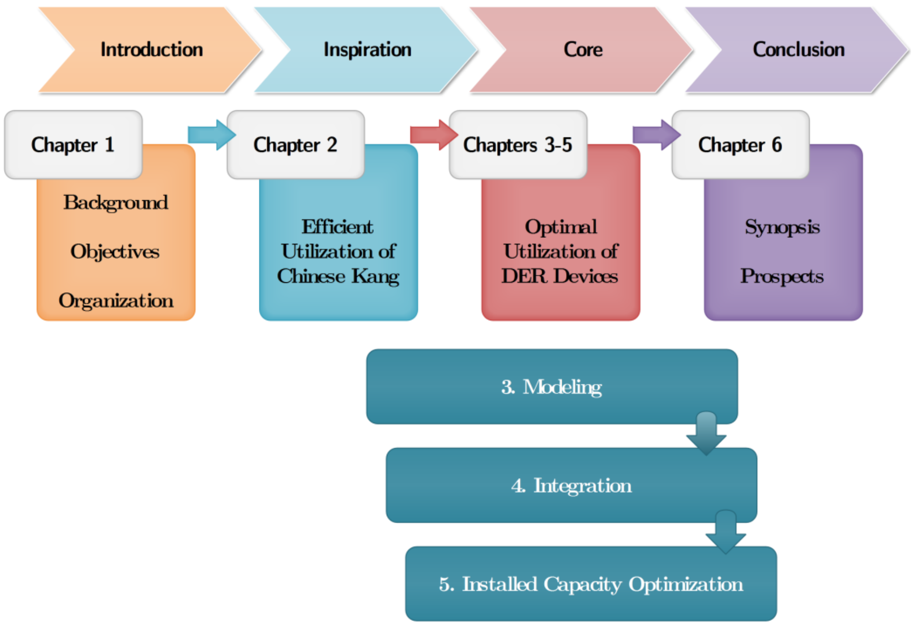

Figure 1-1 Organization of this dissertation

CHAPTER 2

Chinese Kang

Chinese kang use energy in an efficient way and meanwhile improve indoor thermal environment, so that it is an excellent example of energy use filled with the wisdom of ancient Chinese people. Researching on the energy use of Chinese kang can surely help us to make efficient use of energy with modern energy devices.

As a result of the above reasons, this chapter aims to describe the thermal processes of the buildings with Chinese kang and the kang itself, build mathematical models of them, and analyze the calculation results of the field measurements and simulations. By carefully research on the Chinese kang, the energy conservation effect is surely presented and the good experience from Chinese kang can be furthermore used into other kinds of energy devices.

2.1 Background

At present, rural energy uses in northern China are mainly for cooking and heating, of which heating energy use is the most prominent in winter. According to the survey statistics, the energy consumption in northern rural areas takes up to 56% of the country's total energy consumption, of which more than 80% of rural energy is consumed for heating (X. Yang & Jiang, 2008). If the residential heating in rural areas goes through the same way as that the central heating runs in urban areas, it is neither economic nor realistic. There are many kinds of conventional bioenergy in northern rural areas which is easy to be obtained, especially those remainders for harvesting, i.e. the straws and other crop residues, which no doubt play a role for the use of waste. And also, according to statistics, the total bioenergy produced every year in rural areas of China, i.e. the straw, firewood, etc., is approximately 6 million tons, of which about 60% is used as fuel for heating and cooking (J. Li, Bai, & Ralph, 1998). Therefore, the heating methods including the kang which can use the bioenergy for heating are more in line with the rural lifestyle. Meanwhile, it is no doubt a more scientific and rational way to ensure energy heating requirements. Among the various heating methods, the kang is the most widely used form of heating. According to the statistics from Ministry of Agriculture, PRC, there are about 66.85 million kangs existed in China by 2004, which are used by nearly 43.64 million rural households (approximately 175 million people), i.e. every two families have 3 kangs (BERC, 2008). In 2006, according to the research on energy and environment of rural households in northern China by Tsinghua University, the utilization rate of the kang in the north of China is 73.3%, in the northwest, it is 86.3%, and in the northeast, it is up to 96.2% (EEGNRA, 2007).

According to the survey, rural residential areas in the northern China have many problems with indoor air temperature, energy consumption in winter and pollution. The consumption in rural residential areas is up to 30-40 kg/m^2 of standard coal, but it can only maintain the indoor air temperature at about 10 °C, which is about twice of that used for urban heating (BERC, 2008). With the improving living standards and urbanization, the prospects of the traditional heating method are not so optimistic in rural areas. From the 1980s, the commercial energy resources used in the rural areas, i.e. commercial coal, electricity and natural gas, gradually increase. At present, the consumption of commercial coal, electricity and natural gas have taken up to 60% of the total energy consumption in rural areas in China (X. Yang & Jiang, 2008). In 2006, Li Y. found that there is a trend that the northern rural areas have a commercial energy based heating mode and is adopting non-commercial energy for heating according to their research on the comprehensive utilization of energy in northern rural areas, i.e. Heilongjiang, Liaoning and Gansu provinces (Y. Li, Sun, & Yang, 2006). In accordance with this situation, there bound to be heavy pressure on economic and social sustainable development of China. Thus, on basis of the unique characteristics of the rural areas in the north of China, seeking a proper heating method to improve the indoor thermal environment without heavy energy consumption will be an important issue for building energy conservation.

2.2 Outline of thermal process

Kang is not only a heating facility, but also a part of the building. The ultimate goal of this chapter is to analyze its impact for indoor thermal environment. The rooms with kang as the heating method generally do not need active control to adjust the indoor air temperature, and its thermal environment is determined by its dynamic thermal process, thus, according to the systematic research on dynamic thermal process of the room and the kang, the effect that the kang effects on the indoor thermal environment can be quantitatively analyzed in practice.

The indoor thermal environment depends on the equilibrium state of heat transfer, which includes the convection between each interior surface and the indoor air, the radiation between the surfaces, and the conduction from the building envelopes. For kang, the exterior surface temperature of the kang's faceplate is much higher than the indoor air temperature and the interior surface temperatures of the building envelopes. The calculation of heat dissipation on the exterior surface of kang's faceplate should include convection with the indoor air, and radiation with interior surfaces of the building envelopes.

As radiation involves all the interior surfaces, thermal balance equations of every surface need to be established. Thus, the research of indoor thermal environment of kang-heating room is more complex than that of the normal convective heating room. As it is shown in Figure 2-1, the core of the mathematical model of indoor thermal environment of the kang-heating room is the thermal balance equations, composed by the indoor air, interior surface of the building envelopes and exterior surfaces of the kang. The completed model should also include control equations established by the control channel and the interference channel. The control channel is composed of heat medium, air inside the kang, interior surfaces and exterior surfaces of the kang. And the interference channel is composed of exterior ambient, exterior surfaces and interior surfaces of the building envelopes.

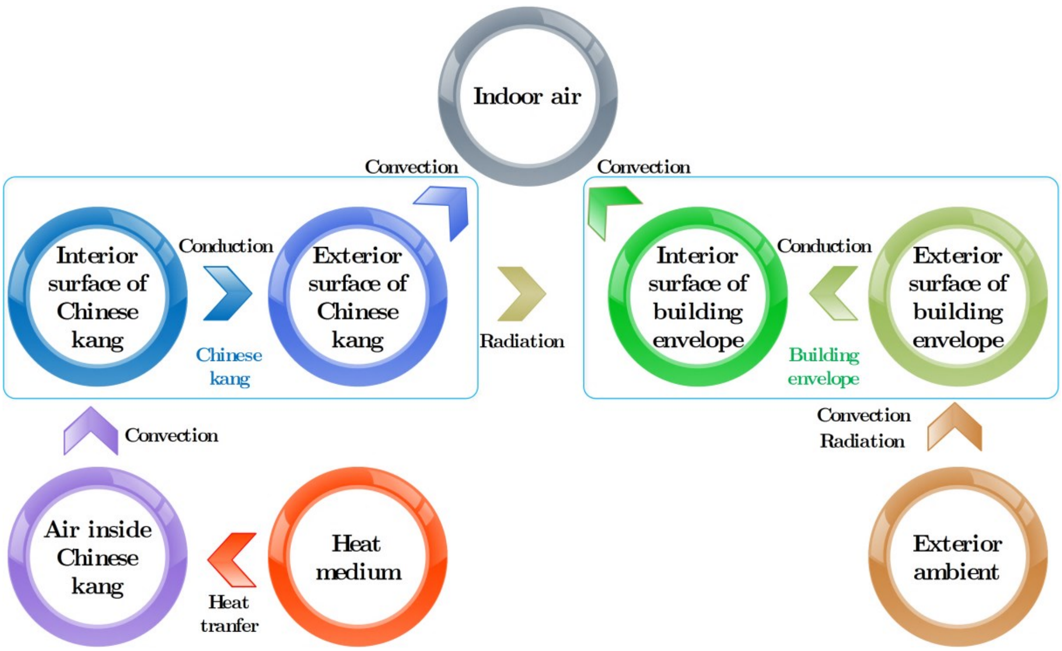

Figure 2-1 Thermal process diagram of the room with the kang

2.2.1 Outdoor interferences

Outdoor interferences include outdoor weather conditions (i.e. outdoor ambient temperature, solar radiation, wind speed and direction, etc.) and outdoor thermal environment (i.e. surface temperature of the surrounding ambient, etc.). Notably, the neighboring room's thermal environment can be regarded as an exterior interference for the kang-heating room. The interferences affect the temperatures of the interior surfaces of the room through the building envelopes in the way of conduction, and then affect the indoor air temperature in the way of convection. In addition, as materials of most building envelopes have attenuation and lag effects on the impact from outdoor interferences due to their large thermal resistances and heat capacities, walls, roofing, and flooring should be calculated by the way of unsteady-state heat transfer. However, the windows and doors are thin and have small heat capacities, so that they can be calculated in steady-state way.

2.2.2 Heat transfer of kang

Basically, the kang is the only indoor heating equipment in kang-heating rooms, which can make full use of waste heat of the smoke exported from the stove in order to improve the indoor thermal environment. During the cooking time, air in the kitchen goes into the stove by thermal pressure, the temperature of which become higher heated in the stove, and then it flows through the inside of the kang while heating the plates, subsequently transfers the heat into the room in the way of convection and radiation, and finally flows the whole way to the outdoor from the chimney leaving most of its heat inside the kang. Although there is no high-temperature airflow comes into the kang while we are not cooking, the remaining high-temperature airflow inside the kang constantly transfers heat in a convective and radiative way into the room through the kang’s faceplate. As to prevent the airflow flowing out, maintain the heat inside the kang and slow down the heat loss, the kang is used to be sealed strictly with a smoke flapper when heating is stopped. In a summary, the kang plays the role as a heat transfer staff that the interior surfaces of the kang gain heat by exchanging with the high-temperature airflow inside the kang, and then the heat is transferred into the interior of the room through the exterior surfaces of the kang.

The exterior surface of the kang's faceplate mainly affects the indoor thermal environment through the convection with the indoor air, as well as the radiation with the interior surfaces of the building envelopes. The convection and radiation performances of the exterior surface of the kang's faceplate reflect the heating capacity of the kang. Considering the size and heat transfer characteristics of the kang's faceplate, convection on the surface of the kang's faceplate can be dealt with following the way of natural convection of an infinite horizontal plate. In addition, convection on the interior vertical surfaces of the room can be calculated as natural convection of an infinite vertical plate, and radiation on exterior surface of the kang's faceplate can be calculated by angular coefficient method.

Considering the coupling heat transfer effecting between the interior surfaces of the kang and the airflow flowing through the stove, the kang and the chimney, and the coupling heat transfer effecting among the kang, the indoor air and the interior surfaces of the building envelopes, a macroscopic model is applicable and feasible to be used to analyze the thermal process of the kang.

2.2.3 Indoor interferences

Indoor interferences in the kang-heating room can be divided into two parts as latent heat interference and sensible heat interference. The humidity loss from the human bodies and the equipment is accompanied with the latent heat loss, which directly impact on the enthalpy of the indoor air immediately. The sensible heat from the lighting, the human bodies and the equipment can be separated into two forms. One of the forms is heat transfer with indoor air by convection directly, and the other one is heat transfer by radiation with each surrounding surface, through which the sensible heat will be transferred to the indoor air by convection.

2.2.4 Ventilation

Outdoor air flows into the room and directly intermixes with the indoor air, mainly in the way of natural ventilation or infiltration. The heat and moisture of the outdoor air effect on the indoor air immediately, so that the temperature and humidity of indoor air changes.

Notably, as the main topic in this chapter is the thermal process of the kang, only the air temperature changes affected by the ventilation or infiltration are focused on, and the coupling effect of heat and moisture transfer are not considered.

2.3 Mathematical modeling

2.3.1 Kang-heating room

The dynamic thermal process can be divided into the following sections for creating the equations:

- Thermal balance equation of indoor air
- Thermal balance equations of interior surfaces of envelopes
- Thermal balance equations of exterior surfaces of envelopes
- Control equations of heat transfer through envelopes

Among these four sections, only three of which are needed to form the final equations, as they are repeated for some extent. Thermal balance equation of indoor air, thermal balance equations of interior surfaces of envelopes, and control equations of heat transfer through envelops are selected for building the equations

1) *Thermal balance equation of indoor air*

The indoor air temperature of kang-heating room is a function of the spatial and time coordinates, which is usually calculated by the *Lumped Heat Capacity Method* for simplicity. With latent heat of human-beings and heat transfer from the phase transition of the indoor air ignored, the thermal balance equation is made as

$$V_i c_p \rho_i \frac{dt_i(\tau)}{d\tau} = Q_c(\tau) + Q_V(\tau) + Q_G(\tau) + Q_F(\tau) \tag{2.1}$$

where

V_i is the volume of the indoor air, m^3;

c_p is the specific heat of the indoor air, J/(kg·K);

ρ_i is the density of the indoor air, kg/m^3;

$Q_c(\tau)$ is the convective heat exchange between the interior surfaces of the building envelopes and the indoor air at the time of τ, J/h;

$Q_V(\tau)$ is the heat exchange by infiltration between the indoor and outdoor air at the time of τ, J/h;

$Q_G(\tau)$ is the heat exchange by natural convection between the indoor and outdoor air at the time of τ, J/h;

$Q_F(\tau)$ is the heat gain from indoor anthropogenic sensible heat and the lighting (constant value, changing by the actual conditions) at the time of τ, J/h.

2) *Thermal balance equations of interior surfaces of envelopes*

It is assumed that there is no phase changes existing in the envelope structure, thermal parameters are constant, heat exchange by the permeability of the water vapor inside the envelope structure is not considered, the indoor air flows sufficiently, and it can be thought as a lumped heat capacity system, with the heat gain direction of the interior surface of the building envelope acts as the positive direction, thus, the thermal balance equation explaining the interior surfaces of the building envelopes can be built as

$$Q_{cj}(\tau)+Q_{rj}(\tau)+Q_{sj}(\tau)+Q_{\lambda j}(\tau)=0 \tag{2.2}$$

where

$Q_{cj}(\tau)$ is the convective heat exchange between the jth interior surface of the building envelope and the indoor air at the time of τ, J/h;

$Q_{rj}(\tau)$ is the radiative heat exchange between the jth interior surface of the building envelope and the other interior surfaces at the time of τ, J/h;

$Q_{sj}(\tau)$ is the heat gain from the interior surfaces of the building envelopes by solar radiation (appears only when solar radiation) at the time of τ, J/h;

$Q_{\lambda j}(\tau)$ is the heat exchange between the jth exterior surface of the building envelope and the outdoor ambient through building envelopes at the time of τ, J/h.

3) Control equations of heat transfer through envelopes

Heat transfer control equations should be led into the calculation of mathematical model of the kang-heating room. It can be divided into 3 categories according to the heat transfer characteristics of the building envelopes, which are respectively discussed below.

- *Finite thickness plates (Roofing and walls)*

The types of the exterior building envelopes are various, as well as a large amount of boundary conditions, so that it cannot be calculated easily. As a result of the homogeneity in the direction of thickness, and that the value of thickness is much smaller than that of length and width, heat transfer control equation is usually simplified as one-dimensional unsteady-state heat transfer equation as

$$\rho_w c_w \frac{\partial t_w(x,\tau)}{\partial \tau} = \lambda_w \frac{\partial^2 t_w(x,\tau)}{\partial x^2} \tag{2.3}$$

where

ρ_w is the density of the building envelope, kg/m^3;

c_w is the specific heat of the building envelope, J/(kg·K);

λ_w is the thermal conductivity coefficient of the building envelope, J/(m·K·h);

$t_w(x,\tau)$ is the instantaneous temperature along the thickness of the envelope at the time of τ, °C.

The boundary condition of the interior surface of the building envelope is actually the heat transfer with the outdoor ambient at the instant time. Based on *Fourier's Law*, there is equation as

$$-\lambda_w \left.\frac{\partial t_w(x,\tau)}{\partial x}\right|_{in} = \frac{Q_{\lambda j}(\tau)}{F_j} \tag{2.4}$$

where, F_j is the area of the jth building envelope, m^2.

The boundary condition of the exterior surface of the building envelope is actually determined by the thermal balance of itself. Based on *Fourier's Law*, there is equation as

$$-\lambda_w \left.\frac{\partial t_w(x,\tau)}{\partial x}\right|_{out} = \alpha_{ecj}[t_z(\tau) - t_{ej}(\tau)] \tag{2.5}$$

where

α_{ecj} is the convective heat transfer coefficient of the exterior surface of the jth envelope, J/(m^2·K·h);

$t_z(\tau)$ is the outdoor sol-air temperature at the time of τ, °C;

$t_{ej}(\tau)$ is the temperature of the exterior surface of the jth envelope at the time of τ, °C.

There are so many kinds of methods for solving these equations, including C.O. Mackey and L.T. Wright's equivalent temperature method (US), A.M. Шкловер's harmonic reaction coefficient method (former Soviet Union), Carrier company's thermal storage coefficient method (US), D.G. Stephenson and G.P. Mitalas's thermal reaction coefficient method (Canada), and the derived thermal reaction coefficient method of room and Z transfer function method, etc.

The thermal reaction coefficient method is adopted in this study, by which the exchanging heat power between interior surfaces of the building envelopes and the outdoor ambient at the instant time can be calculated as (Yan & Zhao, 1986)

$$Q_{\lambda j}(\tau) = F_j \sum_{u=0}^{\infty} Y_j(u) t_z(\tau - u) - F_j \sum_{u=0}^{\infty} Z_j(u) t_j(\tau - u) \tag{2.6}$$

where

$Y_j(u)$ is the reaction coefficient of heat transfer of the jth envelope, J/(m²·K·h);

$t_z(\tau - u)$ is the outdoor sol-air temperature at the time of $\tau - u$, °C;

$Z_j(u)$ is the reaction coefficient of heat absorption of the interior surface of the jth envelope, J/(m²·K·h);

$t_j(\tau - u)$ is the temperature of the interior surface of the jth envelope at the time of $\tau - u$, °C.

Liu J. separates and derives the thermal reaction coefficient into two categories, according to whether the thermal reaction of the air boundary layer of the interior surface is considered or not (Liu, 1998). In this study, not only the indoor air temperature should be calculated, but also the temperature of each interior surface of the envelope should be calculated, thus, the above selected thermal reaction coefficients are all belonging to the second class without considering the thermal reaction of the air boundary layer of the interior surfaces.

- *Semi-infinite thickness plate (Flooring)*

Heat transfer of flooring is more complex than that of walls, roofing, windows and doors, because the heat transfer of flooring involves heat transfer in soil, rather than in air, which has relationships with soil properties and other factors. The flooring is semi-infinite, if the accuracy is required, one-dimensional unsteady heat transfer method as used in the exterior walls cannot be used. Chen Q. proposed a method of adding heat flow into the calculation of the heat transfer of flooring (Q. Chen, 1988). Although it is an approximate algorithm and only used for steady-state heat transfer calculation, this method can basically reflect the heat transfer principle of flooring. Considering the condition of the climates, elevation difference of indoor and outdoor flooring and the construction of the flooring, this method is a relatively more accurate algorithm compared with the others.

Taking into account the complexity and difficulty on simplifying the calculation of two-dimensional calculation, the heat transfer of flooring is simplified as semi-infinite one-dimensional non-steady state heat transfer in this study. As simplified like this, heat transfer equation of the flooring will be the same as that of the roofing and the walls, but only with the boundary condition changed, and the boundary condition in the infinite distance can be calculated as

$$t(\infty,\tau) = t_{\infty} \tag{2.7}$$

where, t_{∞} is the temperature of infinite depth of the shallow ground, °C.

When the shallow ground reaches a certain depth, its temperature is closed to the constant temperature, which is approximately equal to the long year annual mean temperature. As the heat transfers to the room from infinite distance, there is hardly any heat exchange with interior surfaces of the ground. Therefore, heat transfer between the interior surface of the flooring and the infinite depth of shallow ground at an instant time also can be calculated by using thermal reaction coefficient method. The equation of which is made as

$$Q_{\lambda j}(\tau) = -F_j \sum_{u=0}^{U} Z_j(u) t_j(\tau - u) \tag{2.8}$$

- *Lightweight building envelope (Door and window)*

For doors, windows and other lightweight building envelopes, the thermal storage effect can be ignored due to their small heat capacities, so that the steady-state calculation method is adopted. There is control equation as

$$Q_{\lambda j}(\tau) = K_j[t_e(\tau) - t_i(\tau)]F_j \qquad (2.9)$$

where

K_j is the heat transfer coefficient of the jth lightweight building envelope (considered heat transfer coefficient of the surface), J/(m^2·K·h);

$t_e(\tau)$ is the outdoor air temperature at the time of τ, °C;

$t_i(\tau)$ is the indoor air temperature at the time of τ, °C.

2.3.2 Chinese kang

The traditional ground kang is adopted as the target for calculation. As for simplify, the sidewalls of the kang are considered as two kinds, one kind of which towards the inside, the other kind of which faces outside of the room. Good insulation measures are adopted between the kang and building envelopes, so that the process of the heat exchange of the sidewall facing outside can be thought as steady-state heat transfer. Considering the consistency of the calculation, the heat transfer happens in the sidewall facing inside are thought as unstable heat transfer.

1) Thermal balance equation of the air inside the kang

As the heat produced by the air phase change ignored, the thermal balance equation is made as

$$V_a c_p \rho_a \frac{dt_a(\tau)}{d\tau} = Q_{kc}(\tau) + Q_{kG}(\tau) \qquad (2.10)$$

where

V_a is the volume of air inside the kang, m^3;

c_p is the specific heat of the air inside the kang, J/(kg·K);

ρ_a is the density of the air inside the kang, kg/m^3;

$Q_{kc}(\tau)$ is the heat exchange between the interior surfaces of the kang and the air inside the kang at the time of τ, J/h;

$Q_{kG}(\tau)$ is the difference of the convective heat gain from inlet port of the kang and heat loss from outlet port of the kang, i.e. instantaneous heat gain from the heat medium inside the kang (ignoring heat loss by building envelopes in the process of exhausting) at the time of τ, J/h.

2) *Thermal balance equation of the interior surfaces of the kang*

It is assumed that there is no phase changes existing in the kang structure, thermal parameters are constant, heat exchange by the permeability of the water vapor inside the kang structure is not considered, the air flows sufficiently inside the kang, and it can be thought as a lumped heat capacity system, with the heat gain direction of the interior surface of the kang acts as the positive direction, thus, the thermal balance equation explaining the interior surfaces of the kang can be built as

$$Q_{kcn}(\tau)+Q_{krn}(\tau)+Q_{k\lambda n}(\tau)=0 \quad (2.11)$$

where

$Q_{kcn}(\tau)$ is the convective heat exchange between the nth interior surface of the kang and the air inside the kang at the time of τ, J/h;

$Q_{krn}(\tau)$ is the radiative heat exchange between the nth interior surface of the kang and other interior surfaces at the time of τ, J/h;

$Q_{k\lambda n}(\tau)$ is the heat exchange between the nth interior surface of the kang and the indoor air through envelopes of the kang at the time of τ, J/h.

3) *Control equations of heat transfer through kang's envelopes*

The kang transfers heat through the faceplate, the exterior heat transfer of which includes convection with the indoor air and radiation with other surfaces of the interior building envelopes, the interior heat transfer of which includes the convection with the airflow in the kang and radiation with other interior surfaces of the kang. Since the thickness of the faceplate is much smaller than its length and width, heat transfer of the kang can be considered as one-dimensional non-steady state heat transfer, thus the complete mathematical description is as

$$\rho_k c_k \frac{\partial t_k(x,\tau)}{\partial \tau} = \lambda_k \frac{\partial^2 t_k(x,\tau)}{\partial x^2} \tag{2.12}$$

where

ρ_k is the density of the kang's structure, kg/m^3;

c_k is the constant pressure specific heat of the kang's structure, J/(kg·K);

λ_k is the thermal conductive coefficient of the kang's structure, J/(m2·K·h);

$t_k(x,\tau)$ is the instantaneous temperature along the kang's thickness at the distance of x, at the time of τ, °C.

The boundary condition of the interior surface of the kang is actually the heat transfer with the indoor air at the instant time. Based on *Fourier's Law*, there is an equation as

$$-\lambda_k \left.\frac{\partial t_k(x,\tau)}{\partial x}\right|_{in} = \frac{Q_{k\lambda n}(\tau)}{F_n} \tag{2.13}$$

where, F_n is the area of the nth surface of the kang, m^2.

The boundary condition of the exterior surface of the kang is actually determined by the thermal balance of itself. Based on *Fourier's Law*, there is equation as

$$-\lambda_k \left.\frac{\partial t_k(x,\tau)}{\partial x}\right|_{out} = \frac{Q_{cn}(\tau) + Q_{rn}(\tau) + Q_{sn}(\tau)}{F_n} \tag{2.14}$$

where

$Q_{cn}(\tau)$ is the convective heat exchange between the nth exterior surface of the kang and the indoor air at the time of τ, J/h;

$Q_{rn}(\tau)$ is the radiative heat exchange between the nth exterior surface of the kang and other interior surfaces of the kang at the time of τ, J/h;

$Q_{sn}(\tau)$ is the heat gain of the nth exterior surface of the kang by solar radiation at the time of τ (appears only when solar radiation), J/h.

The calculation of the control equations of the kang is the same as that of the building envelopes, using thermal reaction coefficient method. The heat gain of the interior surface of the kang from indoor air at the instant time can be calculated as

$$Q_{k\lambda n}(\tau) = F_n \sum_{u=0}^{\infty} Y_n(u) t_n(\tau - u) - F_n \sum_{u=0}^{\infty} Z_n(u) t_a(\tau - u) \tag{2.15}$$

where

$Y_n(u)$ is the reaction coefficient of heat transfer of the nth kang's plate, J/(m^2·K·h);

$t_n(\tau - u)$ is the temperature of the nth exterior surface of the kang's plate at the time of $\tau - u$, °C;

$Z_n(u)$ is the reaction coefficient of heat absorption of the nth interior surface of the kang's plate, J/(m^2·K·h);

$t_a(\tau - u)$ is the temperature of the air in the kang at the time of $\tau - u$, °C.

As described in the previous section, the thermal reaction coefficient can be separated into two categories. As the particularity of the kang, it is better not to consider the heat reaction of the air boundary layer on both interior and exterior surfaces, which can be called the third class thermal reaction coefficient.

2.3.3 Programs of modeling

According to the above modeling of the kang-heating room and the kang, a program made by mathematical software MATLAB is proposed to calculate the indoor air temperature and exterior surface temperature of the kang's faceplate, which contains a subroutine for calculating thermal reaction coefficient. The diagram of the program is shown in Figure 2-2, and the program is attached in Appendix I.

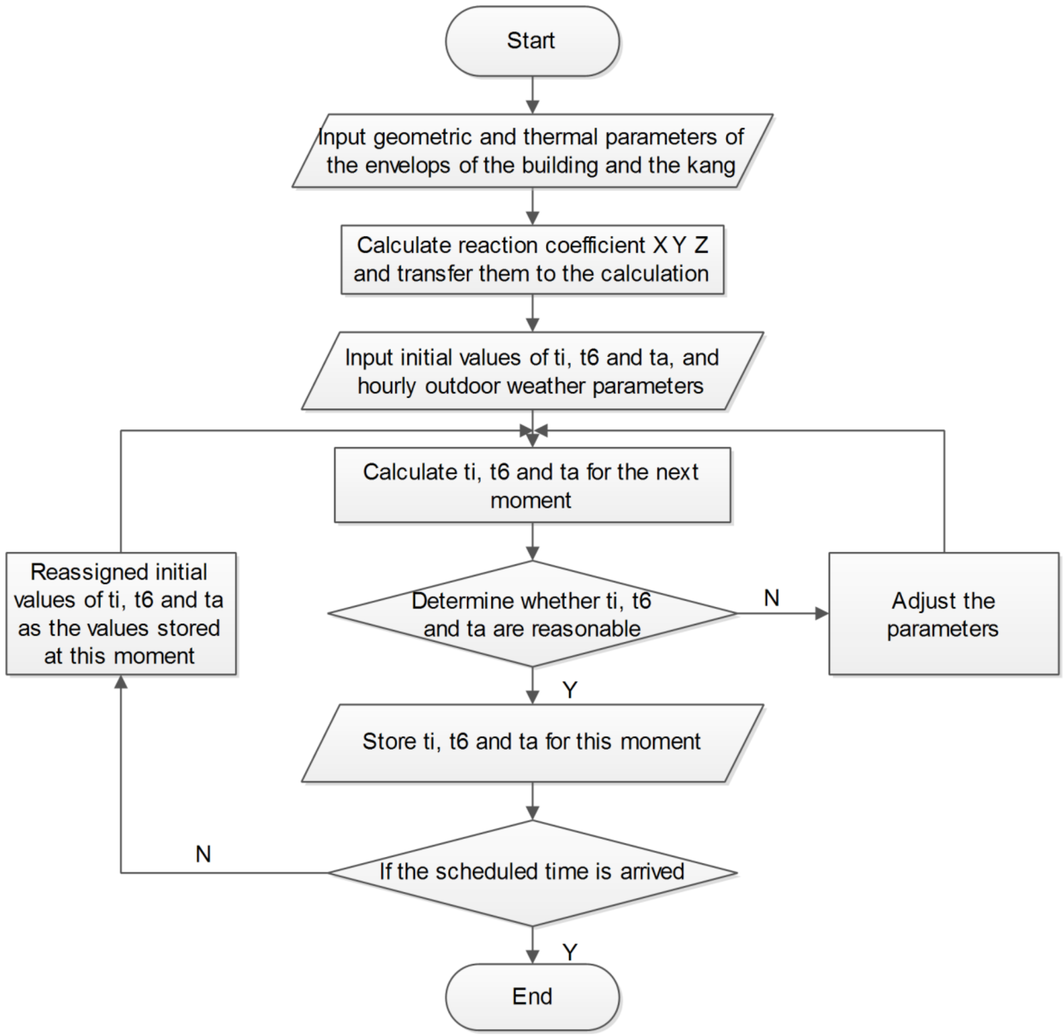

Figure 2-2 Diagram of the program for calculating temperatures regarding the kang

2.4 Field measurement

2.4.1 Conditions and scheme

1) Measurement conditions

The period for measurement is from 12:00, January 9, 2009 to 12:00, January 11, 2009, the measurement site is Qinmao Village, Muhuguan Town, Shangluo City, Shaanxi

Province, and the objective building is a typical house with the kang.

Qinmao village is located in the hinterland of Qinling Mountains, 1420 meters above the sea level. It has a humid mountain climate that the annual average temperature is 10.3 °C, and the wind is blowing from the west all year around. It is cool in summer and cold in winter, and the temperature difference between day and night in summer is very large.

As shown in Figure 2-3, a traditional building made by rammed earth is selected in our research. The size of the main bedroom is 4.0 m × 3.7 m, and the size of the kang in the main bedroom is 3.1 m × 1.8 m. The external walls are constructed by the rammed earth with a thickness of 400 mm, and the internal walls are constructed by the thick adobe with a thickness of 150 mm. The building adopted a gable roof, the construction of which is explained as follow that, the thin woods are nailed onto the pine rafters, on which 20-30 mm thick raw soil is laid, and then gray tiles are covered. The ground is compacted by raw soil. The pine boards are adopted for the bedroom ceiling, and they are 2.7m high above the ground. The building has a layout of simple three-bay. The front door is set in the middle bay, which is a traditional wooden double-door with the size of 2.8 m × 1.5 m, and the windows are set symmetrical on both sides of the door, which is made of wood-framed glass, and the dimensions are 1.45 m × 1.5 m.

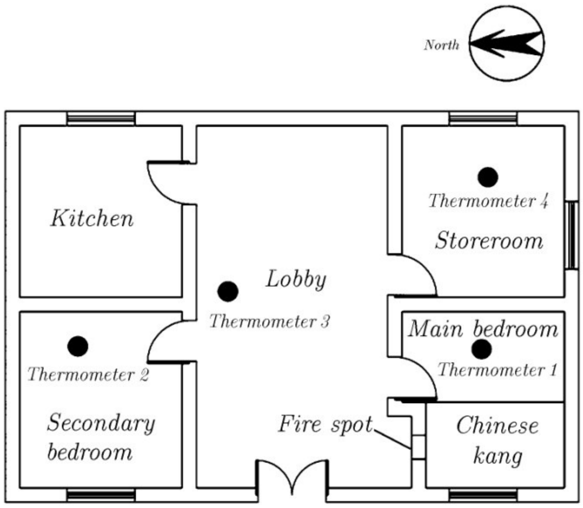

Figure 2-3 Floor plan of the objective building and distribution of thermometers

2) Measurement scheme

It was sunny during the process of the measurement. The contents included measuring the indoor and outdoor air temperature of each room, surface temperature of the kang's faceplate. Air temperatures were measured by the self-recording thermometers, the accuracy of which is up to 0.2 °C. The indoor air temperature measuring points were set 0.5 to 1.0 m high above the ground, the distribution of which is labeled in Figure 2-3. The thermometers which are used to measure the outdoor temperature were placed in the shade and sheltered with the cardboard sleeves. Surface temperature of the kang's faceplate is measured by the thermocouples. The interval for collecting the data is 1 hour, during the entire measurement period.

2.4.2 Results and discussions

Figure 2-4 shows the regression curves of the measured temperatures, including the indoor air temperature of main bedroom and lobby, outdoor ambient and sol-air temperature, and surface temperatures of kang's faceplate. A continuous period of 48 hours was selected as the measurement period for studying on temperatures and heat transfer of the kang, which was from the noon time of the first days to the noon time of the third day.

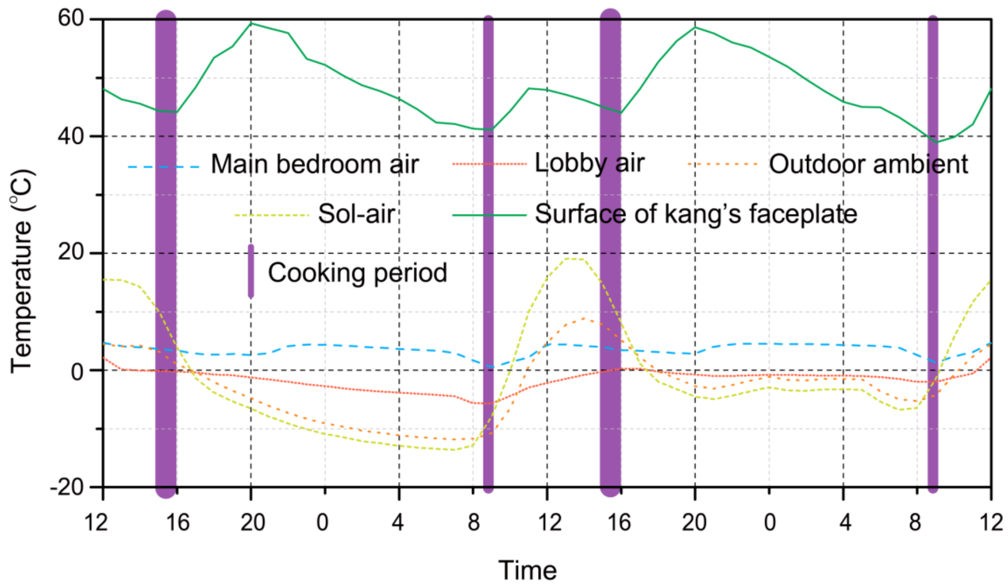

Figure 2-4 Regression curves of the measured temperatures in 48 hours

According to the actual situation, the local residents are generally working outdoor or in the lobby except the cooking time during the day. They usually get heated around the fire spot of the kang at the cooking times, which are from 8:30 to 9:00 and from 15:00 to 16:00 in one day.

It can be seen from Figure 2-4, due to the influence of the thermal inertia of the materials of the kang, temperature of the kang's faceplate begin to rise gradually after the fire is extinguished. If the cooking time last for 1 hour, the rising of the temperature of the kang's faceplate can maintain about 4 hours. After that, the kang continues to radiate the heat to the indoor environment for 9 hours, ensuring that in the most period of day time, there is a continuous heat source heating the indoor environment.

Figure 2-4 also shows that surface temperature of the kang's faceplate is about 45 °C higher than the indoor air temperature, which fully meets the needs for the rest at the night. It is stipulated in the standard *Indoor Air Quality Standard (GB/T 18883-2002)* (GAQSIQ, MEP, & MOH, 2002), that heating temperature in winter should be 16 °C to 24 °C. Although the rural residential heating requirement is not the same as in the city, in order to meet the needs of human beings' thermal comfort, it still should be 15 °C to 18 °C. However, during the day time, the indoor air temperature is very low, which is only 0 °C to 5 °C, which is far below 15 °C.

It is also shown in Figure 2-4, the changes of the indoor air and outdoor ambient temperatures. Throughout the measurement period, the outdoor ambient temperature changes the most deeply, the average temperature of which is -2.7 °C. The minimum values of the outdoor ambient temperatures appear from 4:00 to 8:00, which are around -11 °C, the highest temperatures appear from 13:00 to 15:00, which are around 8 °C, and the difference reaches about 20 °C. The air temperatures of the main bedroom are above 0 °C, and the average value is 3.2 °C, while the air temperatures of the other rooms (only the curve of the indoor air temperatures of the lobby is shown in Figure 2-4, as the curve of the indoor air temperature in other rooms have almost the same trend and the values with that in the lobby) are basically below 0 °C, and the average value is -2 °C. The difference of the indoor air temperatures of different rooms has much relationship with whether there is a kang, indicating that the kang has a great effect on improving the indoor air temperatures.

For the sol-air temperature, it is shown that from 8:00 to 17:00, it is much higher than the outdoor ambient temperature, but it is lower in the other period. The reason is that the sol-air temperature is the integrated by the solar radiation and the outdoor ambient temperature.

As to the air temperature in the lobby, it is can be seen that it changes consistent with the outdoor ambient temperature. When the outdoor ambient temperature reaches the top or drops at the bottom, the air temperature in the lobby appears the same, which are respectively 2 °C and -6 °C.

Improvement of the indoor air temperature by the kang is deeply influenced by the insulation properties of the building envelopes. The exterior walls are made by adobe, which has large thermal mass, thermal resistance and thermal inertia index, heat gains and losses through which are small, i.e. it has a good insulation property. As a result of that, the indoor air temperature is supposed to be enhanced to a very high degree, but the actual indoor air temperature is very low, which forms a great contrast with the surface temperature of the kang's faceplate. It is analyzed that, besides the impact of thermal insulation performance of the building envelopes, the airtightness of the room is another important reason for the low temperature of the indoor air. More airtight the room is, deeper effects the kang does on the indoor air temperature. However, it is a habit of the local residents that they used to open the main door and the bedroom doors, thus the airtightness is very poor, and inevitably lead to the loss of part of the heat by the air exchange between indoor and outdoor. As a result of that, the enhancement of the indoor air temperature by the kang is greatly weakened.

2.5 Model verifying

As shown in Figure 2-5, x-axis represents time from 12:00 of the first day to 11:00 of the subsequent day, and y-axis represents the temperatures which we want to calculated, including indoor air temperature (T_i), exterior surface temperature of the kang's faceplate (T_n), and the outdoor ambient temperature (T_a). In order to verify the accuracy of the model, the measured value is compared with the calculated value by indoor air temperature and exterior surface temperature of the kang's faceplate (the temperature refers the one on the bed which is laid on the top of the kang's faceplate) respectively, the results are shown in Figure 2-6 and Figure 2-7.

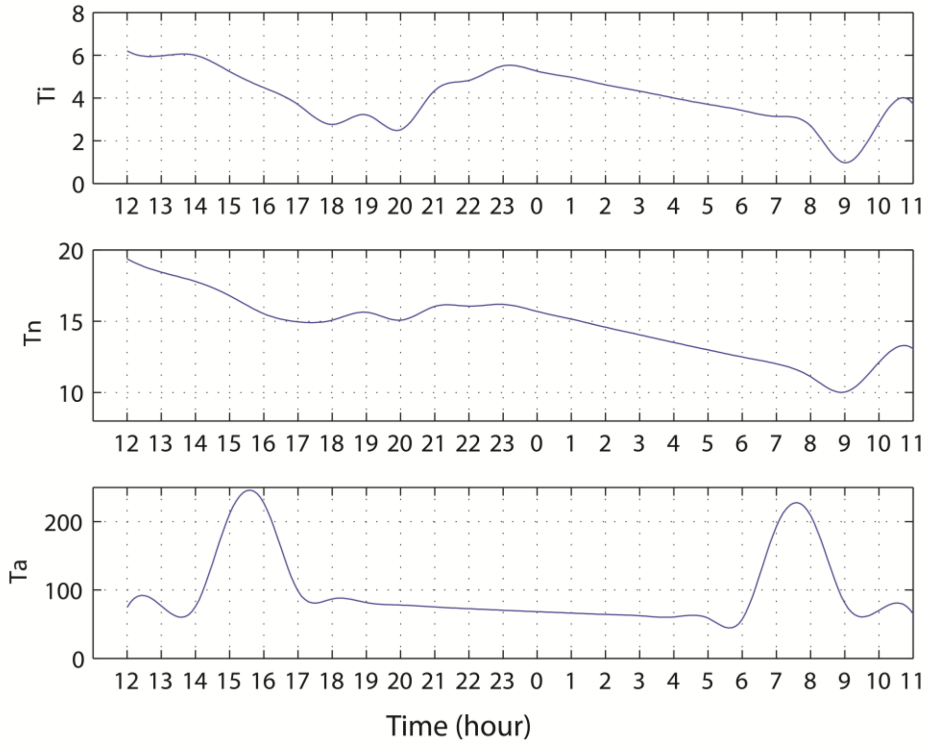

Figure 2-5 Calculated value of the temperatures

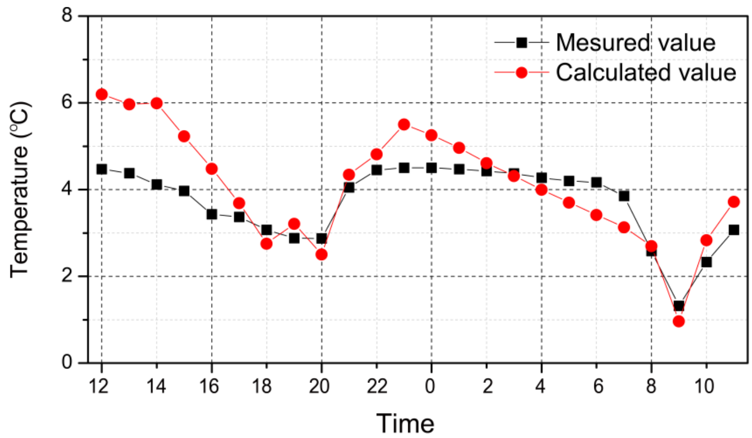

Figure 2-6 Measured and calculated values of indoor air temperature

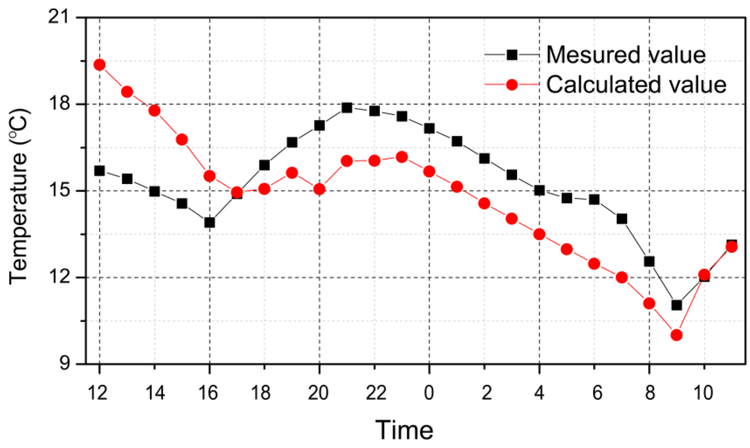

Figure 2-7 Measured and calculated values of exterior temperature of the kang's faceplate

To illustrate the high level of accuracy between measured and calculated values, software *IBM SPSS Statistics* is used to make an independent sample T-test for two groups, the result of which is tabulated in Table 2-1.

The *Sig.* appearing in Table 2-1 stands for the significance or the probability, of which *Sig. (2-tailed)* value is the probability of Pearson two-sided testing, and the *Sig.* value is a probability of one-sided testing. Generally, if this *Sig.* value is bigger than 0.05, it indicates the average values are equal in a probability which is bigger than 5% , and not equal in a probability which is smaller than 95%. In this case, it is thought that the probability of the average value being compared is quite large, indicating that the difference between the two sets of data is not significant, i.e. the two sets of data are thought to be equal. However, if the *Sig.* value is smaller than 0.05, it indicates the average values are equal in a probability which is smaller than 5% , and not equal in a probability which is bigger than 95%. In this case, it is thought that the probability of the equality of the average values is relatively small, indicating that the difference between the two sets of data is significant, i.e. the two sets of data are not thought to equal.

As tabulated in the Table 2-1, the *Sig.* value and *Sig. (2-tailed)* value are much larger than 0.05 in this test, which illustrates that there is only a very small difference between the measured and calculated values, thus the aforementioned model is considered accurate.

Table 2-1 Independent samples test of measured and calculated values

			Indoor Air Temperature		Exterior Temperature of Kang's Faceplate	
			EVA [a]	EVNA [b]	EVA [a]	EVNA [b]
Levene's Test for EV [c]	F		3.698		1.029	
	Sig.		0.061		0.316	
T-test for EM [d]	t		-1.216	-1.216	0.822	0.822
	df		46	39.942	46	43.879
	Sig. (2-tailed)		0.230	0.231	0.415	0.415
	Mean Difference		-0.38374	-0.38374	0.49017	0.49017
	Std. Error Difference		0.31567	0.31567	0.59613	0.59613
	95% CID [e]	Lower	-1.01915	-1.02176	-.70977	-.71134
		Upper	0.25166	0.25427	1.69011	1.69168

a Abbreviation of *Equal variances assumed*

b Abbreviation of *Equal variances not assumed*

c Abbreviation of *Equality of Variances*

d Abbreviation of *Equality of Means*

e Abbreviation of *95% Confidence Interval of the Difference*

Based on the above analysis, it can be explained that the methodology we proposed which can accurately calculate the indoor air temperature and exterior surface temperature of the kang's faceplate, can be used to estimate the temperatures under certain conditions. Therefore, by changing the input parameters, different temperatures can be calculated, by which the optimal measures that we should take to improve the indoor thermal environment of the kang-heating room can be found.

Conclusion

In order to show how the Chinese kang use energy in an efficient way and meanwhile improve indoor thermal environment, thermal processes of the kang-heating building and the kang itself are described in this chapter. Mathematical models of them are built according to the thermal processes, and the results are compared with that of the field measurements.

As studied in this chapter, the success and persistence of traditional Chinese kang make it an excellent example for inspiring us with the idea as using one kind of energy in two ways to make efficient use of energy in the modern energy devices.

The photovoltaic device can only generate the electricity, and the solar water heating device can only generate the hot water. However, with the idea of using one kind of energy in two ways from the research of the kang, the idea of integrating the photovoltaic and solar water heating devices, as well as the fuel cell device to make full use of the electricity and the hot water is proposed. In Chapters 3 to 5, the integrated system of these three devices will be the main topic of this dissertation.

CHAPTER 3

3 Modeling of DER Devices

As researched in the previous chapter, the Chinese kang is a traditional device using energy in efficient ways, which is an excellent example of using one kind of energy in two ways. However, this device is only used in the rural buildings, and not suitable for urban buildings, due to many reasons, i.e. regional limitation, air pollution, etc. Thus, modern energy devices should be promoted to be used in the urban buildings, using the inspiration from the good experience of the kang.

Recent increases in electric grid coupled with electric generation capacity shortages have prompted some residential customers to evaluate distributed energy resource (DER) solutions for their energy needs. DER devices, as mentioned in this research, refer to electricity and hot water generating and storage devices that can be located close to the load they serve. DER devices are playing increasing roles in providing the electric power quality and reliability required by economy of recent, accompanied with hot water, heat, etc.

Overall, there are three types of DER devices studied in this research, which are photovoltaic (PV), solar water heating (SWH) and solid oxide fuel cell (SOFC) devices. Among these three devices, PV and SWH devices use solar energy, and SOFC device utilize natural gas as the resource; PV and SOFC can supply with electricity, and SWH and SOFC can supply with hot water.

This chapter aims to build the mathematical models of these three devices mentioned above by researching on their working principles, and analyze the generation capacity and efficiency of each device to verify the model that we built.

3.1 Photovoltaic device

Photovoltaic device is a device which can use photons from the sun to generate electricity by the photovoltaic effect. A photovoltaic device typically includes an array of PV modules since a single module can produce only a limited amount of power, and each module is packaged and connected assembly of photovoltaic cells.

3.1.1 Mathematical modeling

Working principles of the photovoltaic module can be expressed as a diode electricity equivalent circuit as shown in Figure 3-1. It includes a diode, a series resistance, a parallel resistance and a current source, of which, the diode represents the p-n junction of a PV cell; series resistance contains the integrated bulk resistance, surface resistance and electrode conductor resistance, etc.; parallel resistance refers to the resistance caused by the leakage currents; and current source generates the photogenerated current from the incident solar radiation.

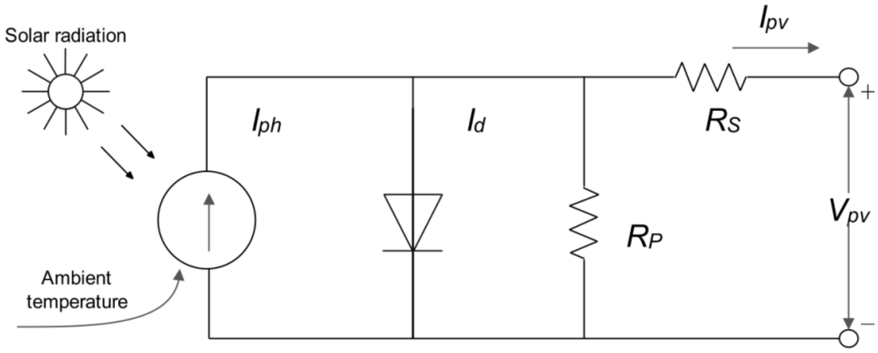

Figure 3-1 Equivalent circuit diagram of the photovoltaic module

According to the *Kirchhoff's Circuit Laws* and *Shockley Equation*, the relationship between the current and the voltage of a PV module can be expressed as

$$I_{mo} = I_{ph} - I_0 \left\{ \left[exp\left(\frac{V_{mo} + I_{mo} R_S}{V_t} \right) \right] - 1 \right\} - \frac{V_{mo} + I_{mo} R_S}{R_P} \tag{3.1}$$

where

I_{mo} is the current of a PV module, A;

I_{ph} is the photogenerated current, A;

I_0 is the diode p-n junction reverse saturation current, A;

V_{mo} is the voltage of a PV module, V;

R_S is the series resistance, Ω;

R_P is the parallel resistance, Ω;

V_t is the diode emission factor, which can be expressed as

$$V_t = nkT_{ref} / q \tag{3.2}$$

where

n is the diode emission factor;

k is the Boltzmann constant, which is 1.38×10^{-23} J/K;

T_{ref} is the temperature at the reference condition, K;

q is the charge of electron, which is 1.602×10^{-19} C.

In order to show the relationship between the involved current, voltage and resistance, there are equations expressed as (DECEE)

$$\frac{V_t}{I_d} = \left(\frac{V_{mo}}{I_{mo}} - R_S\right) R_P \Big/ \left(R_P - \frac{V_{mo}}{I_{mo}} + R_S\right) \tag{3.3}$$

where I_d is the diode current, A.

Photogenerated current is directly proportional to solar radiation, considering the effects of irradiance and temperature on the photogenerated current, it can be expressed as (Chenni, Makhlouf, Kerbache, & Bouzid, 2007)

$$I_{ph} = \frac{G}{G_{ref}} \left[I_{ph,ref} + C_T \left(T_a - T_{ref} \right) \right] \tag{3.4}$$

where

G	is the incident solar radiation, J/(s·m^2);
G_{ref}	is the incident solar radiation in reference condition, J/(s·m^2);
$I_{ph,ref}$	is the photogenerated current in reference condition, A;
C_T	is the temperature coefficient;
T_a	is the ambient temperature, K;
T_{ref}	is the reference temperature, K.

The performance of the photovoltaic module is measured by the manufacture, from which the power that the module will produce can be predicted. Current-voltage (I-V) relationships, which measure the electrical characteristics of photovoltaic devices, are depicted by I-V curves. These I-V curves are obtained by exposing the module to a constant level of light while maintaining a constant module temperature, varying the resistance of the load, and measuring the current that is produced (NI).

The I-V curve of an illuminated PV module has the shape shown in Figure 3-2. The vertical axis refers to current, and the horizontal axis refers to voltage. The actual I-V curve typically passes through two significant points (NI):

- The short circuit current (I_{sc}) corresponds to the short circuit condition when the impedance is low and is calculated when the positive and negative terminals of the module are short-circuited and the voltage between the terminals is zero, which corresponds to a load resistance of zero. I_{sc} occurs at the beginning of the forward-bias sweep and is the maximum current value in the power quadrant.

- The open-circuit voltage (V_{oc}) is the voltage across the positive and negative terminals under open-circuit conditions occur when there is no current passing through the module, which corresponds to a load resistance of infinity. V_{oc} is also the maximum voltage difference across the module for a forward-bias sweep in the power quadrant.

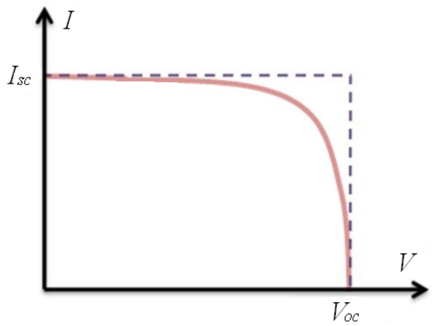

Figure 3-2 Illuminated I-V sweep curve

The module may be operated over a range of voltages and currents. By varying the load resistance from zero (a short circuit) to infinity (an open circuit), the highest efficiency can be determined as the point at which the module delivers maximum power. The power produced by the module can be easily calculated along the I-V sweep by multiplying voltage and current. At the I_{sc} and V_{oc} points, the power will be zero and the maximum value for power will occur between the two. The voltage and current at this maximum power point are denoted as voltage at maximum power (V_{mp}) and current at maximum power (I_{mp}) respectively. Therefore, on the I-V curve, the maximum-power point occurs where the product of current timing voltage is a maximum. This point represents the maximum efficiency of the solar device at converting sunlight into electricity (NI).

Accordingly, Equation 3.1 can be transformed into three equations, respectively at three significant points as

(1) Short-circuit point

$$I_{ph,ref} = I_0\left[exp\left(\frac{I_{sc}R_S}{V_t}\right)-1\right]+\frac{I_{sc}R_S}{R_P}+I_{sc} \tag{3.5}$$

where I_{sc} is the short circuit current, A.

(2) Open-circuit point

$$0 = I_{ph,ref} - I_0\left[exp\left(\frac{V_{oc}}{V_t}\right)-1\right]-\frac{V_{oc}}{R_P} \tag{3.6}$$

where V_{oc} is the open circuit voltage, V.

(3) Maximum power point

$$I_{mp} = I_{ph,ref} - I_0\left[exp\left(\frac{V_{mp}+I_{mp}R_S}{V_t}\right)-1\right]-\frac{V_{mp}+I_{mp}R_S}{R_P} \tag{3.7}$$

where

I_{mp} is the current at maximum power, A;

V_{mp} is the voltage at maximum power, V.

As solar radiation and ambient temperature determined, an I-V curve under current condition can be shaped approximately by the above equations. As mentioned before, there is a maximum value of product of voltage and current, and that is the output power of the module at that time.

For an array of PV modules, the shape of the I-V curve does not change. However, it is scaled based on the number of modules connected in series and in parallel. When N_S is the number of cells connected in series, N_P is the number of cells connected in parallel, and I_{sc} and V_{oc} are values for individual modules, the I-V curve is shown in Figure 3-3.

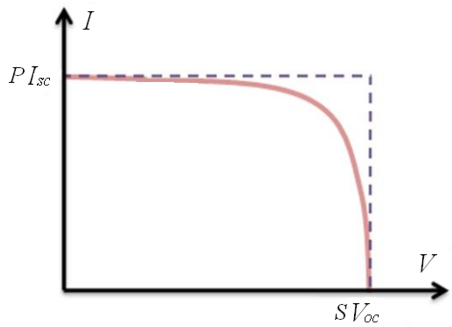

Figure 3-3 I-V curve for arrays

The maximum power output of the PV device can be expressed in equation as

$$P_{pv}(t) = N_S N_P \left[V_{mo}(t) I_{mo}(t) \right]_{max} \eta_{mppt} \tag{3.8}$$

where

P_{pv} is the power output of a PV device, W;

N_S is the number of cells connected in series;

N_P is the number of cells connected in parallel;

η_{mppt} is the maximum power point tracking efficiency.

Although the maximum power point tracking efficiency is variable according to different working conditions, in order to make effective use of solar energy, photovoltaic cells are always working in the vicinity of maximum power point in the practical application, a constant value of 100% is assumed to simplify the calculations in this research (H. Yang et al., 2008).

3.1.2 Generation capacity & efficiency analysis

Energy conversion efficiency of a photovoltaic cell is the percentage of the solar energy shining on a photovoltaic module that is converted into electrical energy, i.e. the ratio of the electrical output of a photovoltaic cell to the incident energy in the form of sunlight (DOE). Energy conversion efficiency is the most important specification of a photovoltaic module as improving it can help make photovoltaic technologies cost-competitive with more traditional sources of energy.

The specification data of the PV devices provided by the PV manufacturers are generally tested with reference to standard test conditions and nominal conditions, the model of which adopted in this work is tabulated in Table 3-1.

Table 3-1 Typical performance characteristics of a photovoltaic module

Typical performance characteristic	Unit	Value
Maximum power	W	195
Voltage at maximum power	V	22.32
Current at maximum power	A	8.74
Open circuit voltage	V	27.41
Short circuit current	A	9.40
Occupancy area of a module	m^2	1.2

The selected PV device was simulated by the mathematical model that we proposed in the previous section.

The daily electricity generation capacities of the selected PV module compared with the daily amounts of effective solar radiation in a year are shown in Figure 3-4. It can be seen that the daily electricity generation capacities of the PV module fluctuate from 0.14 MJ to 4.73 MJ. The rapid fluctuation is mainly caused by the randomness of effective solar radiation and the quarterly changeable outdoor ambient temperature. The annual average daily electricity generation capacity of the PV module is 2.59 MJ, which is 19% of the annual average daily amount of effective solar radiation.

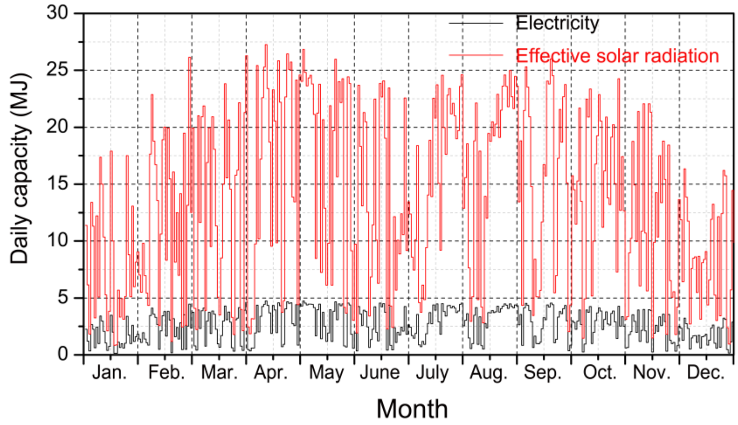

Figure 3-4 Daily electricity generation capacity of the selected PV module

Figure 3-5 presents the daily average efficiency of the PV module. It can be seen that the efficiencies fluctuate from 16.5% to 20%, the amplitude of which is not heavy. The annual average efficiency is calculated as 19%.

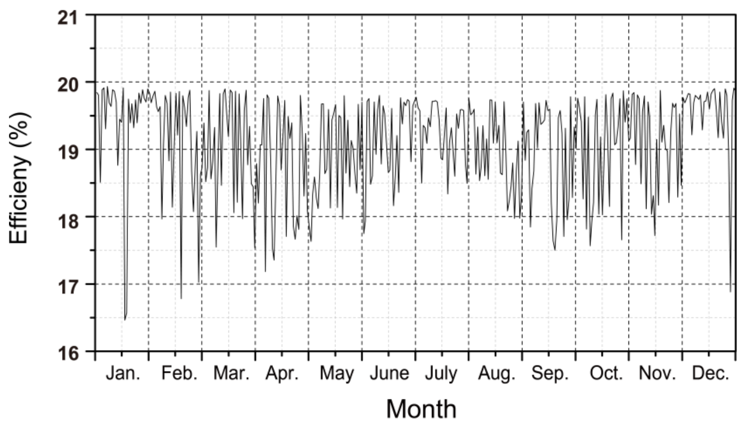

Figure 3-5 Daily average efficiency of the selected PV module

3.2 Solar water heating device

Solar water heating device mainly contains a solar thermal collector, a water tank and sometimes with a pump. Solar thermal collector plays the most important part in this device, which captures and retains heat from the sun and uses it to heat a liquid. Heat pipe evacuated tubular collector is studied in this research, which is recognized as one of the highest efficient types of the solar thermal collectors recently, and has excellent thermal performance used in the low ambient temperature and refluxed with high mass temperature (Ayompe, Duffy, Mc Keever, Conlon, & McCormack, 2011; Lane, 2004).

Two important physical principles govern the technology of solar thermal collectors:

- Whatever hot object ultimately returns to thermal equilibrium with its environment, due to heat loss from the hot object.
- Heat loses more rapidly if the temperature difference between a hot object and its environment is larger.

3.2.1 Mathematical modeling

The detailed arrangement of the heat pipe evacuated tubular collector is shown in Figure 3-6. The portion of the heat pipe being touched with the fin is the boiler portion. The condenser is a short section in good thermal contact with the pipe or duct through which the fluid will be heated and pumped.

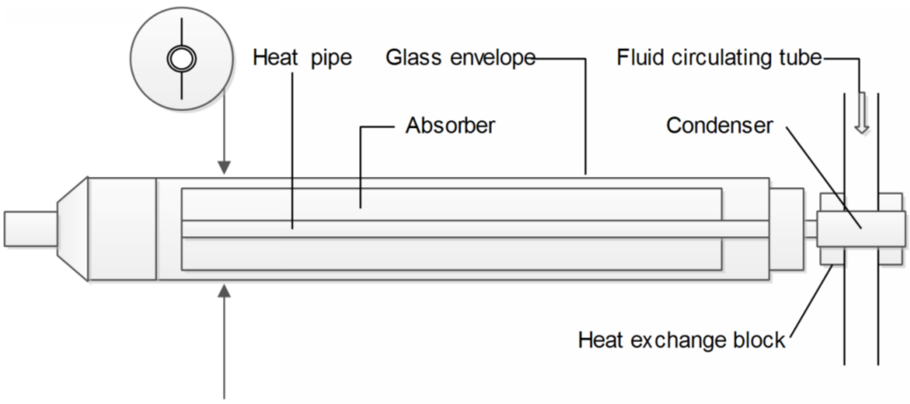

Figure 3-6 Detailed arrangement of heat pipe evacuated tubular collector

Solar radiation is projected on the metallic absorber plate through the enclosure of the evacuated tube, and converted to heat by the absorber plate, making the heat-transfer medium vaporized in the boiler portion of the heat pipe. Once the vapor rises to the condenser section of the heat pipe, the heat is transferred to the fluid in the fluid circulating tube through the heat exchanger block with the vapor itself condensed into liquid and flowing back into the boiler portion by gravity. The above process is repeated circularly, making the temperature of the fluid in the fluid circulating tube increasing ceaselessly. At the same time, the heated absorber plate and the fluid circulating tube dissipate part of the heat to the surrounding environment via various pathways inevitably.

Equivalent thermal network of the heat pipe evacuated tubular collector is shown in Figure 3-7. If all losses are assumed occurring to a common sink temperature, following *Energy Conservation Law*, rates of actual useful energy gain from the solar can be calculated as

$$\dot{Q}_u = N_{tu} A_p \left[G\left(\tau_g \alpha_p\right) - \left(U_t + U_b\right)\left(T_p - T_a\right) \right] \tag{3.9}$$

where

$\dot{Q}_u$	is the rates of addition of energy from solar collector to the load, J/s;
N_{tu}	is the tube number;
A_p	is the absorbed plate area of a SWH tube, m^2;
τ_g	is the transmittance of glass pipe;
α_p	is the absorptance of absorbed plate;
U_t	is evacuated tube heat loss coefficient, W/(m^2·K);
U_b	is the insulation box heat loss coefficient, W/(m^2·K);
T_p	is the mean absorbed plate temperature, assumed as a constant value, K.

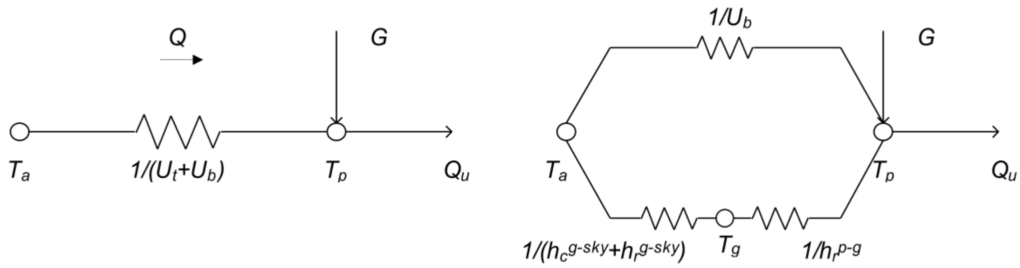

Figure 3-7 Equivalent thermal network of heat pipe evacuated tubular collector

There are radiation and convection between the glass envelope and the ambient environment, but there are only radiation between absorber plate and the glass envelope as we considering no convection and conduction in the vacuum space. Therefore, evaluated tube heat loss coefficient can be expressed as

$$U_t = \left(\frac{1}{h_r^{p-g}} + \frac{1}{h_c^{g-sky} + h_r^{g-sky}} \right)^{-1} \tag{3.10}$$

where

h_r^{p-g} is the radiation heat transfer coefficient between absorber plate and glass envelope, W/(m²·K);

h_c^{g-sky} is the convection heat transfer coefficient between glass envelope and background sky, W/(m²·K);

h_r^{g-sky} is the radiation heat transfer coefficient between glass envelope and background sky, W/(m²·K).

According to the *principle of radiation heat transfer* (Holman, 1997; John, Lienhard, John, & Lienhard, 2008), the two radiation heat transfer coefficients can be deduced and expressed as

$$h_r^{p-g} = \frac{2\sigma\left(T_p^4 - T_g^4\right)}{T_p - T_g} / \left[\left(\frac{1}{\varepsilon_p} - 1 \right) + \frac{2A_p}{A_g A^{p-g}} \left(\frac{1}{\varepsilon_g} - 1 \right) \right] \tag{3.11}$$

where

σ is the Stefan-Boltzmann constant which is 5.6697×10^{-8} W/(m²·K⁴);

T_g is the glass tube temperature, K;

ε_p is emissivity of absorbed plate;

A_g is the glass tube surface area, m²;

A^{p-g} is the area between absorber plate and glass envelope, m²;

ε_g is the emissivity of glass tube.

$$h_r^{g-sky} = \frac{\varepsilon_g \sigma \left(T_g^4 - T_{sky}^4\right)}{T_g - T_a} \tag{3.12}$$

where, T_{sky} is the background sky temperature, K.

In accordance with the principle of thermal balance, the heat loss of the evacuated tube can be expressed in another form as

$$U_t\left(T_p - T_a\right) = h_r^{p-g}\left(T_p - T_g\right) \tag{3.13}$$

Collector heat removal factor is defined as a quantity that relates the actual useful energy gain of a collector to the useful gain if the whole collector surface was at the fluid inlet temperature. In equation form it is

$$F_R = \frac{C_p r^{\cdot}}{A_p\left(U_t + U_b\right)}\left\{1 - exp\left[-\frac{A_p\left(U_t + U_b\right)F^{'}}{C_p r^{\cdot}}\right]\right\} \tag{3.14}$$

where

F_R is the collector heat removal factor;

C_p is the water specific heat at constant pressure, which is 4.2×10³ J/(kg·K);

$r^{\cdot}$ is the mass flow rate of fluid in the fluid circulating tube, kg/s;

$F^{'}$ is the collector efficiency factor, which can be calculated by various parameters of the absorb plate, i.e. collector heat lost coefficient and values of heat transfer coefficient between boiler portion of heat pipe and absorber plate (Duffie & Beckman, 1991).

Therefore, rates of actual useful energy gain from the solar can be rewritten by solving the resulting equations simultaneously, that is to say, Equation 3.9 can be expressed as

$$\dot{Q}_u \quad \cdot \cdot_{\tau} \cdot \cdot_{p} F_R \left[G\left(\tau_g \alpha_p\right) - \left(U_t + U_b\right)\left(T_i - T_a\right) \right] \tag{3.15}$$

where T_i is the fluid inlet temperature, which is equals to the water temperature in water storage tank, K.

Considering about the energy loss from the ducts and pipes leading to and returning from the collector, equation for calculating the useful energy gain of the SWH device can be expressed as the same form as Equation 3.15, only with the value of $\left(\tau_g \alpha_p\right)$ and $\left(U_t + U_b\right)$ being corrected, following the research of Beckman (1978) (Duffie & Beckman, 1991).

As shown in Figure 3-8, the heat is transferred by sending hot water from the collector to the water tank, and replenishing the water from the water tank simultaneously, sending the hot water in the water tank ahead of the load, with the municipal water supplied in return. As the water tank involved is thought of an unstratified tank filling with water, the time-dependent temperature of which is assumed to be uniform in this paper, at any instant, the energy balance of the tank yield can be expressed as

$$C_p \rho V_{tank,sw} \frac{dT_{s,sw}}{dt} = \dot{Q}_u \quad \dot{-}_{s,sw} \quad (\cdot_{tank} A_s)_{sw} \left(T_{s,sw} - T_{a,sw}'\right) \tag{3.16}$$

where

ρ	is the density of water, 1 kg/ L;
$V_{tank,sw}$	is the tank volume of SWH, L;
$T_{s,sw}$	is the water temperature in water storage tank of SWH, K;
t	is the time instant, s;

$\dot{L}_{s,sw}$	is the rates of removal of energy from SWH to the load, J/s;
$(U_{tank}A_s)_{sw}$	is the heat loss coefficient-surface area product of water storage tank of SWH, W/K;
$T_{a,sw}^{'}$	is the ambient temperature for water storage tank of SWH, K.

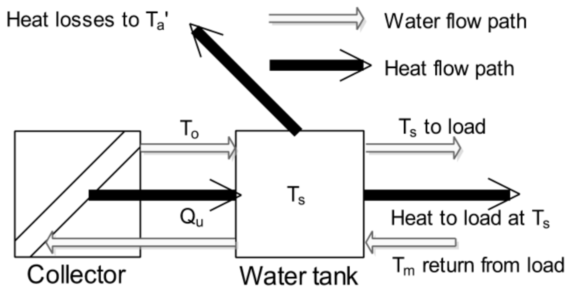

Figure 3-8 Water and heat flow path of a typical solar thermal collector with an unstratified water tank

Specially, when the temperature in the tank reaches an upper limit value, the excess heat will be exhausted, that is while $dT_{s,sw}/dt = 0$.

3.2.2 Generation capacity & efficiency analysis

A SWH device using heat pipes evacuated tube collector was selected and set parallel to the roof. The collector contains 8 tubes, taking an area of 1.2 m^2, the parameters of which are shown in Table 3-2. The number of tubes selected in the device is considered by repeated measurements using the program, considering the balance between the heat gain in summer and that in winter. The water storage tank is thought to be 200 L according to the ordinary situation.

Table 3-2 Typical performance characteristics of a solar thermal collector

Typical performance characteristic	Unit	Value
Area of absorber plant	m^2	0.175
Absorbance of absorber plate	——	0.92
Outside diameter of tube	m	0.1
Occupancy area of a tube	m^2	0.3
Transmittance of tube glass	——	0.9
Absorbance of tube glass	——	0.12
Thermal conductivity of insulation material	W/(m·K)	0.048
Mean thickness of insulation material	m	0.05

The selected SWH device was simulated by the mathematical model that we proposed in the previous section.

Figure 3-9 demonstrates daily heat generation capacity of the selected SWH device. It can be calculated that the annual average daily heat generation capacity of the selected SWH device is 5.9 MJ, which is 42.7% of the effective solar radiation. The maximum value of the daily heat generation capacity reaches 11.2 MJ, and the minimum value is only 0.4 MJ. The rapid fluctuation of the average capacities is also caused by the randomness of effective solar radiation and the quarterly changeable outdoor ambient temperature as that of PV.

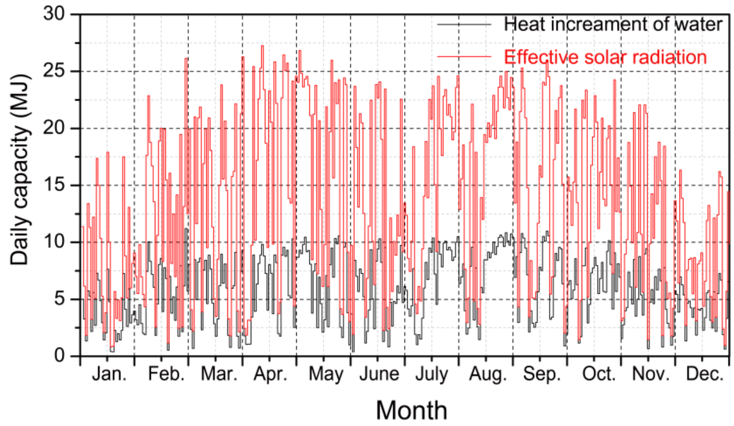

Figure 3-9 Daily heat generation capacity of the selected SWH device

Figure 3-10 shows the daily average efficiency of the SWH device. It can be seen that the efficiencies fluctuate from 21% to 83.5%, the amplitude of which is very large due to heat loss from the collector and the tank changes rapidly between days. The annual average efficiency is calculated as 42.7%, which is much larger than that of the selected PV module.

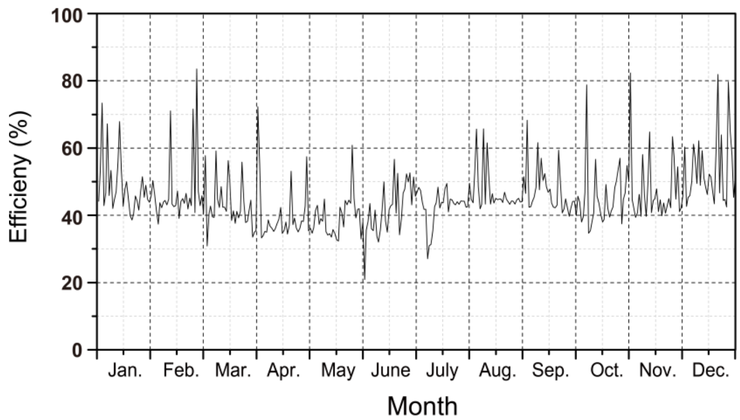

Figure 3-10 Daily average efficiency of the selected SWH device

3.3 Fuel cell device

A fuel cell is a device that converts the chemical energy from a fuel into electricity through a chemical reaction with oxygen or another oxidizing agent. The solid oxide fuel cell (SOFC) device studied in this research is a type of fuel cell that produces electricity directly by oxidizing hydrogen reformed from municipal gas, and simultaneously recovering the exhausted heat to warm the water in a water tank.

3.3.1 Mathematical modeling

The arrangement of SOFC device is shown in Figure 3-11 that it contains a reformer, a cell stack and a heat exchanger, which consist of the generation unit, and a water tank unit is also included. Hydrogen that is generated from the natural gas is used as the fuel to generate electricity.

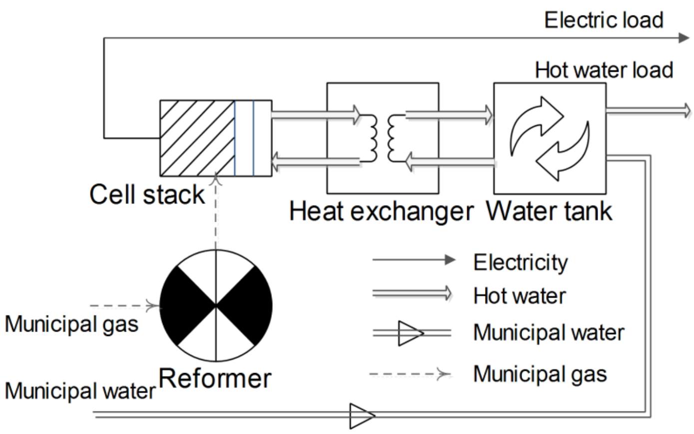

Figure 3-11 Block diagram of the SOFC device

The electric power output of the fuel cell (P_{fc}) varies depending on the electric power load (P_L). If the power load at that instant is smaller than the rated power of the fuel cell (P_r) at the same time, the power output equals the power load, otherwise, it equals the rated power, which may be expressed as

$$P_{fc} = \begin{cases} P_L & P_L < P_r \\ P_r & P_L \geq P_r \end{cases} \tag{3.17}$$

where

P_{fc} is the instant electric power of fuel cell, W;

P_L is the electric power load, W;

P_r is the rated electric power of fuel cell, W.

The value of the electric power generating efficiency (η_e) and exhausted heat recovery efficiency (η_h) changes with the variations of the partial load factor, which is the quotient of P_{fc} and P_r, according to our regression of the experimental data, which are provided by the fuel cell manufacturer. The fuel cell adopted in this work has a rated value of η_e at 42.75%, and a rated value of η_h at 39.15%.

As shown in Figure 3-12, the exhausted heat is recovered in the form of hot water, and subsequently transformed into the form of heat received by a heat exchanger, and then transformed again into the form of water flowing into the water tank. Meanwhile, the hot water in the water tank flows to the load and is supplied with municipal water in the same way on return.

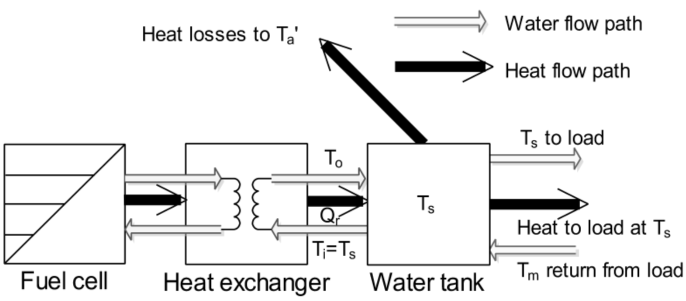

Figure 3-12 Water and heat flow path of a typical fuel cell device with an unstratified water tank

The relationship of electricity generating efficiency and residual heat recovery efficiency as a function of the partial load factor can be given by the regression analysis of testing data, where partial load factor is defined as quotient of electric power generated and the rated power, which are expressed as

$$\dot{Q}_{gas} = \dot{E}_{fc} / \eta_e \tag{3.18}$$

where

$\dot{Q}_{gas}$ is the gas consumption of fuel cell evaluated in heat, J/s;

η_e is the electricity generating efficiency of fuel cell.

$$\dot{Q}_r = \dot{Q}_{gas} \cdot \eta_h \tag{3.19}$$

where

$\dot{Q}_r$ is the rates of recovered exhausted heat from fuel cell unit to the load, J/s;

η_h is the residual heat recovery efficiency.

Likewise, as the water tank is assumed to be unstratified and filled with water at time-dependent uniform temperature as proposed in the previous section, at any instant, the energy balance of the tank yield is expressed in the same form as Equation 3.16 as

$$C_p \rho V_{tank,fc} \frac{dT_{s,fc}}{dt} = \dot{Q}_r - \dot{L}_{s,fc} - (U_{tank} A_s)_{fc} \left(T_{s,fc} - T_{a,fc}'\right) \tag{3.20}$$

where

$V_{tank,fc}$ is the tank volume of fuel cell, L;

$T_{s,fc}$ is the water temperature in water storage tank of fuel cell, K;

$\dot{L}_{s,fc}$ is the rates of removal of energy from fuel cell to the load, J/s;

$(U_{tank} A_s)_{fc}$ is the heat loss coefficient-surface area product of water storage tank of fuel cell, W/ K;

$T_{a,fc}'$ is the ambient temperature for water storage tank of fuel cell, K.

Similarly to that of SWH, when the temperature in the tank rises up to an upper limit value, the excess residual heat will be also exhausted, that is while $dT_{s,fc}/dt = 0$.

3.3.2 Generation capacity & efficiency analysis

A new type of SOFC device was selected in this study, the parameters of which are shown in Table 3-3. The water storage tank is thought to be 90 L according to the typical situation.

Table 3-3 Typical performance characteristics of a generation unit of SOFC device

Typical performance characteristic	Unit	Value
Rated output of power generation	W	700
Rated power generation efficiently (HHV)	——	42.8%
Rated exhaust heat recovery efficiently (HHV)	——	39.2%

The selected SOFC device was simulated by mathematical model made by the efficiency curve of the rated power and that of the exhaust heat which we proposed in the previous section.

The daily average generation capacities of electricity and heat were calculated and shown in Figure 3-13. The heat mentioned here is the effective exhaust heat, which is transferred to the domestic water. It interprets that the electricity generation capacities and the total generation capacities of the SOFC device are larger in winter and summer, smaller in middle seasons, especially in winter, which is caused by the large thermal load in winter. The daily average heat generation capacities are little larger in winter than other seasons. The maximum value of the daily average electricity generation capacity is 667 W, and the minimum value is only 304 W. The maximum capacity almost reaches the rated output of the SOFC device, but the minimum capacity is less than half of the rated output.

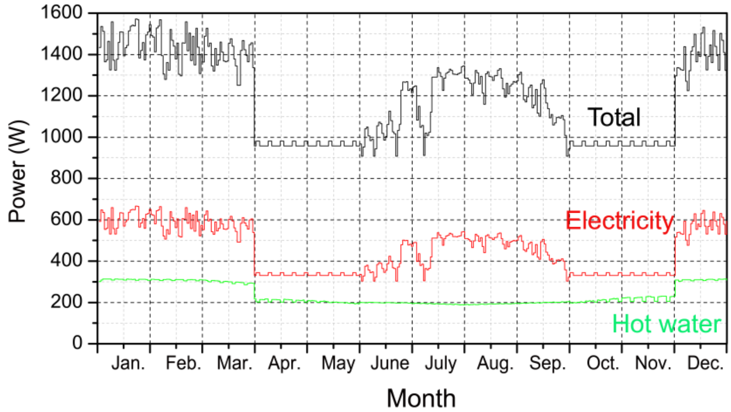

Figure 3-13 Daily average generation capacities of the selected SOFC device

Figure 3-14 interprets that the daily average total generation efficiencies of SOFC device drop into 54% in summer and reach 64% in winter. The reason is that the utilization of the exhaust heat is much higher in winter than in summer due to the initial water temperature and the ambient temperature. The annual average total generation efficiency is calculated as 53%.

The daily average electricity generation efficiencies of SOFC device fluctuate from 33.4% to 42.4%, which is higher in winter and summer than the other seasons. The annual average electricity generation efficiency is calculated as 38.4%, which is a little smaller than the rated power generation efficiency.

The daily average heat generation efficiencies of SOFC device fluctuate from 14% to 25.3%, which is higher in winter than the other seasons. The annual average heat generation efficiency is calculated as 20%, which is a much smaller than the exhaust heat recovery efficiently. That is because there is heat loss from the water tank, especially when the hot water thermal load is smaller than the heat stored in the water tank.

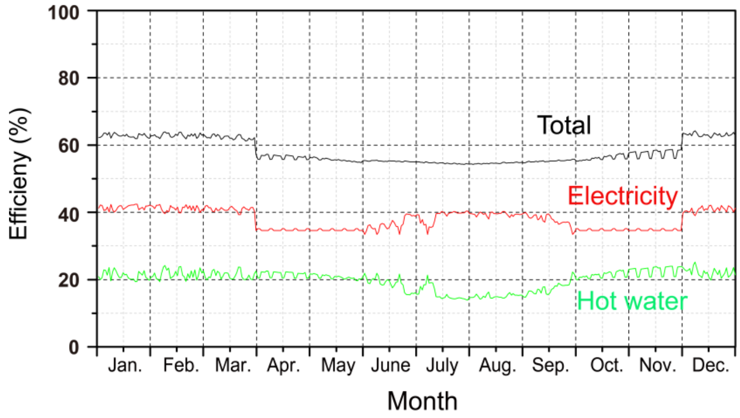

Figure 3-14 Daily average efficiency of the selected SOFC device

Conclusion

The selected DER devices have been mathematical modeled, which are PV device, SWH device and SOFC device. Especially, the dynamic model of PV with effects of ambient temperature and that of SWH with effects of the heat loss from the collector are originally developed.

And, selected types of the DER devices are analyzed in specific conditions, including analyzing the generation capacity and efficiency of each DER device. It demonstrates that the selected DER devices are all existed with a relatively high efficiency in generating energy for residential use.

However, modeling is not the final goal that we pursuit, but a beginning and the base of our core research. Next step of the research for the three selected DER devices is the integration of their electric power generation and hot water supply, which is the topic that is the focus of Chapter 4.

CHAPTER 4

4 Integration of DER devices

A single PV or SWH device is very unlikely to provide a stable electrical or hot water supply, due to the low energy density and high randomness of solar energy. A single SOFC device is also unlikely to provide enough end-use energy in a highly-efficient manner, due to its working principles that the generation efficiency diminishes as the load drops. Thus, integrated operation of the DER devices is necessary for the residential customers.

This chapter focuses on the operation strategies of electric power and hot water required to integrate DER devices modeled in the previous chapter into an overall system and interconnects it with the grid. Weather and municipal water data should be collected first to calculate electrical and hot water loads. In order to show energy conservation effect of integrated operation of the DER devices and compare with each other, the strategies are applied to a supposed building in Fukuoka City in Japan.

4.1 Data collection and calculation

4.1.1 Introduction of objective building

The selected building model is the standard building provided by *Architectural Institute of Japan* (AIJ), which can stand for the normal types in Japan. The plan view of the building is shown in Figure 4-1, and the function of each room is labeled in the floor plans. The elevational and cross-sectional views are shown in Figure 4-2.

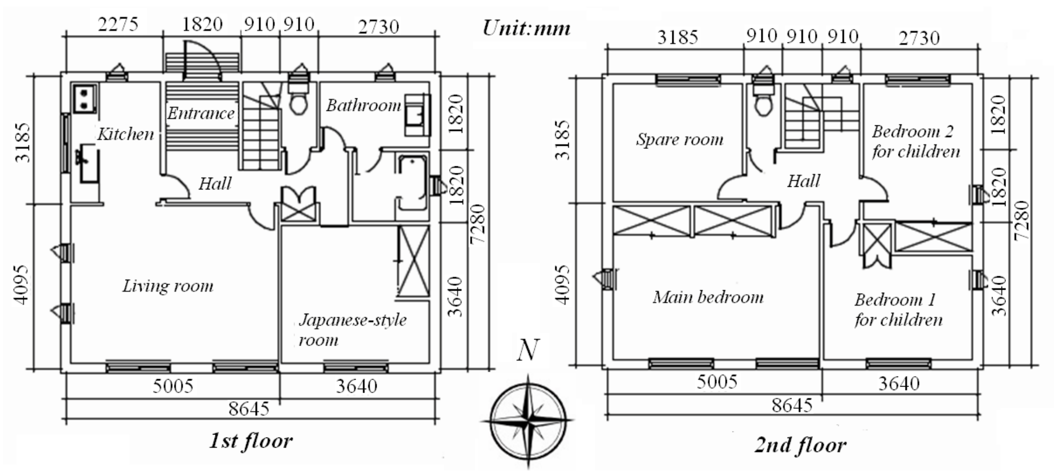

Figure 4-1 Plan view of the standard building

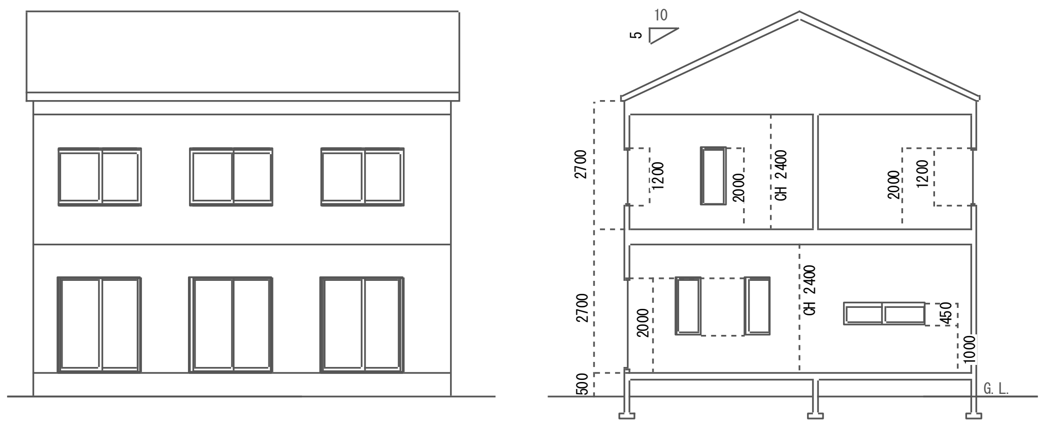

Elevational view of south

Cross-sectional view of north-south

Figure 4-2 Elevational and cross-sectional view of the standard building

It was set to be only parents and two children living in the building, which is the standard situation in Japan recently. The living schedules of the four persons can be decided according to the *Report of National Life Time* (NHK, 2010).

4.1.2 Data collection

Fukuoka City is selected as the location of our research objective, which has a humid subtropical climate that is hot humid in summer and relatively mild in winter. Along with many of the cities in Fukuoka Prefecture, Fukuoka City has a moderate climate with an annual average temperature of 16.3 °C, average humidity of 70% and 1,811 annual daylight hours, and generally 40% of the year is cloudy (AIJ, 2005). In Fukuoka City, the winter is not cold with temperatures rarely dropping below 0 °C; the spring is warm and sunnier; the summer is humid and hot with temperatures peaking around 37 °C; the autumn is mild and dry.

With the hourly meteorological data of the typical meteorological year (AIJ, 2005) and the municipal water data (FCWB.WPD, 2004) obtained, the hourly values of solar radiation in the normal vector of the roof are presented in Figure 4-3, hourly values of the average outdoor air temperature are shown in Figure 4-4, and hourly temperatures of municipal water are displayed in Figure 4-5.

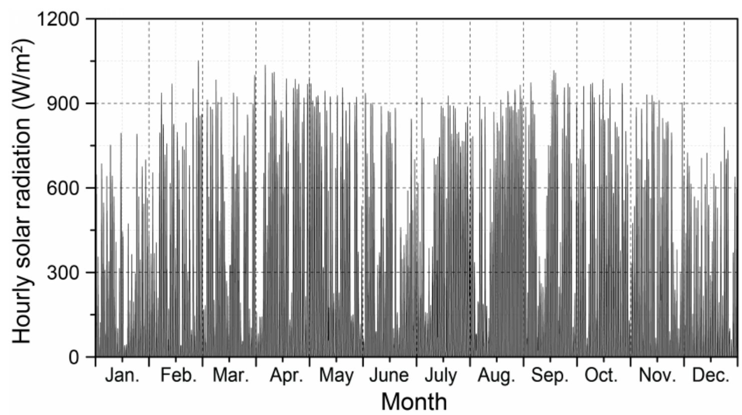

Figure 4-3 Hourly average solar radiation in the normal vector of the roof plot by the data collected from the database (AIJ, 2005)

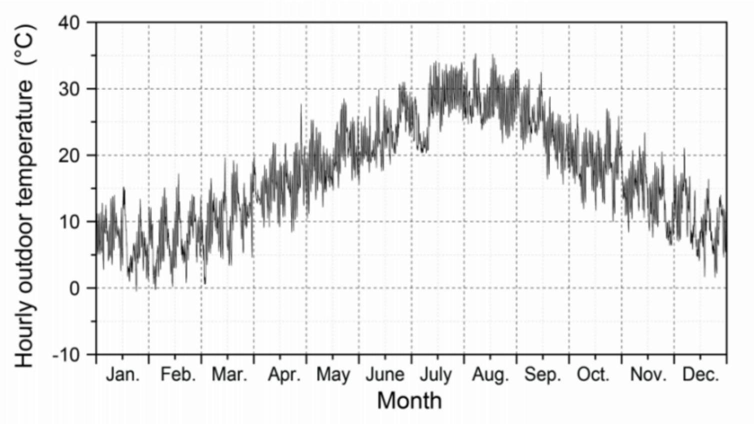

Figure 4-4 Hourly average outdoor air temperatures plot by the data collected from the database (AIJ, 2005)

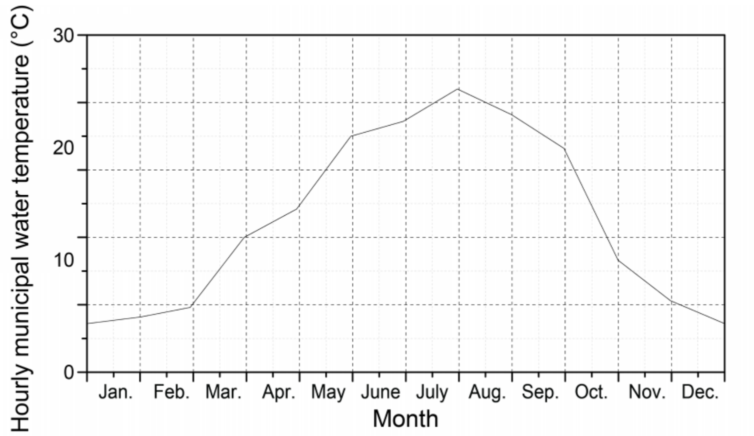

Figure 4-5 Hourly temperatures of the municipal water plot by the data collected from the database (FCWB.WPD, 2004)

4.1.3 Electric power load calculation

Electric power load is calculated by two parts, one part from air conditioning and the other part indicating without air conditioning, which can be calculated by an automatic life style calculation program called *SCHEDULE Ver.2.0* (SHASC.CESR, 2000), and a dynamic simulation program called *THERB* (Ozaki, Watanabe, Takase, & Iwaoka, 2001). Hourly total electric power load was calculated by summing up the part from air conditioning and the left part hour by hour, and it appears for a period of one year is shown in Figure 4-6.

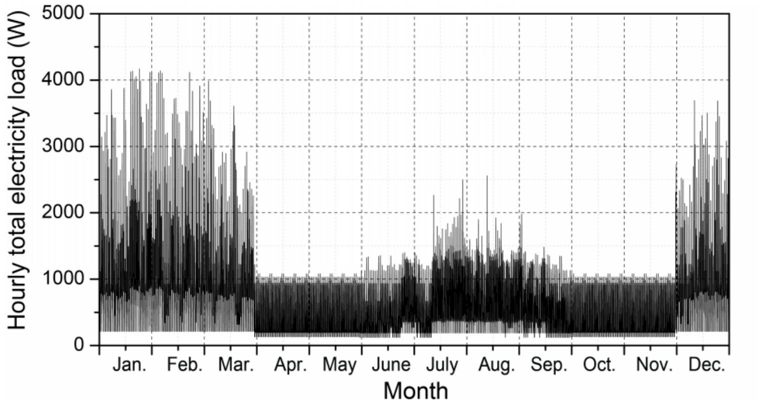

Figure 4-6 Hourly electric power load distribution

4.1.4 Hot water thermal load calculation

SCHEDULE Ver.2.0 (SHASC.CESR, 2000) was used again to calculate the consumption and proper temperatures of domestic hot water. As a special custom of taking a bath every day by Japanese, the use of water is divided into two ways, which are bath use and other uses. Each of the use has its suitable temperature for each season, and there is little difference between hourly volume consumptions of hot water for each season, and they are depicted in Figure 4-7.

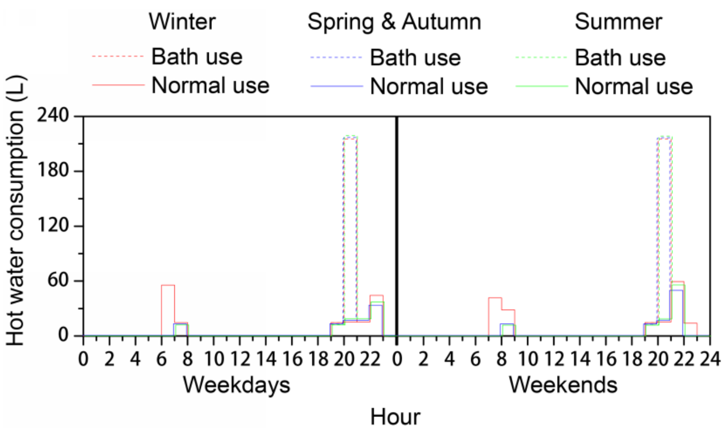

Figure 4-7 Hourly hot water load distribution

4.2 Operation strategy design

An integrated system is not merely a combination of the individual devices as PV, SWH and SOFC, but also with operation strategies employed. As configured in Figure 4-8, the integrated system studied in this paper consists of PV, SWH and SOFC devices, of which switches and valves are respectively used for carrying out the operation strategies of electric power controlling and hot water controlling. The operation strategies adopted in this work makes the first use of the referred individual devices while ensuring a reliable system operation, stating that the supply from the integrated system can exactly satisfy the electric power load demand and hot water load demand all the time with municipal electricity from the power plant and hot water supplied by the sub-boiler as an assist.

4.2.1 Electric power operation modes

The electric power operation strategy follows the supplying sequence that the SOFC first, followed by the PV, and finally the power plant, according that the SOFC will has the highest efficiency if it operates under a full load condition. The operation modes are determined in this work by controlling the switches (*S.1, S.2* and *S.3*), turning them on or off as shown in Figure 4-8.

Overall five operation modes are studied as shown in the process chart in Figure 4-9, labeled as *Mode 1-1* – *Mode 1-5* following the presented strategy.

(1-1) If electrical load is zero, all the switches are turned off; if electrical load is not zero, there are next four operation modes.

(1-2) In case that electric power from SOFC can meet the load, *S.1* and *S.3* are turned on and all electric power from PV is delivered to the grid.

(1-3) In case that the load can be exactly fulfilled when both the electric power from SOFC and PV are activated, *S.1* and *S.2* are turned on. All electric power from PV is exported to the load.

(1-4) In case that the load can be fulfilled only when both the electric power from SOFC and PV are activated, *S.1, S.2* and *S.3* are turned on. Electric power from PV is distributed into two parts, one of which is exported to the load, and the other is exported to the grid.

(1-5) In case that both the electric power from SOFC and PV are unlikely to meet the load, all electric power from PV is used within the building, and electric power from power plant is activated to make up for the remaining load. In this case, *S.1, S.2* and *S.4* are turned on.

At any instant, the distribution of electric power to the load and the gird can be expressed by the electric power of PV (P_{pv}), rated electric power of SOFC (P_r) and total electric power load (P_L) in equations for each operation mode, which are tabulated in Table 4-1.

Table 4-1 Expressive equations of electric power distribution to the load and the grid

Operation mode	P_{fc}	$P_{pv,du}$	$P_{pv,ex}$	P_{pp}
(1-1) No switch on	*0*	*0*	P_{pv}	*0*
(1-2) *S.1,S.3 on*	P_L	*0*	P_{pv}	*0*
(1-3) *S.1,S.2 on*	P_r	P_{pv}	*0*	*0*
(1-4) *S.1,S.2,S.3 on*	P_r	$P_L - P_r$	$P_{pv} - (P_L + P_r)$	*0*
(1-5) *S.1,S.2,S.4 on*	P_r	P_{pv}	*0*	$P_L - \left(P_r + P_{pv}\right)$

4.2.2 How water operation modes

The hot water supply complies with the operation strategy as follows. Above all, in case the instant temperature of hot water in the water tanks of SOFC is not lower than the load temperature at the corresponding time, use the hot water from SOFC tank mixed with appropriate volume of municipal water. Hereafter, so does the hot water in the water tank of SWH. Last, in case the instant hot water temperatures from both water tanks are not enough for the use, the water temperature of which is slightly higher is selected to be used by reheating with the sub-boiler to the degree of the load temperature at the corresponding time. The hot water operation modes are recognized by opening and closing the valves (*V.1, V.2, V.3, V.4 and V.5*), as shown in Figure 4-8.

A total of seven operation modes are studied as shown in the process chart in Figure 4-9, labeled as *Mode 2-1 – Mode 2-7* following the proposed strategy.

(2-1) If hot water mass load is zero, all the valves are closed; if hot water mass load is not zero, there are next six operation modes.

(2-2) In case water temperature from SOFC is larger than load temperature, municipal water is needed to be mixed with the hot water from SOFC, so that *V.2, V.3* and *V.4* are opened.

(2-3) In case water temperature from SOFC exactly equals to load temperature, only hot water from SOFC is used, so that *V.2* and *V.4* are opened.

(2-4) In case water temperature from SOFC is smaller than load temperature, but water temperature from SWH is larger than load temperature, municipal water is needed to be mixed the hot water from SWH, so that V.1, V.3 and V.4 are opened.

(2-5) In case water temperature from SOFC is smaller than load temperature, but water temperature from SWH exactly equals to load temperature, only hot water from SOFC is used, so that V.1 and V.4 are opened.

(2-6) In case both water temperature from SOFC and SWH is smaller than load temperature, water temperature from SOFC is larger than that from SWH, only hot water from SOFC is used, but it needs to be heated by sub-boiler, so that V.2 and V.5 are opened.

(2-7) In case both water temperatures from SOFC and SWH are smaller than load temperature, water temperature from SOFC is smaller than that from SWH, only hot water from SWH is used, but it needs to be heated by sub-boiler, so that V.1 and V.5 are opened.

At any instant, the removal rates of energy distribution to the load can be expressed in equations by the temperature of the hot water from the water tank of SWH ($T_{s,sw}$) and SOFC ($T_{s,fc}$), the mass flow rate of hot water to the load ($\dot{r}$), the temperature of hot water load (T_L), and the municipal water temperature (T_m) for each operation mode, which are tabulated in Table 4-2.

Table 4-2 Expressive equations of removing rates of energy distribution to the load

Operation mode	$\dot{L}_{s,sw}$	$\dot{L}_{s,fc}$	$\dot{L}_{s,sb}$
(2-1) No valve open	*0*	*0*	*0*
(2-2) *V.2, V.3, V.4* open	*0*	$C_p \dot{r}$ ([illegible])	*0*
(2-3) *V.2, V.4* open	*0*	$C_p \dot{r}$ ([illegible])	*0*
(2-4) *V.1, V.3, V.4* open	$C_p \dot{r}$ ([illegible])	*0*	*0*
(2-5) *V.1, V.4* open	$C_p \dot{r}$ ([illegible])	*0*	*0*
(2-6) *V.2, V.5* open	*0*	$C_p \dot{r}$ ([illegible] $_m$)	$C_p \dot{r}$ ([illegible] $_{,fc}$)
(2-7) *V.1, V.5* open	$C_p \dot{r}$ ([illegible] $_m$)	*0*	$C_p \dot{r}$ ([illegible] $_{,sw}$)

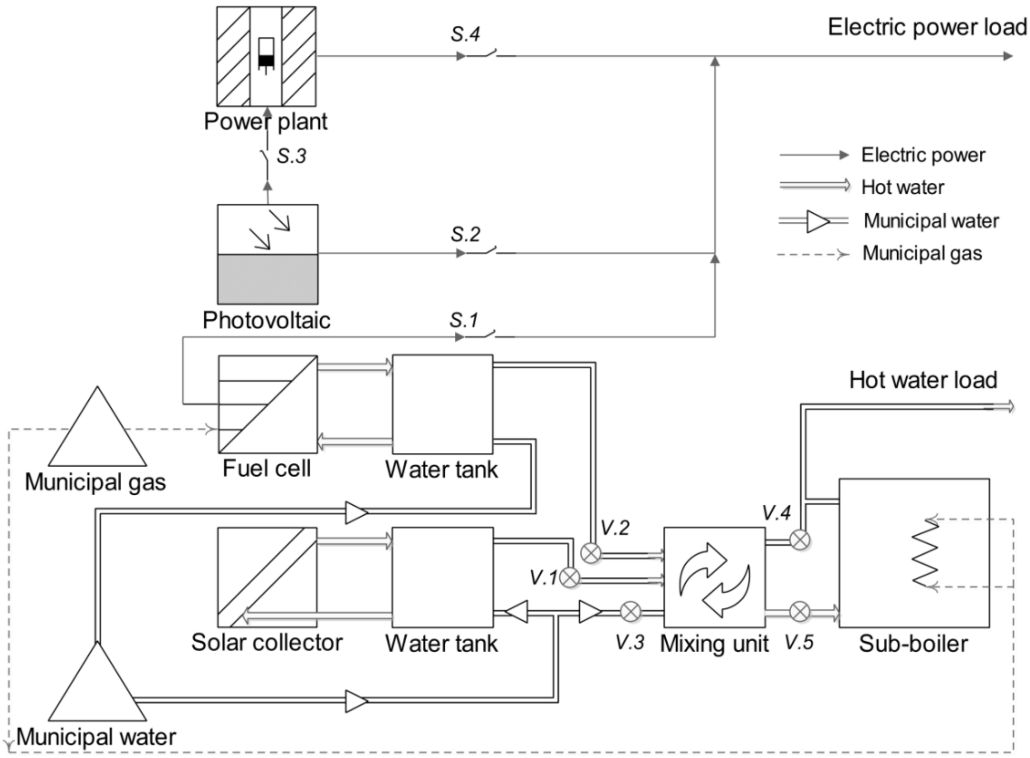

Figure 4-8 Block diagram of the integrated DER device

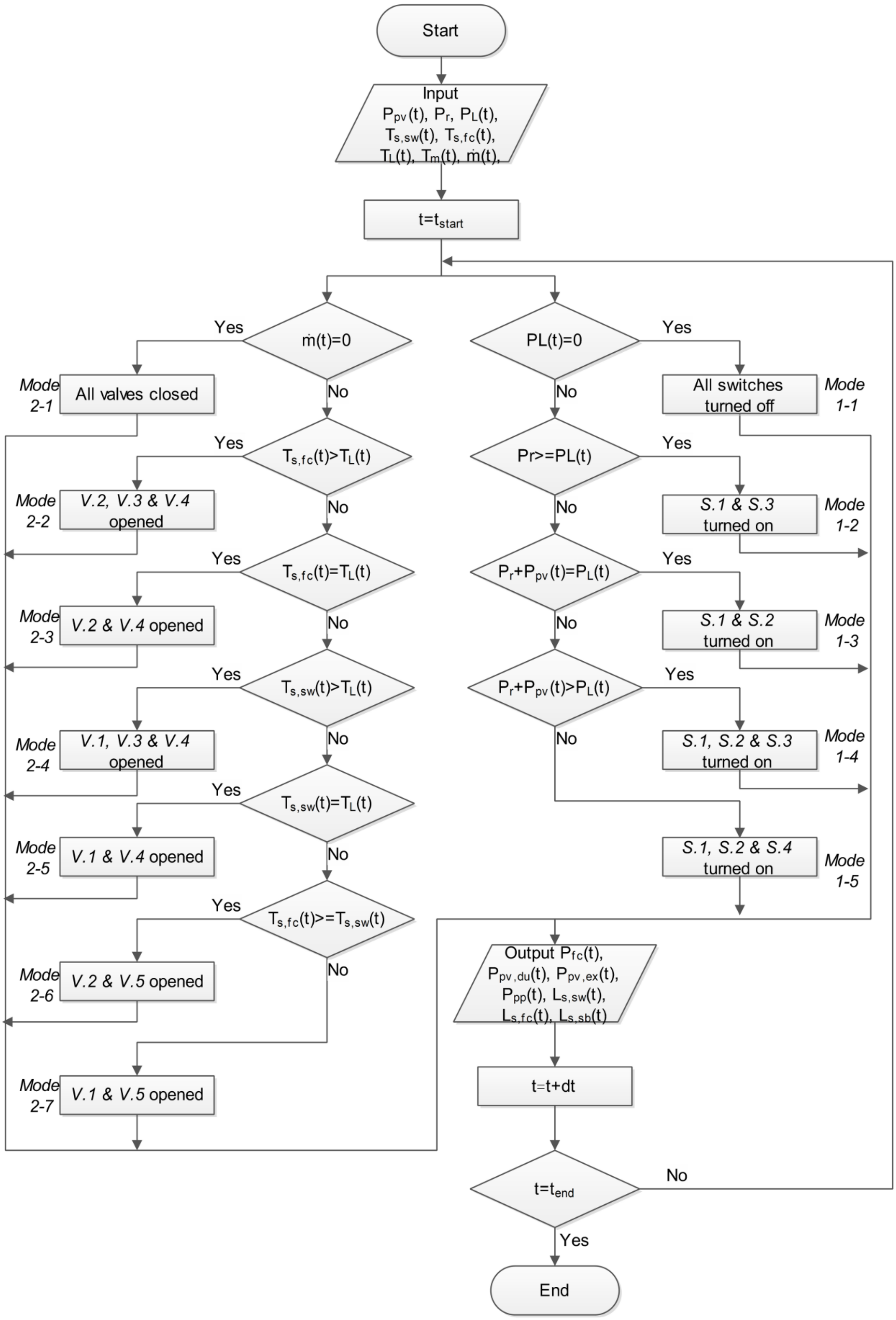

Figure 4-9 Process chart indicating the operation modes of electric power and hot water

4.3 Case study

After each model of these devices was established, energy consumption of integrated system can be calculated. Comparisons between using and not using the integrated system from the aspect of reduction of conventional energy consumption can be studied.

Though species of the combination of the devices are various, as the surplus electricity generated by the PV device can be send to the gird to make profits, it is thought to be used in every case of integrated system, and as much capacity as possible. Meanwhile, since only the SWH and SOFC devices cannot generate hot water as required, but respectively depends on the electric power load and the weather condition, sub-boiler needs to be used in every case to make up for insufficient hot water.

In this research, according to the choice of using or not using the SWH and SOFC device, overall four cases are selected for analyzing, which are

- PV
- PV+SWH
- PV+SOFC
- PV+SWH+SOFC

In order to make the results more comparable with each other, the insulation effects of PV modules and SWH panels for the building are not considered, i.e. thermal load of the building is thought to be the same as that when PV modules and SWH panels are not installed.

4.3.1 Only photovoltaic device

Case 1 is set containing only PV device. For the purpose of simplification, only the south roof area of the objective building is considered to be the place for installing the PV modules. Since the south roof area is 36 m^2, and the PV modules are selected as the type shown in Table 3-1, at most 30 selected modules can be installed.

Figure 4-10(a) presents the monthly distribution of electricity consumption as calculated in Case 1, only using PV device. The results are described as

- For monthly electric load, 15.4% (in Dec.) to 41.5% (in May) is supplied from the PV device in a year. This percentage is relatively high in summer, and low in winter.

  And totally in a year, the percentage is about 27.4%, which means 72.6% of electric load should be supplied by the power plant.
- The monthly consumption of the electricity supplied from the PV device for direct home use is from 0.27 GJ (in Nov.) to 0.65 GJ (in Aug.) in a year, and the value is much larger in summer than in other seasons. The reason is that the daytime is longer and more electricity is used at the daytime in summer than in other seasons.

  And totally in a year, this amount is about 5.27 GJ, which means PV can contribute an annual reduction of electricity consumption of 5.27 GJ in this case for direct home use.
- The monthly consumption of the electricity supplied from the PV device being sent to the grid is from 1.03 GJ (in Jan.) to 2.69 GJ (in May) in a year, and the value is much larger in the middle seasons than in summer and winter.

  And totally in a year, this amount is about 23.15 GJ, which means PV can contribute an annual reduction of electricity consumption of 23.15 GJ in this case for the society by the surplus electricity sent to the grid.
- The home use ratio of the electricity generated by the PV device is relatively high in summer and winter, and low in the middle seasons, which is the same trend with the monthly electric load in a year.

  And the whole year home use ratio is 18.5%, which means 18.5% of electricity generated by PV is for the direct home use.

Figure 4-10(b) shows the monthly distribution of hot water thermal consumption as calculated in Case 1, only using PV device. In this case, it can be seen that hot water is totally supplied by the sub-boiler, as PV can only supply electricity.

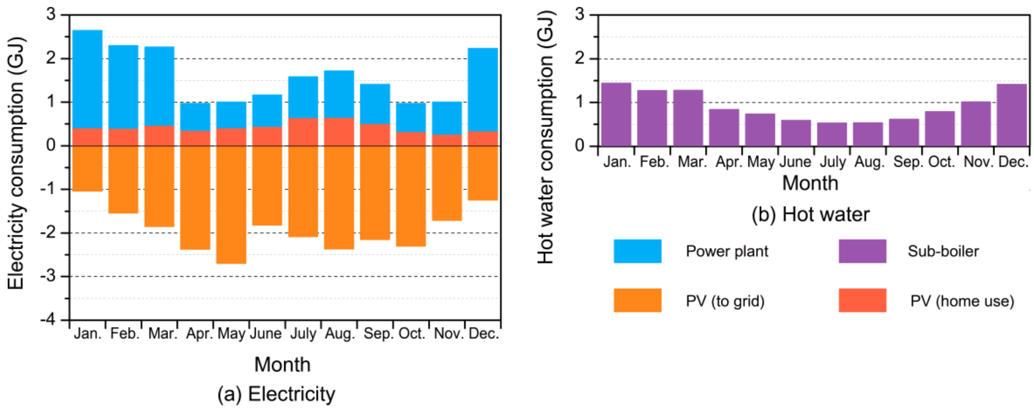

Figure 4-10 Monthly distribution of energy consumption in Case 1

(a) Electricity consumption (b) Hot water thermal consumption

Figure 4-11 presents the monthly reduction of conventional energy consumption as calculated in Case 1, only containing PV device. The results are described as

- The reduction comes from only the PV device, but it is divided into two parts. One part is for home use, and the other part is sent to the grid. If the part sent to the grid can be thought as an reduction of conventional energy consumption for the society, the monthly conventional energy consumption reduction can reach 3.9 GJ (in Jan.) to 8.4 GJ (in May).
- Totally 77 GJ of conventional energy consumption can be reduced in a year. It consists of two parts, for the part from the electricity generated by PV for direct home use, the reduction is 14.3 GJ, and the part from the electricity generated by PV being sent to the grid, the reduction is 62.7 GJ.

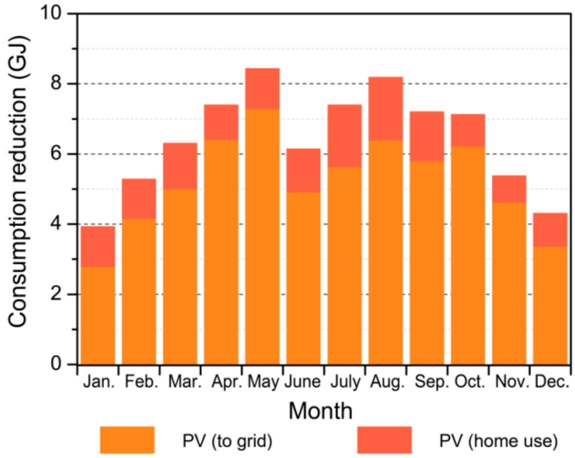

Figure 4-11 Monthly reduction of conventional energy consumption in Case 1

4.3.2 Integrated PV+SWH system

Case 2 is set containing PV device and SWH device. The SWH device is assumed to have 8 tubes, occupying a space of 2.4 m^2, which depends on the result of the repeated calculation by changing the values of the parameters to balance the demands and the generating ability. Since the SWH device takes 2.4 m^2, the remaining area can be installed at most 28 modules of PV.

The monthly distribution of electricity consumption calculated in Case 2, is shown in Figure 4-12(a), which contains PV and SWH devices. The results are shown as

- For monthly electric load, 15.1% (in Dec.) to 41.2% (in May) is supplied from the PV device in a year. This percentage is still relatively high in summer, low in winter, and just a little bit smaller than that in Case 1.

  And totally in a year, the percentage is about 27.0%, which means 73.0% of electric load should be supplied by the power plant, which is almost the same with the percentage calculated in Case 1.
- The monthly consumption of the electricity supplied from the PV device for direct home use is from 0.27 GJ (in Nov.) to 0.64 GJ (in Aug.) in a year, and the value is almost the same as that in Case 1.

And totally in a year, this amount is about 5.19 GJ, which is only a little less than that in Case 1.

- The monthly consumption of the electricity supplied from the PV device being sent to the grid is from 0.95 GJ (in Jan.) to 2.49 GJ (in May) in a year, which is smaller than that in Case 1. It is because in this case, less PV modules are installed than in Case 1.

  And totally in a year, this amount is about 21.32 GJ, which is less than that in Case 1.

- The home use ratio of the electricity supplied from the PV device is from 13.2% (in Oct.) to 29.8% (in Jan.). This ratio is also relatively high in summer and winter, and low in the middle seasons, which is the same trend with that calculated in Case 1.

  And the whole year home use ratio is 19.6%, which is a little larger than that in Case 1. That is because the amount of the electricity generated by PV for direct home use is almost the same as in Case 1, but the amount sent to the grid reduced.

The monthly distribution of hot water thermal consumption calculated in Case 2, is shown in Figure 4-12(b), which contains PV and SWH devices. The results are shown as

- For monthly hot water load, 14.7% (in Jan.) to 79% (in Aug.) is supplied from the SWH device in a year. This percentage is relatively high in summer, and low in winter. The reason is that, the municipal water temperature is much lower in winter than in summer, which caused the fact that more heat is need to heat the water into the proper temperature in winter than in summer. And also, the proper temperature that we need is lower in summer than in winter.

  And totally in a year, the percentage is about 35.2%, which means 64.8% of hot water load should be supplied by the sub-boiler.

- The monthly thermal consumption of the hot water supplied from the SWH device is from 0.21 GJ (in Jan.) to 0.42 GJ (in Aug.) in a year.

And totally in a year, this amount is about 3.89 GJ, which means SWH can contribute an annual reduction of hot water thermal consumption of 5.27 GJ in this case.

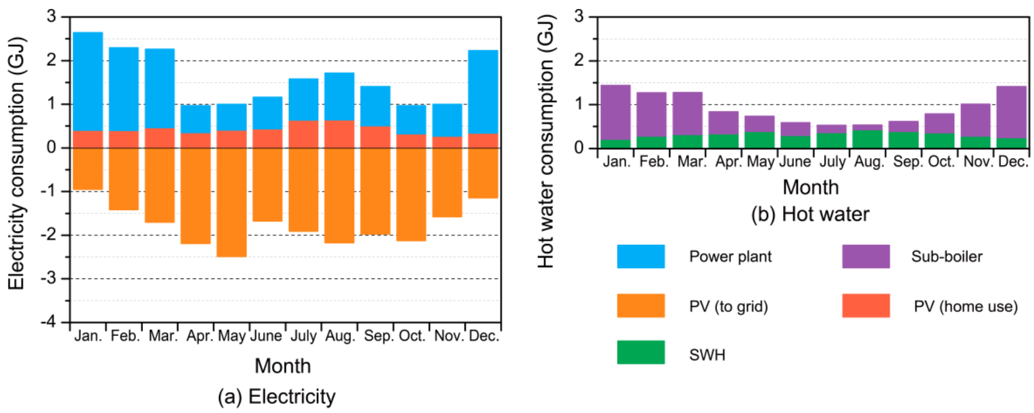

Figure 4-12 Monthly distribution of energy consumption in Case 2

(a) Electricity consumption (b) Hot water thermal consumption

Figure 4-13 presents the monthly reduction of conventional energy consumption as calculated in Case 2, containing PV device and SWH device. The results are described as

- The reduction comes from PV and SWH, but the part from PV can be further divided into two parts. One part is for home use, and the other part is sent to the grid. If the part sent to the grid can be thought as an reduction of conventional energy consumption for the society, the monthly conventional energy consumption reduction can reach 3.9 GJ (in Jan.) to 8.4 GJ (in May), which is almost the same as that in Case 1.
- Totally 77.1 GJ of conventional energy consumption can be reduced in a year, which is almost the same as that in Case 1. It consists of three parts, for the part from the electricity supplied by PV for direct home use, the reduction is 14.1 GJ, the part from the electricity generated by PV being sent to the grid, the reduction is 57.8 GJ, and the part from the hot water supplied by SWH, the reduction is 5.2 GJ.

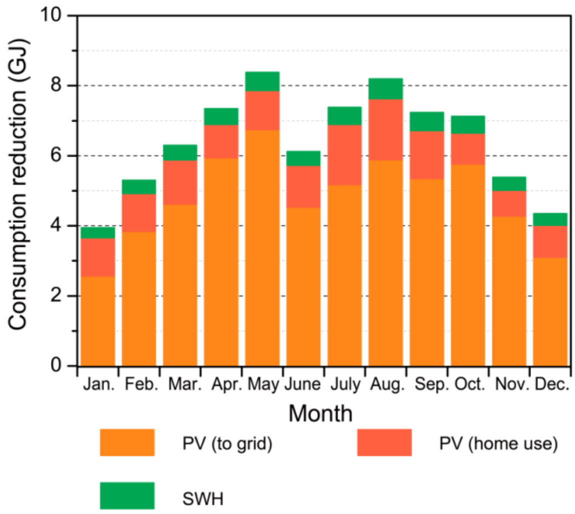

Figure 4-13 Monthly reduction of conventional energy consumption in Case 2

4.3.3 Integrated PV+SOFC system

The SOFC device and the PV device are used in Case 3, and 30 selected modules of the PV modules are installed, which is the same as in Case 1.

Figure 4-14(a) illustrates the monthly distribution of electricity consumption as calculated in Case 3, using PV device and SOFC device. The results are described as

- For monthly electric load, very little part is supplied from the PV device, but much part is supplied from the SOFC, it is about 61.6% (in Jan.) to 89.6% (in Oct.). This percentage is relatively high in summer, and low in winter.

  And totally in a year, the percentage is about 74.7%, which means only 25.3% of electric load should be supplied by the power plant.
- The monthly consumption of the electricity supplied from the PV device for direct home use is from 0.01 GJ (in Nov.) to 0.13 GJ (in July) in a year, and the value is much larger in summer than in other seasons.

  And totally in a year, this amount is about 0.71 GJ, which means PV can contribute an annual reduction of electricity consumption of 0.71 GJ in this case for direct home use.

- The monthly consumption of the electricity supplied from the PV device being sent to the grid is from 1.38 GJ (in Jan.) to 3.08 GJ (in May) in a year, and the value is much larger in the middle seasons than in summer and winter.

  And totally in a year, this amount is about 27.7 GJ, which means PV can contribute an annual reduction of electricity consumption of 27.7 GJ in this case for the society by the surplus electricity sent to the grid.
- The home use ratio of the electricity generated by the PV device is very small in all seasons.

  And the whole year home use ratio is 2.5%, which means only 2.5% of electricity generated by PV is for the direct home use, the other part is sent to the grid.
- The monthly consumption of the electricity supplied from the SOFC device is from 0.87 GJ (in Apr.) to 1.63 GJ (in Jan.) in a year, and the value is much larger in the middle seasons than in summer and winter.

  And totally in a year, this amount is about 14.38 GJ, which means SOFC can contribute an annual reduction of electricity consumption of 14.38 GJ in this case.

Figure 4-14(b) presents the monthly distribution of hot water thermal consumption as calculated in Case 1, using PV device and SOFC device. The results are shown as

- For monthly hot water load, 57.9% (in Jan.) to 95.7% (in Aug.) is supplied from the SOFC device in a year. This percentage is relatively high in summer, and low in winter.

  And totally in a year, the percentage is about 67.7%, which means only 32.3% of hot water load should be supplied by the sub-boiler.
- The monthly thermal consumption of the hot water supplied from the SOFC device is from 0.5 GJ (in July) to 0.83 GJ (in Jan.) in a year.

  And totally in a year, this amount is about 7.48 GJ, which means SOFC can contribute an annual reduction of hot water thermal consumption of

7.48 GJ in this case.

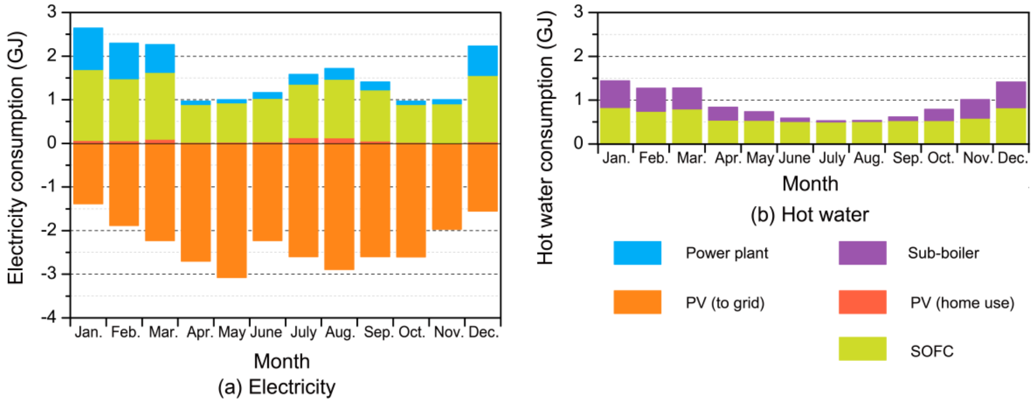

Figure 4-14 Monthly distribution of energy consumption in Case 3

(a) Electricity consumption (b) Hot water thermal consumption

Figure 4-15 presents the monthly reduction of conventional energy consumption as calculated in Case 3, containing PV device and SOFC device. The results are described as

- The reduction comes from PV and SWH, but the part from PV can be further divided into two parts. One part is for home use, and the other part is sent to the grid. If the part sent to the grid can be thought as an reduction of conventional energy consumption for the society, the monthly conventional energy consumption reduction can reach 5.5 GJ (in Jan.) to 9.1 GJ (in Aug.), which is much larger than that in Case 1 & Case 2.
- Totally 88.5 GJ of conventional energy consumption can be reduced in a year, which is much more than that in Case 1 & Case 2. It consists of three parts, for the part from the electricity supplied by PV for direct home use, the reduction is 1.9 GJ, the part from the electricity generated by PV being sent to the grid, the reduction is 75.1 GJ, and the part from the hot water supplied by SWH, the reduction is 11.6 GJ.

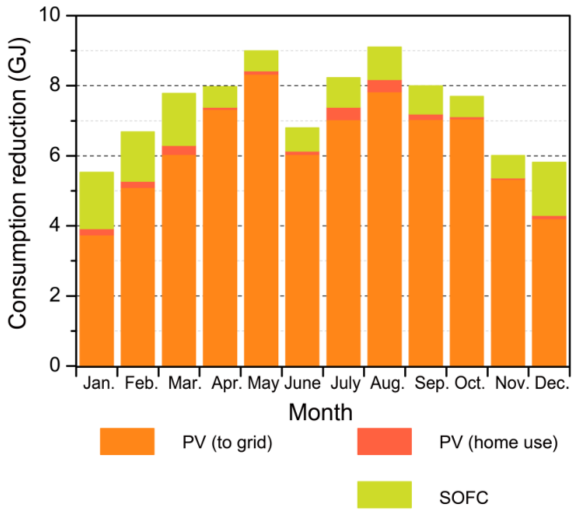

Figure 4-15 Monthly reduction of conventional energy consumption in Case 3

4.3.4 Integrated PV+SWH+SOFC system

It contains the whole three devices as the PV device, the SWH device and the SOFC device in Case 4. The installation numbers of the PV modules and the SWH panels in Case 4 are the same as that in Case 2.

The monthly distribution of electricity consumption calculated in Case 4, is shown in Figure 4-16(a), which contains PV, SWH and SOFC devices. The results are shown as

- For monthly electric load, very little part is supplied from the PV device, but much part is supplied from the SOFC. The percentage is the same as that in Case 3, because the electricity supplied by SOFC is used first, and the generation capacity is the same.

  And totally in a year, the percentage is also about 74.7%, which is also the same as that in Case 3.
- The monthly consumption of the electricity supplied from the PV device for direct home use is from 0.01 GJ (in Nov.) to 0.13 GJ (in July) in a year, which is almost the same as that in Case 3.

  And totally in a year, this amount is about 0.69 GJ, which means PV can contribute an annual reduction of electricity consumption of 0.69 GJ in this case for direct home use.

- The monthly consumption of the electricity supplied from the PV device being sent to the grid is from 1.29 GJ (in Jan.) to 2.87 GJ (in May) in a year, which is a little smaller than that in Case 3.

  And totally in a year, this amount is about 25.8 GJ, which means PV can contribute an annual reduction of electricity consumption of 25.83 GJ in this case for the society by the surplus electricity sent to the grid.

- The home use ratio of the electricity generated by the PV device is very small in all seasons.

  And the whole year home use ratio is 2.6%, which means only 2.6% of electricity generated by PV is for the direct home use, the other part is sent to the grid.

- The monthly consumption of the electricity supplied from the SOFC device is the same as that in Case 3.

  And totally in a year, this amount is about 14.38 GJ, which is also the same as that in Case 3.

The monthly distribution of hot water thermal consumption calculated in Case 4, is shown in Figure 4-16(b), which contains PV, SWH and SOFC devices. The results are shown as

- For monthly hot water load, 68.3% (in Feb.) to 95.7% (in Aug.) is supplied from the SOFC device in a year, and 4.3% (in Aug.) to 26.6% (in Oct.). The reason why the percentage supplied from SWH is so low is that SOFC can supply most of the hot water in this case.

  And totally in a year, the percentage supplied by SOFC is about 74.4%, and by SWH is about 13.9%, which means only 11.7% of hot water load should be supplied by the sub-boiler.

- The monthly thermal consumption of the hot water supplied from the SOFC device is from 0.5 GJ (in July) to 1 GJ (in Jan.) in a year.

And totally in a year, this amount is about 8.21 GJ, which means SOFC can contribute an annual reduction of hot water thermal consumption of 8.21 GJ in this case.

- The monthly thermal consumption of the hot water supplied from the SWH device is from 0.02 GJ (in Aug.) to 0.21 GJ (in Oct.) in a year.

  And totally in a year, this amount is about 1.53 GJ, which means SWH can contribute an annual reduction of hot water thermal consumption of 1.53 GJ in this case.

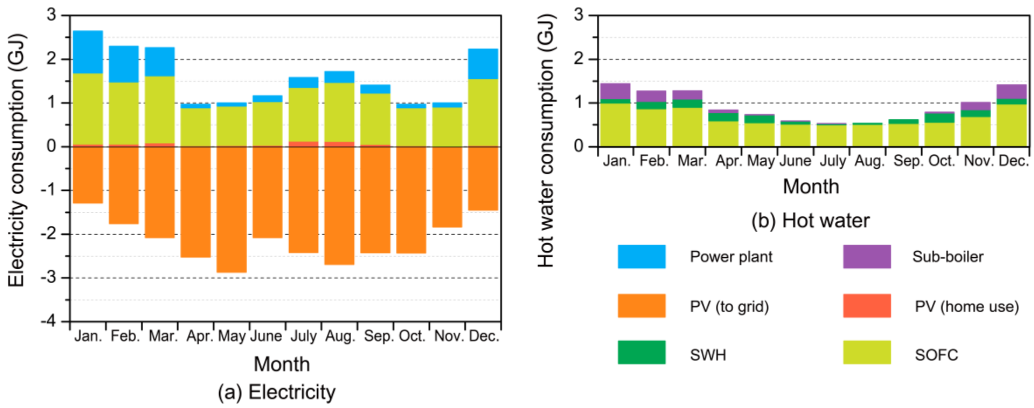

Figure 4-16 Monthly distribution of energy consumption in Case 4

(a) Electricity consumption (b) Hot water thermal consumption

Figure 4-17 presents the monthly reduction of conventional energy consumption as calculated in Case 4.

- The reduction comes from PV, SWH and SOFC, but the part from PV can be further divided into two parts. One part is for home use, and the other part is sent to the grid. If the part sent to the grid can be thought as an reduction of conventional energy consumption for the society, the monthly conventional energy consumption reduction can reach 5.6 GJ (in Jan.) to 8.7 GJ (in May), which is a little smaller than that in Case 3.
- Totally 86.5 GJ of conventional energy consumption can be reduced in a year, which is a little smaller than that in Case 3. It consists of four parts, for the

part from the electricity supplied by PV for direct home use, the reduction is 1.87 GJ, the part from the electricity generated by PV being sent to the grid, the reduction is 70.02 GJ, the part from the hot water supplied by SWH, the reduction is 2.04 GJ, and the part from the hot water supplied by SOFC, the reduction is 12.53 GJ.

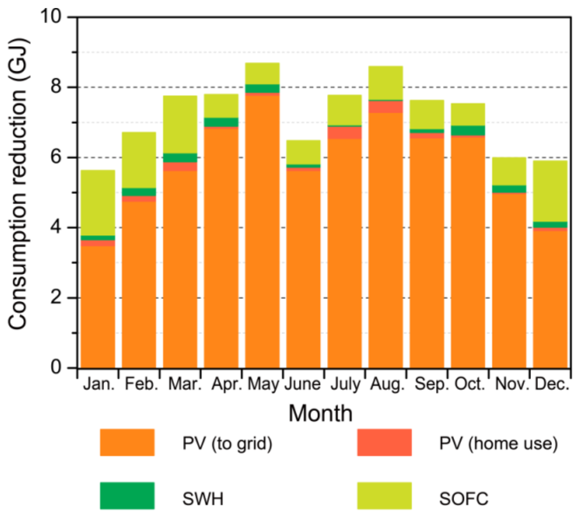

Figure 4-17 Monthly reduction of conventional energy consumption in Case 4

4.3.5 Summary of the results

In summary of the above, four cases of combinations of DER devices have been proposed. From the conventional energy consumption distributions and the reductions shown in this section, four conclusions can be achieved according to the integration with the operation strategies that we proposed in this chapter.

- In the case that the SOFC device and the SWH device are used at the same time (Case 4), the SWH device makes little contribution to reduce conventional energy consumption, especially in summer, which is much less than that in the case without combination of the SOFC device (Case 2).
- In the case that the SOFC device is used (Case 3 & 4), the reduction of conventional energy consumption by the PV device is more than that in the case

that the SOFC device is not used, due to the generation capacity of the SOFC device. Of the consumption reduction, the electricity being sent to the grid contributes much more than that being used directly for the own house.

- It is shown in Figure 4-18, as for the reduction of conventional energy consumption for direct use in the own house, it is better to use the combination proposed in Case 2 than in the other three cases. The annual reduction for own house in Case 2 is 19.2 GJ, which is about 14.7% more than that in Case 4, about 25.9% more than that in Case 1, and about 30% more than that in Case 3.
- It is shown in Figure 4-18, as for total reduction of conventional energy consumption, including the surplus electricity being sent to the gird to equal a reduction for the society, it is better to use the combination proposed in Case 3 than in the other three cases. The annual reduction in Case 3 is 88.5 GJ, which is only about 2.4% more than that in Case 4, and about 13% more than that in Case 1 & 2.

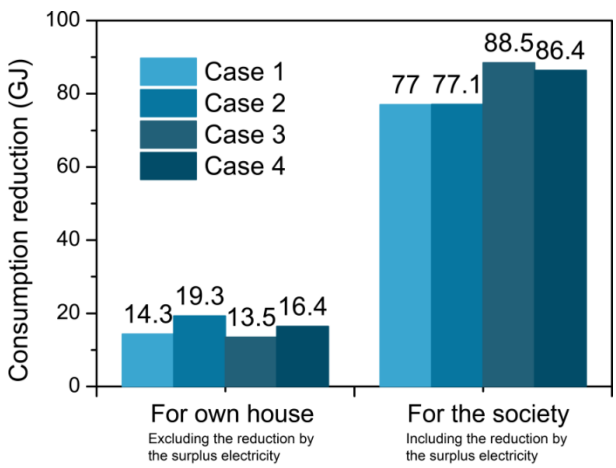

Figure 4-18 Comparison of reduction of conventional energy consumption between cases

Conclusion

In this chapter, energy conservation effects of four kinds of combinations of the devices are analyzed. Initially, a full year of electric power and hot water load is estimated according to a long term weather and municipal water database collecting the solar radiation, outdoor temperature and municipal water temperature on hourly basis. Subsequently, strategies for integrating the use of electricity and hot water by the PV, SWH and SOFC device are developed. At last, four kinds of combinations of the DER devices are proposed for the analysis of energy conservation effects.

The results shows that the combination of PV device and SWH device is the optimal one if the integrated device is not interconnected with the grid, and the total energy reduction is 19.2 GJ/year; but the combination of PV device and SOFC device is the optimal one if the integrated device is interconnected with the grid, and the total energy reduction is 88.5 GJ/year.

As the effects of energy conservation of the integrated use of DER devices are very obvious shown in this chapter, future researches should be done to make optimal use of the integrated devices, which is the topic that is the focus of Chapter 5.

CHAPTER 5

Installed Capacity Optimization

Only analyzing on the energy conservation effect of several specific combinations of the distributed energy resource (DER) devices cannot afford us with an optimal combination of optimal sized DER devices. However, on the other hand, the previous chapter provided conditions and basis for installed capacity optimization of the DER devices.

As it is known, optimization strategies are various in finding the optimal solution of a simulation, but a proper methodology can save much time for us and provide us with more accurate solutions. Thus, a proper optimization methodology, which is genetic algorithm, is adopted in this chapter.

This chapter aims to apply a genetic algorithm to optimize the installed capacities of the DER devices, aiming at reducing the conventional energy consumption and the life cycle costs, so as to achieve a pervasive methodology for selecting the optimal kinds and confirming the optimum installed capacities of the DER devices for residential use.

5.1 Global optimization strategies

5.1.1 Introduction

Global optimization is a branch of applied mathematics and numerical analysis that deals with the optimization of a function or a set of functions according to some criteria. Typically, a set of bound and more general constraints is also present, and the decision variables are optimized considering also the constraints (Wikipedia).

Approaches to access the global optimization are various and they mainly can be sorted into deterministic methods, stochastic methods and heuristics methods.

(1) Deterministic methods:

- Inner approximation
- Outer approximation
- Cutting plane methods
- Branch and bound methods
- Interval methods / Interval algebra
- Methods based on real algebraic geometry

(2) Stochastic methods:

- Simulated annealing
- Direct Monte-Carlo sampling
- Stochastic tunneling
- Parallel tempering

(3) Heuristics methods:

- Evolutionary algorithms (e.g., genetic algorithms and evolution strategies)
- Swarm-based optimization algorithms (e.g., particle swarm optimization, multi-swarm optimization and ant colony optimization)
- Memetic algorithms, combining global and local search strategies
- Reactive search optimization (i.e. integration of sub-symbolic machine learning techniques into search heuristics)
- Differential evolution
- Graduated optimization

Heuristic approaches are often applied to computationally intractable problems which consume an exponential amount of computation time to be solved exactly, as in our research.

5.1.2 Genetic algorithm

Just as the name implies, genetic algorithms (GAs) are inspired by Darwin's theory about evolution (Goldberg, 1989). GAs are categorized as global search heuristic strategies that provide methods using techniques inspired by evolutionary biology for optimization of NP-hard problems for which an exponentially number of steps is required to generate the exact or approximate answer.

The basic algorithm of GA may be described as follows:

- Choose the initial population of individuals;
- Evaluate the fitness of each individual in that population;
- Select the best-fit individuals for reproduction;
- Breed new individuals through crossover and mutation operations to give birth to offspring;
- Evaluate the individual fitness of new individuals;
- Replace least-fit population with new individuals;

- Repeat on generations until termination, i.e. time limit, sufficient fitness achieved.

From a theoretical point of view, a GA process may converge to an optimum solution if some conditions are met, with an appropriate initial parameters and termination rules, for instance, population size, generation and variable range.

Thus, in order to use GA to solve our problem, objective function, decision variables and constraint conditions should be prepared first, which is presented in following sections.

5.2 Installed capacity optimization

5.2.1 Objective function

As is known, energy and economy are two important criteria for verifying an energy system. Therefore, two objective functions are selected in this work, respectively aiming at the energy conservation and the cost economization, which are detailed as follows.

1) Aiming at energy conservation

The main stages of the energy transformed and flowing from solar via the integrated system to the load are depicted in Figure 5-1. The energy involved in this paper distributes in different quality that cannot be summed up directly, thus, conventional energy equivalent value should be used in the calculation. As what considered, the annual conventional energy consumption ($ACEC$) is selected as the objective function while aiming at energy conservation in this work, which consists of three parts including the part of the power plant, the part of the SOFC device, and the part of the sub-boiler. Notably, solar energy is not included in the calculation of the objective function in this study, since large flows of low-quality solar energy equals exponentially smaller volumes of the conventional energy, which has an exponentially higher quality (Odum, 1988). Instead, the PV device generates electricity in the way not only for direct use within the buildings but also for exporting to the grid, so that the excessive electric power from PV should be considered in the calculation, as it is a reduction of the conventional energy consumption for the society.

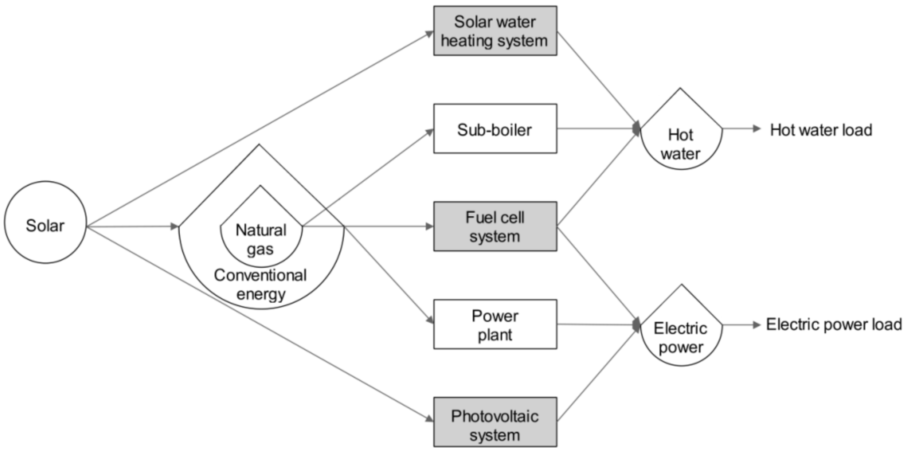

Figure 5-1 Energy transformed and flowing from solar via the DER devices to the load

With the calculation step set at one minute, $ACAE$ can be expressed as

$$ACEC(X) = \int_{t_{min}=0}^{t_{min}=365*24*60} \begin{bmatrix} P_{pp}(t_{min},X)t_{min}/\eta_{pp} + P_{fc}(t_{min},X)t_{min}/\eta_{e} \\ +\dot{L}_{s,sb}(t_{min},X)t_{min}/\eta_{sb} - P_{pv,ex}(X)t_{min}/\eta_{pp} \end{bmatrix} \quad (5.1)$$

where

$ACEC$ is the annual conventional energy consumption, J;

t_{min} is the time, minute;

η_{pp} is the efficiency of the power plant, typical values of which appears as 36.9%, according to the analyzing data (IBEC, 2009);

η_{sb} is the efficiency of the sub-boiler, typical values of which appears as 73.6%, according to the analyzing data (IBEC, 2009).

2) Aiming at cost economization

The life cycle cost is developed to be the objective function in this study while aiming at cost economization. As shown in Table 5-1, the PV module and SWH tube are assumed to have the longest life cycle among the components, so that the overall lifetime of the integrated system is set as twenty years, the same as that of the PV module and SWH tube. With interest rate and inflation rate disregarded, and maintenance cost ignored, the life cycle cost of the whole integrated energy system LCC is composed of the initial capital cost (C_i), replacement cost (C_r), monthly costs of municipal electricity and gas (C_m) and monthly profit made by excessive electricity from PV (P_m), the equation of which is expressed as

$$LCC = C_i + C_r + \sum_{t_m=1}^{t_m=20*12} [C_m(t_m) - P_m(t_m)] \tag{5.2}$$

where

LCC is the life cycle cost of the system, JPY;

C_i is the initial capital cost, JPY;

C_r is the replacement cost, JPY;

t_m is the time, month;

C_m is the monthly costs of electric power and gas, JPY;

P_m is the monthly profit by selling excess electricity, JPY.

As tabulated in Table 5-1, five main parts are considered in calculating C_i, which are the PV module, power inventor, SWH tube, SOFC unit and sub-boiler. Besides that, the other parts have very little or no relationship with the decision variables and are relatively cheap, thus, they are recognized as an overall quantitative in this work, named *other components*. Withal, the power inventor, SOFC unit and sub-boiler should be replaced at half the life cycle of the integrated system, since their lifetimes are assumed to be ten years as tabulated in Table 5-1, thus, only the cost of the power inventor, SOFC unit and sub-boiler are considered in the calculation of C_r.

Table 5-1 Costs and lifetimes of the system components

	Initial capital cost	**Replacement cost**	**Lifetime (year)**
PV module	95,000 JPY/m^2	Null	20
Power inventor	85,000 JPY/kW	85,000 JPY/kW	10
SWH tube	65,000 JPY/m^2	Null	20
SOFC unit	2,600,000 JPY/kW	360,000 JPY/kW	10
Sub-boiler	200,000 JPY	200,000 JPY	10
Other components	100,000 JPY	Null	Null

C_m and P_m can be respectively calculated according to each line chart of unit price as shown in Figure 5-2, which are provided by a local electric power company and a gas company (KEP; SG). Notably, there are two lines shown the recovering unit price of the excessive electricity from PV in the line chart of Figure 5-2(d), the higher one of which is announced by the Japanese government (IBEC, 2012), referring to the initial ten years, and the lower one is assumed for subsequent ten years.

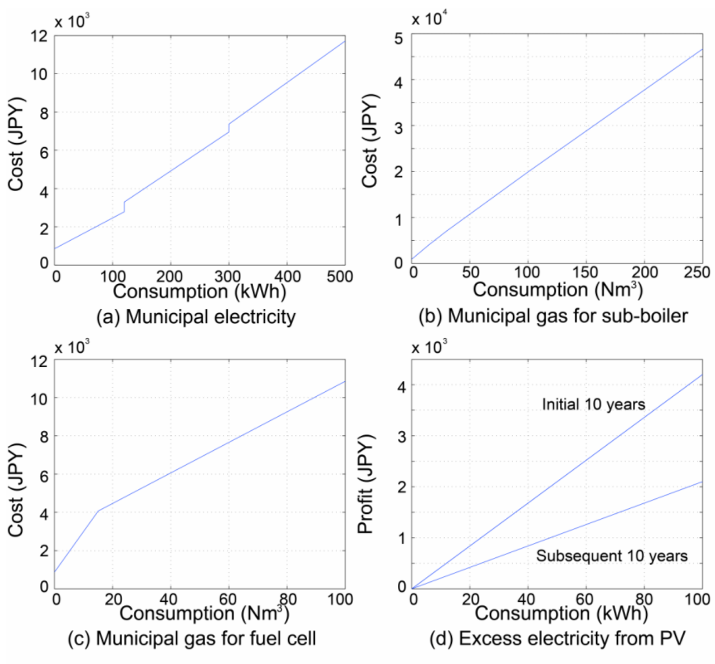

Figure 5-2 Price curves of electric power and natural gas

5.2.2 Decision variables

1) Aiming at energy conservation

Capacities of the DER devices are selected as the decision variables for the object function, which are listed in a matrix as follows

$$X = \left[N_{mo}, N_{tu}, V_{tank,sw}, V_{tank,fc}, P_r\right] \tag{5.3}$$

where X is the matrix enumerating the decision variables for energy conservation analysis.

2) Aiming at cost economization

As assumed in Table 5-1, SOFC unit should be replaced at half lifetime of the integrated DER device, and the unit price of it will reduce heavily as technology developed (ANRE, 2009). Therefore, the volume of water storage tank of replaced SOFC and rated electric power of replaced SOFC should be added to the decision variables in Equation 5.3, which is transformed as

$$X' = \left[N_{mo}, N_{tu}, V_{tank,sw}, V_{tank,fc}, P_r, V_{tank,fc,rep}, P_{r,rep}\right] \tag{5.4}$$

where

X' is the matrix enumerating the decision variables for cost economization analysis;

$V_{tank,fc,rep}$ is the volume of water storage tank of replaced SOFC, L;

$P_{r,rep}$ is the rated electric power of replaced SOFC, W.

5.2.3 Constraint conditions

The ranges of decision variables, considered according to the nature of the PV, SWH and SOFC devices, are set as the constraint conditions, which are described as follows.

The number of PV modules and the SWH tubes are linearly related, in that the total acreage of the modules plus the tubes has an upper bound limited according to the areas where it is possible to install the system components, which is expressed as

$$N_{mo}A_{mo} + N_{tu}A_{tu} \le A_{in,ub} \tag{5.5}$$

where, $A_{in,ub}$ is the upper bound limit of total area for installing PV modules and SWH tubes, m^2.

The volumes of the water tanks of SWH and SOFC have an upper bound limited by the spaces for installing, which is expressed as

$$\left[V_{tank,sw}, V_{tank,fc}, V_{tank,fc,rep}\right] \le V_{tank,ub} \tag{5.6}$$

where

$V_{tank,fc,rep}$ is the volume of the replaced water tank for fuel cell, L.

$V_{tank,ub}$ is the upper bound limit of volume of water tank, L.

The rated electric power of SOFC has an upper bound limited by the technologies of fuel cell industry, which is expressed as

$$\left[P_r, P_{r,rep}\right] \le P_{r,ub} \tag{5.7}$$

where

$P_{r,rep}$ is the rated electric power of the replaced fuel cell, W.

$P_{r,ub}$ is the upper bound limit of rated electric power of fuel cell, W.

5.3 Simulation results and discussions

Exhibited in Figure 5-3 are two plots of fitness against generations, through the genetic algorithm convergence process, refering to the results of the two objective functions respectively, as proposed previously, from which it is seen that all the best and mean fitness of individuals among an entire population converge toward a minimum value, namely the optimization solutions that are our goal.

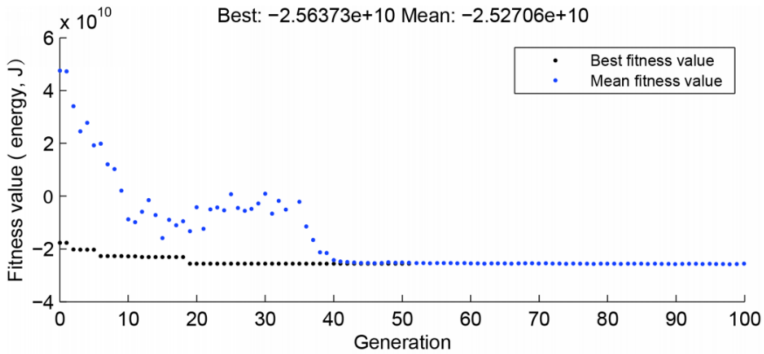

(a) Aimed at energy conservation

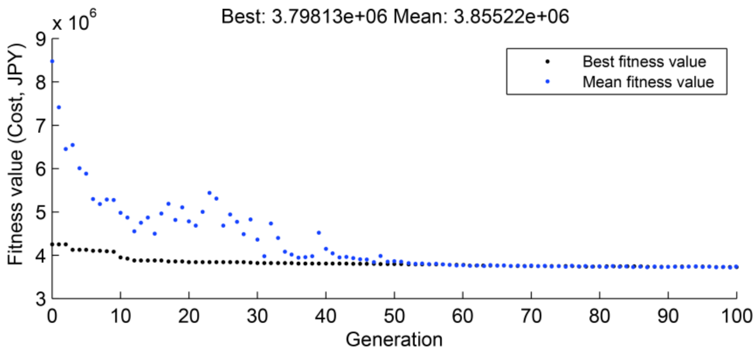

(b) Aimed at cost economization

Figure 5-3 Convergence curve of the genetic algorithm

5.3.1 Effect analysis of energy conservation

The optimum values of the decision variables aiming at energy conservation are tabulated in Table 5-2. It is better not to install any SWH device for energy conservation, leaving the total roof area for installing the PV modules, as the SOFC device can support enough hot water for the demand. Meanwhile, the SOFC device is optimized with having a capacity of 740 W and a tank volume of 200 L.

Table 5-2 Optimum values of the decision variables aiming at energy conservation

Decision Variable	Unit	Value
N_{mo}	module	30
N_{tu}	tube	0
V_{sw}	L	0
V_{fc}	L	200
P_r	W	740

With the standard calorific value of natural gas valued at 45.6 MJ/Nm^3, the annual quantity of energy distribution aimed at energy conservation using the optimized integrated system compared with not using.

It is noted that the municipal electric power consumption has been reduced 80% when using the optimized integrated system, accompanied with excess electricity of 7,714 kWh from the PV device, which equals another saving for the society of around 150%.

Although the gas consumption of the sub-boiler has had an enormous decline of more than 90%, the SOFC device consumes an extra volume of more than 2.5 times that of ordinary gas consumption, so that the total consumption of municipal gas increases 170%.

However, overall, as electric power is equivalised into conventional energy and gas is equivalised into thermal units, the result shows that there was a 25% reduction of conventional energy consumption with an annual sale quantity of 7,714 kWh of electric power from the PV device, which makes an extra reduction of conventional energy consumption for the society.

Table 5-3 and Figure 5-4 exhibit the annual quantity of energy distribution aimed at energy conservation using the optimized integrated system compared with not using.

It is noted that the municipal electric power consumption has been reduced 80% when using the optimized integrated system, accompanied with excess electricity of 7,714 kWh from the PV device, which equals another saving for the society of around 150%.

Although the gas consumption of the sub-boiler has had an enormous decline of more than 90%, the SOFC device consumes an extra volume of more than 2.5 times that of ordinary gas consumption, so that the total consumption of municipal gas increases 170%.

However, overall, as electric power is equivalised into conventional energy and gas is equivalised into thermal units, the result shows that there was a 25% reduction of conventional energy consumption with an annual sale quantity of 7,714 kWh of electric power from the PV device, which makes an extra reduction of conventional energy consumption for the society.

Table 5-3 Annual quantity of energy distribution aimed at energy conservation using the optimized integrated system compared with not using

Energy forms	Using DER devices		Without using DER device	
	SR [a]	CEEV [b]	SR [a]	CEEV [b]
Municipal Electricity	1,048 kWh	10,227 MJ [c]	5,345 kWh	52,168 MJ [c]
Municipal gas (sub-boiler)	25 Nm^3 [d]	1,139 MJ	323 Nm^3 [d]	14,726 MJ
Municipal gas (fuel cell)	852 Nm^3 [d]	38,847 MJ	——	——
Excess electricity (PV)[e]	-7,714 kWh	-75,291 MJ [c]	——	——
Total		-25,637 MJ		66,894 MJ

a Abbreviation of *Simulation Result*

b Abbreviation of *Conventional Energy Equivalent Value*

c The efficiency of power plant is valued 36.9% (IBEC, 2009)

d The standard calorific value of natural gas is valued 45.6MJ/Nm^3 (ANRE, 2007)

e Negative numbers represent the part is considered as reduction of energy consumption

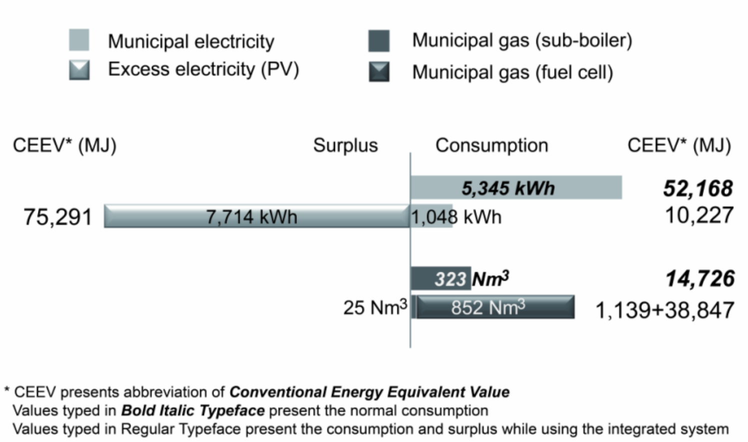

Figure 5-4 Annual quantity of energy distribution aimed at energy conservation using the optimized integrated system compared with not using

5.3.2 Effect analysis of cost economization

The optimum values of the decision variables aiming at cost economization are also tabulated in Table 5-4. It is more economical not to install the SOFC device initially, when its unit price is extremely high. However, when the price of the unit goes down with improving technologies of the fuel cell industry, the SOFC device becomes economical for use with optimum capacity of 630 W and tank volume of 170 L at half the overall lifetime. Simultaneously, the roof area ratio for installing the PV modules and SWH tubes are optimized as 14:1, respectively with 28 modules and 8 tubes.

Table 5-4 Optimum values of the decision variables aiming at cost economization

Decision Variable	Unit	Value
N_{mo}	module	28
N_{tu}	tube	8
V_{sw}	L	150
V_{fc}	L	0
P_r	W	0
$V_{fc,rep}$	L	170
$P_{r,rep}$	W	630

Tabulated in Table 5-5 and shown in Figure 5-5 are the life cycle costs and profits aimed at cost economization using the optimized integrated system. It can be seen that the profit made by selling the excess electricity from the PV in the subsequent ten years are 60% of that in the initial ten years, mostly due to the unit price which is assumed to be reduced 50% in the subsequent ten years, and another 10% due to the installation of SOFC device, the electric power generated by which makes more electricity from the PV device which can be sold.

Overall, although the initial capital cost is high, with heavy reduction on the energy cost and the profit made by selling the excess electricity from the PV device, the optimum total life cycle cost is calculated to be 3,798,200 JPY, which is 16% reducing compared with not installing the integrated system.

Table 5-5 Life cycle cost and profits aimed at cost economization using the optimized integrated system

Cost and profit items	Initial ten years cost (JPY)	Subsequent ten years cost (JPY)
Initial capital cost	3,979,100	——
Replacement cost	——	890,900
Energy cost	1,465,200	1,449,400
Excess electricity profit	-2,488,300*	-1,498,100*
Life cycle cost	3,798,200	

* Negative numbers represent that excess electricity exported from PV makes profit

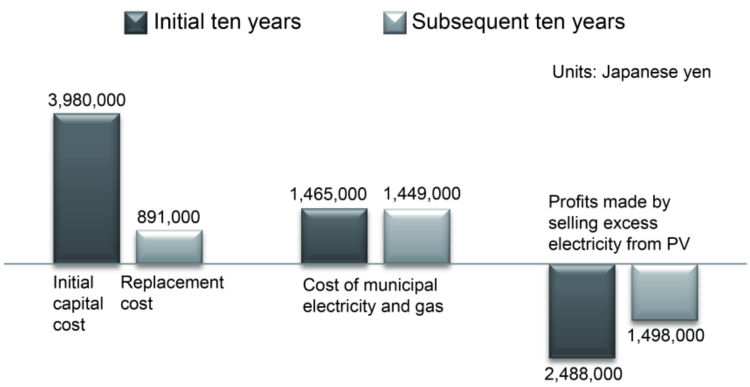

Figure 5-5 Life cycle costs and profits aimed at cost economization using the optimized integrated system

Table 5-6 and Figure 5-6 presents the annual quantity of energy distribution aimed at cost economization using the optimized integrated system.

It is noted that the municipal electricity consumption has been reduced for more than 25% in the initial ten years, and around 75% in the subsequent ten years, accompanied respectively with excess electricity of 5,925 and 7,134 kWh from the PV device, which separately equals additional reduction of 110% and 130%.

In the initial ten years, the consumption of the sub-boiler has had a decline of 35%, and in the subsequent ten years, the decline increased to 95%. However, in the subsequent ten years, the SOFC consumed an extra volume of gas, causing the total consumption of municipal gas in the subsequent ten years to increase 140%.

Overall, as electric power was equivalised into conventional energy and gas was equivalised into thermal units, in the initial ten years, there was a 30% reduction of conventional energy consumption with an annual selling quantiy of 5,925 kWh of electric power from the PV device, which makes extra saving of conventional energy for the society. In the subsequent ten years, the reduction is 25% with an annual selling quantity of 7,134 kWh of electric power from the PV device, which also makes extra saving of conventional energy for the society.

Table 5-6 Annual quantity of energy distribution aimed at cost economization using the optimized integrated system

Energy forms	Initial ten years		Subsequent ten years	
	SR [a]	CEEV [b]	SR [a]	CEEV [b]
Municipal Electricity	3,904 kWh	38,102 MJ [c]	1,367 kWh	13,342 MJ [c]
Municipal gas (sub-boiler)	210 Nm^3 [d]	9,593 MJ	14 Nm^3 [d]	657 MJ
Municipal gas (fuel cell)	——	——	760 Nm^3 [d]	34,669 MJ
Excess electricity (PV)[e]	-5,925 kWh	-57,824 MJ [c]	-7,134 kWh	-69,627 MJ [c]
Total		-10,129 MJ		-20,959 MJ

[a] Abbreviation of *Simulation Result*

[b] Abbreviation of *Conventional Energy Equivalent Value*

[c] The efficiency of power plant is valued 36.9% (IBEC, 2009)

[d] The standard calorific value of natural gas is valued 45.6MJ/Nm^3 (ANRE, 2007)

[e] Negative numbers represent the part is considered as reduction of energy consumption

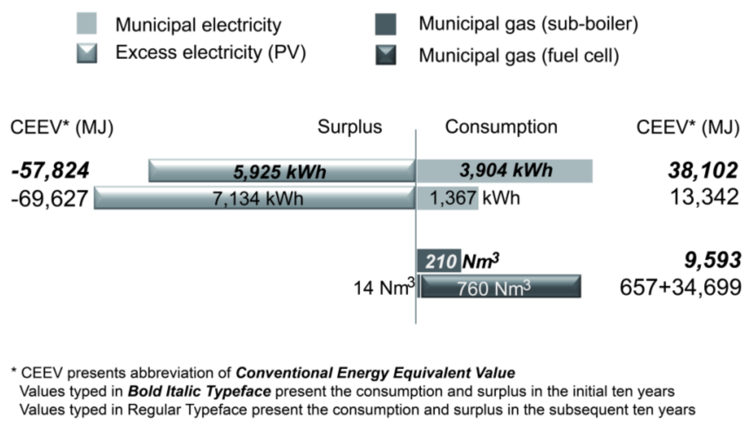

Figure 5-6 Annual quantity of energy distribution aimed at cost economization using the optimized integrated system

Conclusion

In this chapter, with system models developed separately as well as the integration strategy proposed, a capacity optimization model is built in consideration of conventional energy consumption and life cycle costs. The full year of electric power and hot water load is estimated as the same in Chapter 4. On top of that, a genetic algorithm is applied to the solutions of the capacity optimization of the integrated DER device.

The optimum installed capacities of the DER devices are calculated separately on the basis of energy conservation and cost economization performance. In case we aim at energy conservation, the optimum combination of DER devices is simulated consisting of a photovoltaic device and a fuel cell device; in case we aim at cost economization, the optimum combinatorial components change to a photovoltaic device and a solar water heating device, and the fuel cell device is only economic to be used with its unit price decreased in the future.

The methodology that we propose is validated to reduce considerable quantity of residential energy consumption and expense. In case we aim at energy conservation, about 25% of conventional energy consumption can be reduced, meanwhile another 7,714 kWh of excess electric power can be obtained; in case we aim at cost economization, about 16% of the total life cycle cost can be saved.

The procedure allows us to add more DER device models by adding new simulators with capacity variables of the selected adding devices. Also, it is a valuable tool to determine optimum capacities of the DER devices for various energy loads with the fitness function established beforehand.

In summary, the integration and optimization methodology proposed in this chapter can be applied to help the residents reform their existing DER devices with actual energy demands, and also help the designers in designing the hardware of the DER devices on the basis of overall system performance with load profiles estimated by investigation and analysis.

CHAPTER 6

Conclusion

This research aims to propose a method for installed capacity optimization of the integrated DER devices using operation strategies for the generation of electrical and hot water in order to reduce residential energy consumption and expense.

Notably, this research proposes two novel objective functions of a genetic algorithm, separately aiming at energy and cost, for confirming the installed capacities of the integrated DER devices.

Furthermore, cases for confirming the optimal installed capacities of a typical building in Fukuoka City of Japan are studied based on the above mentioned objective functions.

6.1 Synopsis

This dissertation consists of six chapters. The chapter outlines are described as follows:

In Chapter 1, general background of today's situation of dramatically rising energy consumption is revealed. The previous researches on combination and optimization of the DER devices are presented, the objectives of this research are given, and the structure of this dissertation is illustrated.

In Chapter 2, in order to show how the Chinese kang, which is a traditional heating device using surplus exhaust heat from cooking, use energy in an efficient way and improve indoor thermal environment, thermal processes of building with the kang are described, the mathematical models are built, and results of the field measurements and simulations are analyzed. Through the works of this chapter, the success and persistence of the kang inspires us with this kind of idea as using one kind of energy in two ways to make efficient use of energy in researching on the modern energy devices.

In Chapter 3, dynamic models of photovoltaic device, solar water heating device and fuel cell device as three kinds of DER devices are built on the basis of their working principles. Especially, the dynamic model of photovoltaic device with effects of ambient temperature and that of solar water heating device with effects of the heat loss from the collector are originally developed. The electric power and/or hot water generation capacity and efficiency of these devices are analyzed, and each device respectively demonstrates a relatively high efficiency in generating electric power and/or hot water for residential use. This chapter provides the mathematical models for integration of the devices in the next chapter.

In Chapter 4, the models of the DER device, which are built in the previous chapter, are integrated as an overall system with the operation strategies for the generation of electric power and hot water. The simulation program of the overall system with the DER devices installed to a typical residential building located in Fukuoka City is originally developed. The standard weather data, the municipal water temperature data, the electric power and hot water loads calculated by other existing simulation programs are collected as the input data of the system simulation program. Finally, four patterns of combination of the selected DER devices are respectively analyzed. The reduction effects of energy consumption are compared, and the reasonable results validate the integration method of the DER devices. As a result of the case study, the combination of PV device and SWH device is the optimal one if the integrated device is not interconnected with the grid, and the total energy reduction is 19.2 GJ/year; but the combination of PV device and SOFC device is the optimal one if the integrated device is interconnected with the grid, and the total energy reduction is 88.5 GJ/year.

In Chapter 5, a genetic algorithm is applied to optimize the installed capacities of the DER devices. As a result, for the cases selected in this research, the optimum combination of the DER devices for maximum energy reduction includes 30 modules of photovoltaic panel, a fuel cell with the capacity of 740 W and the hot water tank volume of 200 L. In this case, for one year, about 57% of conventional energy consumption can be directly reduced and 7,714 kWh of surplus amount of electric power can be obtained. The optimum combination for maximum cost economization changes to 28 modules of the photovoltaic panel and a solar thermal collector with 8 tubes with the hot water tank volume of 150 L for the initial ten years. In the subsequent ten years, a fuel cell with the capacity of 630 W and the hot water tank volume of 170 L will be additionally installed to the integrated system because the unit price of it would be highly decreased at that time. In this case, as the life time is assumed as 20 years, about 16% of the life cycle cost can be saved.

In Chapter 6, summary of this dissertation is given, and scope for further work is described. The methodology proposed in this dissertation is validated to reduce considerable quantity of residential energy consumption and expenses. The results of this research can help residents reform their existing DER devices, assist developers to equip the newly completed buildings with optimal DER devices, and also support designers in designing the hardware of newer types of DER devices.

6.2 Prospects

As written through the previous chapters, this research has proposed a methodology for us to select proper and DER devices and confirm their installed capacities. However, the methodology is still not so convenient for the normal residents to master, and this study only provided one case of a standard detached house in Fukuoka, Japan. Thus, if more cases referring many kinds of building types and climate zones are researched, different optimal combinations can be analyzed aiming at each case. These combinations can be classified into groups referring different building types and climate zones, and the residents can choose the DER devices conveniently according to their own locations and building types.

And for the models built in this study, indoor thermal environment was adjusted only by the air conditioner. Actually, the radiant floor heating system is widely used recently, and it is recognized more efficient than baseboard heating and usually more efficient than forced-air heating, because it eliminates duct losses, and also it doesn't distribute allergens as forced air systems do. Therefore, the radiant floor heating system is better to be nested into the existed thermal environment simulation program, for the research.

Furthermore, it is significant to synthesize the muti-objective functions as one objective function, so as to achieve an optimal combination of the DER devices and determine an optimal installed capacities of them for every aspect, i.e. the energy conservation, the cost economization, the CO_2 reduction, etc.

Finally, as the DER devices are various and being improved every day, more kinds of proper and high-efficient DER device models can be added to the procedure made in this study by adding new simulators with capacity variables of the selected adding devices.

References

AIJ. (2005). Extended amedas weather data 1981-2000. In (1st ed.). Kagoshima: Kagoshima TLO Co. Ltd.

Andreadis, G., Roaf, S., & Mallick, T. (2012). Tackling fuel poverty with building-integrated solar technologies: The case of the city of dundee in scotland. *Energy and Buildings*.

ANRE. (2007). Investigation results and revision values of the standard calorific applies after year 2005. from http://www.enecho.meti.go.jp/info/statistics/jukyu/resource/pdf/070601.pdf

ANRE. (2009). Current status and prospect of fuel cell technology. Retrieved April 1, 2013, from http://www.meti.go.jp/committee/materials2/downloadfiles/g90225a08j.pdf

ANRE. (2010). Energy in japan, 2010. Retrieved April 1, 2013, from http://www.enecho.meti.go.jp/topics/energy-in-japan/english2010.pdf

Ashok, S. (2007). Optimised model for community-based hybrid energy system. *Renewable energy, 32*(7), 1155-1164.

Ayompe, L., Duffy, A., Mc Keever, M., Conlon, M., & McCormack, S. (2011). Comparative field performance study of flat plate and heat pipe evacuated tube collectors (etcs) for domestic water heating systems in a temperate climate. *Energy, 36*(5), 3370-3378.

BERC. (2008). *China annual report on building energy efficiency (2008)*: China Building Industry Press.

Carvalho, M., Lozano, M. A., & Serra, L. M. (2012). Multicriteria synthesis of trigeneration systems considering economic and environmental aspects. *Applied Energy,* *91*(1), 245-254.

Chen, H. C. (2013). Optimum capacity determination of stand-alone integrated generation system considering cost and reliability. *Applied Energy, 103*, 115-164.

Chen, Q. (1988). *Basis of building thermal physics*. Xi'an: Xi'an Jiaotong University Press.

Chen, Y.-H., Lu, S.-Y., Chang, Y.-R., Lee, T.-T., & Hu, M.-C. (2012). Economic analysis and optimal energy management models for microgrid systems: A case study in taiwan. *Applied Energy*.

Chenni, R., Makhlouf, M., Kerbache, T., & Bouzid, A. (2007). A detailed modeling method for photovoltaic cells. *Energy, 32*, 1724-1730.

DECEE. Renewable sources and efficient electrical systems. Retrieved April 1, 2013, from http://ecee.colorado.edu/~ecen2060/

DOE. Energy efficiency & renewable energy. Retrieved April 1, 2013, from http://www.eere.energy.gov/basics/renewable_energy/pv_cell_conversion_efficiency.html

Duffie, J. A., & Beckman, W. A. (1991). Solar engineering of thermal process. In (2nd ed., pp. 382-426). New York: John Wiley & Sons, Inc.

EEGNRA. (2007). *Summary report of energy and environment group of northern rural area in tsinghua university in 2006*. Tsinghua University, Beijing.

EIA. (2011). International energy outlook 2011. from http://www.eia.gov/forecasts/ieo/index.cfm

Ekren, O., & Ekren, B. Y. (2010). Size optimization of a pv/wind hybrid energy conversion system with battery storage using simulated annealing. *Applied Energy, 87*(2), 592-598.

FCWB.WPD. (2004). *Annual report of water testing: Collection 29*.

Ganguly, A., Misra, D., & Ghosh, S. (2010). Modeling and analysis of solar photovoltaic-electrolyzer-fuel cell hybrid power system integrated with a floriculture greenhouse. *Energy and Buildings, 42*(11), 2036-2043.

GAQSIQ, MEP, & MOH. (2002). Gb/t18883-2002 indoor air quality standard, p.R.China [s]. Beijing.

Goldberg, D. E. (1989). Genetic algorithms in search, optimization, and machine learning.

Groscurth, H.-M., Bruckner, T., & Kümmel, R. (1993). Energy, cost, and carbon dioxide optimization of disaggregated, regional energy-supply systems. *Energy, 18*(12), 1187-1205.

Hamdy, M., Hasan, A., & Siren, K. (2012). A multi-stage optimization method for cost-optimal and nearly-zero-energy building solutions in line with the epbd-recast 2010. *Energy and Buildings*.

Holman, J. (1997). Heat transfer: McGraw-Hill, New York.

IBEC. (2009). *Manual of energy consumption calculation methods for standards of judgment for residential construction clients* (1st ed.). Tokyo: IBEC.

IBEC. (2012). *Design guideline for autonomous housing in quasi-cold regions: Reducing 50% energy consumption by housing design* (1st ed.). Tokyo: IBEC.

John, H., Lienhard, I., John, H., & Lienhard, V. (2008). A heat transfer textbook. *Phlogiston Press, Cambridge*.

Kayo, G., & Ooka, R. (2010). Building energy system optimizations with utilization of waste heat from cogenerations by means of genetic algorithm. *Energy and Buildings, 42*(7), 985-991.

KEP. Retrieved April 1, 2013, from http://www.kyuden.co.jp/rate_mein-menu_index.html

Khatib, T., Mohamed, A., & Sopian, K. (2012). Optimization of a pv/wind micro-grid for rural housing electrification using a hybrid iterative/genetic algorithm: Case study of kuala terengganu, malaysia. *Energy and Buildings, 47*, 321-331.

Khatib, T., Mohamed, A., Sopian, K., & Mahmoud, M. (2011). Optimal sizing of building integrated hybrid pv/diesel generator system for zero load rejection for malaysia. *Energy and Buildings, 43*(12), 3430-3435.

Lane, T. (2004). *Solar hot water systems: Lessons learned 1977 to today* (29th ed.). Gainesville, Florida: Energy Conservation Services.

Li, C.-H., Zhu, X.-J., Cao, G.-Y., Sui, S., & Hu, M.-R. (2009). Dynamic modeling and sizing optimization of stand-alone photovoltaic power systems using integrated energy storage technology. *Renewable Energy, 34*, 815-826.

Li, H., Nalim, R., & Haldi, P.-A. (2006). Thermal-economic optimization of a distributed multi-generation energy system—a case study of beijing. *Applied Thermal*

Engineering, 26(7), 709-719.

Li, J., Bai, J., & Ralph, O. (1998). Assessment of biomass resource availability in china. *China Environmental Science Press, Beijing, China*, 123-270.

Li, Y., Sun, H., & Yang, X. (2006). *Investigation report of the situation of ecological utilization of energy in rural areas in north china*. Hong Kong University, Hongkong.

Liu, J. (1998). *Theory of thermal process of the attached sunspace of yaodong* (Doctoral dissertation ed.). Chongqing: Chongqing University of Architecture.

Lozano, M. A., Ramos, J. C., Carvalho, M., & Serra, L. M. (2009). Structure optimization of energy supply systems in tertiary sector buildings. *Energy and Buildings, 41*(10), 1063-1075.

NHK. (2010). *Data book: Report of national life time 2010*. Tokyo: NHK Publishing Inc. .

NI. from http://www.ni.com/white-paper/7230/en

Odum, H. T. (1988). Self-organization, transformity, and information. *Science, 242*, 1132-1139.

Ozaki, A., Watanabe, T., Takase, S., & Iwaoka, S. (2001). Simulation software to describe the thermal environment of residential buildings based on detailed physical models.

Ren, H., & Gao, W. (2010a). Economic and environmental evaluation of micro chp systems with different operating modes for residential buildings in japan. *Energy and Buildings, 42*(6), 853-861.

Ren, H., & Gao, W. (2010b). A milp model for integrated plan and evaluation of distributed energy systems. *applied energy, 87*(3), 1001-1014.

Ren, H., Gao, W., & Ruan, Y. (2008). Optimal sizing for residential chp system. *Applied Thermal Engineering, 28*(5), 514-523.

Ren, H., Zhou, W., Nakagami, K. i., Gao, W., & Wu, Q. (2010). Multi-objective optimization for the operation of distributed energy systems considering economic and environmental aspects. *Applied Energy, 87*(12), 3642-3651.

Rubio-Maya, C., Uche-Marcuello, J., Martínez-Gracia, A., & Bayod-Rújula, A. A. (2011). Design optimization of a polygeneration plant fuelled by natural gas and renewable energy sources. *Applied energy, 88*(2), 449-457.

SG. Retrieved April 1, 2013, from http://www.saibugas.co.jp/home/rates/price_list/index.htm

SHASC.CESR. (2000). *Auto program of life schedule: Schedule ver.2.0*.

Taghipour Rezvan, A., Shams Gharneh, N., & Gharenpetian, G. B. (2013). Optimization of distributed generation capacities in buildings under uncertainty in load demand. *Energy and buildings, 57*, 58-64.

Wikipedia. Global optimization. Retrieved April 1, 2013, from http://en.wikipedia.org/wiki/Global_optimization

Yamaguchi, Y., Akai, K., Shen, J., Fujimura, N., Shimoda, Y., & Saijo, T. (2012). Prediction of photovoltaic and solar water heater diffusion and evaluation of promotion policies on the basis of consumers' choices. *Applied Energy*.

Yan, Q., & Zhao, Q. (1986). *Building thermal process* (1 ed.). Beijing: China Building Industry Press.

Yang, H., Zhou, W., Lu, L., & Fang, Z. (2008). Optimal sizing method for stand-alone hybrid solar–wind system with lpsp technology by using genetic algorithm. *Solar energy, 82*(4), 354-367.

Yang, X., & Jiang, Y. (2008). *Energy and environment in chinese rural housing: Road to sustainability.* Paper presented at the Proceedings of the First International Conference on Building Energy and Environment, China.

Appendix

I. Programs for Chapter 2

1 Main program

```
function T=test_k(n)
%-------------------------confirmation of maximum value of u---------------
u_max=min([size(X,2) size(Y,2) size(Z,2)]);
%-------------------------assignment for ti t6 ta-------------------------
ti=zeros(u_max-1+n,1);t6=zeros(u_max-1+n,1);ta=zeros(u_max-1+n,1);
ti(u_max:end)=ti(1:u_max-1);
t6(u_max:end)=t6(1:u_max-1);
ta(u_max:end)=ta(1:u_max-1);
%-------------------------p2 p3----------------------------------------
p2=alpha_rk*(F(6)-F_AUST)+X(6,1)*F(6);
p3=-Y(6,1)*F(6)-Y(7,1)*F(7);
%-------------------------w1 w2 w3-------------------------------------
w1=alpha_6;
w2=-alpha_6-Z(6,1);
w3=Y(6,1);
%-------------------------f1 f2 f3-------------------------------------
f1=-Y(7,1)*F(7);
```

```
f2=-Y(6,1)*F(6);
f3=V_a*c_p*Rou_a+2*m*c_p+(Z(6,1)*F(6)+Z(7,1)*F(7)+Z(8,1)*F(8)+Z(9,1)*F(9));
%-------------------------Initialization of ti0 ta0----------------------
ti0=ti(u_max-1);
ta0=ta(u_max-1);
%-------------------------Initialization of A B---------------------------
A=ones(3,3);
B=ones(3,1);
%-------------------------cycling--------------------------------------
for tao=1:1:n
%-------------------------p1-----------------------------------------
p1(tao)=V_i*c_p*Rou_i+(Z(1,1)*F(1)+Z(2,1)*F(2)+Z(3,1)*F(3)+Z(4,1)*F(4)+X(7,1)*F(7))
+F(5)*K5+[N(tao)+G(tao)]*c_p*Rou_e-alpha_rk*(F(6)-F_AUST);
%-------------------------p4-----------------------------------------
s1=0;s2=0;s3=0;s4=0;s5=0;s6=0;s7=0;s8=0;s9=0;s10=0;s11=0;
u=1:u_max;
s1=sum((Y(1,u)*F(1)+Y(4,u)*F(4))'.*td(tao-u+u_max));
s2=sum(Y(3,u)'*F(3).*tz(tao-u+u_max));
u1=2:u_max;
s3=sum((Y(6,u1)*F(6)+Y(7,u1)*F(7))'.*ta(tao-u1+u_max));
s4=sum((Z(1,u1)*F(1)+Z(2,u1)*F(2)+Z(3,u1)*F(3)+Z(4,u1)*F(4)+X(7,u1)*F(7))'.*ti(tao-
u1+u_max));
s5=sum(X(6,u1)'*F(6).*t6(tao-u1+u_max));
s6=sum(Y(6,u1)'.*ta(tao-u1+u_max));
s7=sum(X(6,u1)'.*t6(tao-u1+u_max));
p4(tao)=V_i*c_p*Rou_i*ti(tao+u_max-1)+s1+s2+s3-s4+K5*te(tao)*F(5)-s5+[N(tao)+G(ta
o)]*c_p*Rou_e*te(tao)+QF(tao);
%-------------------------w4-----------------------------------------
w4(tao)=-s6+s7;
%-------------------------f4-----------------------------------------
s10=sum(Y(9,u)*tz(tao-u+u_max)*F(9));
```

```
s8=sum(Y(6,u1)'.*t6(tao-u1+u_max)*F(6));
s9=sum(Y(7,u1)'.*ti(tao-u1+u_max)*F(7));
s11=sum((Z(6,u1)*F(6)+Z(7,u1)*F(7)+Z(8,u1)*F(8)+Z(9,u1)*F(9))'.*ta(tao-u1+u_max));
f4(tao)=V_a*c_p*Rou_a*ta(tao+u_max-1)+s8+s9+s10-s11+m*c_p*(tf(tao)+te(tao));
%--------------------------Solution-------------------------------------
A=[p1(tao) p2 p3;w1 w2 w3;f1 f2 f3];
B=[p4(tao) w4(tao) f4(tao)]';
C=A\B;
ti(tao+u_max-1)=C(1);
t6(tao+u_max-1)=C(2);
ta(tao+u_max-1)=C(3);
%--------------------------Update ti0 ta0---------------------------------
ti0=ti(tao+u_max-1);
ta0=ta(tao+u_max-1);
end
T1=[ti t6 ta];
T=T1(u_max:n+u_max-1,:);
```

2 Subroutine: Reaction coefficient

1) Main

```
function [K root_s XYZ] = thermal_coef(n, Re, Ri, lambda, rou, c, d, num)
syms s real
[Bs As Cs Ds] = get_root_s(Ri, Re, lambda, rou, c, d, n, s);
dt = 0.0001;
dt_Bs = diff(Bs, s);
end_point = -40;
s = end_point:dt:-1e-10;
x = real( subs(Bs, s) );
min_num = 0.002;
[row vol] = find(abs(x) < min_num);
```

```
root_s0 = end_point + (vol - 1) * dt;
for k = 1:length(root_s0)
    temp(k) = fzero(@(ss) get_root_s(Ri, Re, lambda, rou, c, d, n, ss), root_s0(k) );
end
root_s = unique(fix(temp * 1e8) / 1e8);
s = root_s;
K = 1 / ( Re + Ri + sum(d ./ lambda) );
tao = 1;
dB = real(subs(dt_Bs, s));
Aai = real(subs(As, s));
Dai = real(subs(Ds, s));
alf = root_s;
bi = 1 ./ (alf.^2 .* dB);
ai = Aai ./ (alf.^2 .* dB);
ci = Dai ./ (alf.^2 .* dB);
for k =0:num
    if k == 0
        Y(1) = K - bi * (1 - exp(alf * tao))' / tao;
        X(1) = K - ai * (1 - exp(alf * tao))' / tao;
        Z(1) = K - ci * (1 - exp(alf * tao))' / tao;
    else
        temp = (1 - exp(alf * tao)).^2 .* exp(alf * tao * (k-1)) / tao;
        Y(k+1) = sum( bi .*    temp);
        Z(k+1) = sum( ci .*    temp);
        X(k+1) = sum( ai .*    temp);
    end
end
XYZ = [X' Y' Z'];
root_s = root_s';
```

2) Roots of a polynomial B(s)

```
function [Bs As Cs Ds] = get_root_s(Ri, Re, lambda, rou, c, d, n, s)
for k =1:1:n
    a(k)= 3600*lambda(k) / (rou(k)*c(k));
end
T=[1 0;0 1];
for k = 1:1:n
    temp1 = sqrt( s / a(k) ) * d(k);
    temp2 = lambda(k) * sqrt(s/a(k));
    An=cosh( temp1 );
    Bn=sinh( temp1 ) / (temp2);
    Cn = temp2 * sinh( temp1 );
    Dn=An;
    t = [An -Bn;-Cn Dn];
    T=T*t;
end
root_s = [1 -Ri;0 1]*T*[1 -Re;0 1];
%--------------------------Output----------------------------------------
As = root_s(1,1);
Bs = -root_s(1,2);
Cs = -root_s(2,1);
Ds = root_s(2,2);
```

II. Programs for Chapters 3, 4 & 5

1 Subroutine 1: Effective solar radiation

```
function Is=solar(dip)
global SIDN SIdH day hour
waz=0;
lat=33.58*pi/180;
long=130.37667*pi/180;
longs=139.73*pi/180;
IDN=SIDN(day,hour);
IdH=SIdH(day,hour);
sn=day;
w=2*sn*pi/360;
Ed=23.45*sin((360*(284+sn)/365)*pi/180)*pi/180;
td=-0.0002786409+0.1227715*cos(w+1.498311)-0.1654575*cos(2*w-1.261546)-0.00535
3830*cos(3*w-1.157100);
Hs=hour;
omega=(Hs+(long-longs)/15+td/60-12)*15*pi/180;
h=asin(sin(lat)*sin(Ed)+cos(lat)*cos(Ed)*cos(omega));
saz=acos((sin(h)*sin(lat)-sin(Ed))/(cos(h)*cos(lat)));
if omega>=0
    saz=saz;
else saz=-saz;
end
cosi=cos(dip)*sin(h)+sin(dip)*cos(h)*cos(saz-waz);
if cosi>=0
    cosi=cosi;
```

```
else
    cosi=0;
end
ID=IDN*cosi;
Id=IdH*cos(dip/2)^2;
Is=ID+Id;
```

2 Subroutine 2: Power output from PV module

1) Equations solution

```
G=csvread('IS.csv');
T=csvread('TA.csv');
T=T+273.15*ones(365,24);
P_MAX=zeros(365,24);
for m=1:365
    for n=1:24
        g=G(m,n);
        t=T(m,n);
        if g~=0
        SimOut=sim('pv_array.mdl');
% 'pv_array.mdl' is shown in Figure I and Figure II
        P_max=max(PV.signals.values(:,1));
        P_MAX(m,n)=P_max*N;
        end
    end
end
csvwrite('P_MAX.csv',P_MAX)
```

2) Equations establishment

```
Ns=round(Voc/0.61);
Gref=1000;
```

```
Tref=298.15;
Ct=2.3e-3;
k=1.381e-23;
e=1.602e-19;
A=1.3*Ns;
Vt=A*k*Tref/e;
Rp=100*Voc/Isc;
Vdm=Voc;
for i=1:10
    Idm=Isc-Ir-Vdm/Rp;
    Io=(Isc-Voc/Rp)/(exp(Voc/Vt)-1);
    Vdm=Vt*log(Idm/Io+1);
    Rs=(Vdm-Vr)/Ir;
    Rd=(Vr/Ir - Rs)*Rp/(Rp-Vr/Ir+Rs);
    Idm=Vt/Rd;
    Rp=Vdm/(Isc-Ir-Idm);
end
```

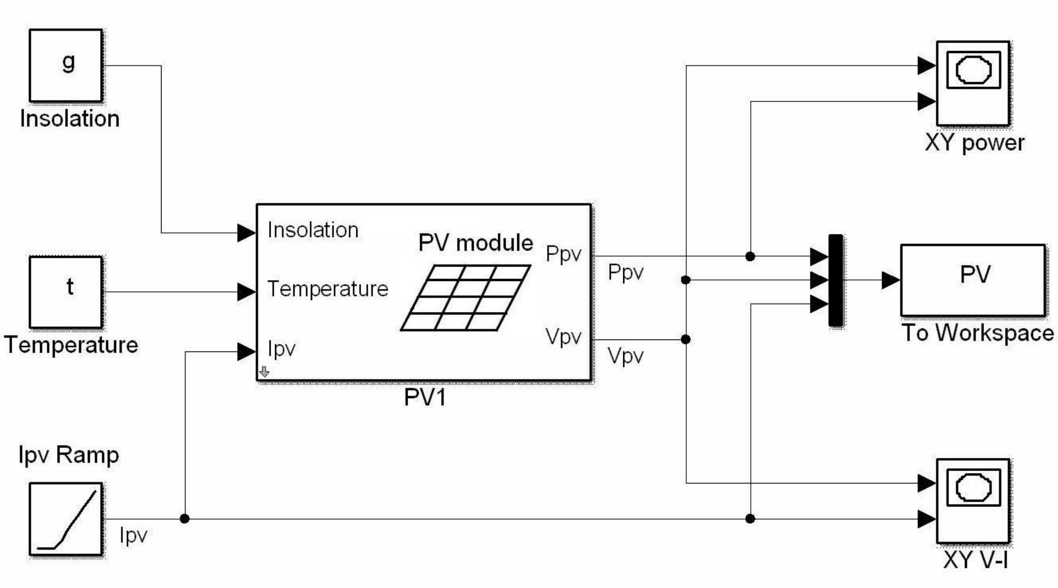

Figure I Simulation model of the PV module ('pv_array.mdl')

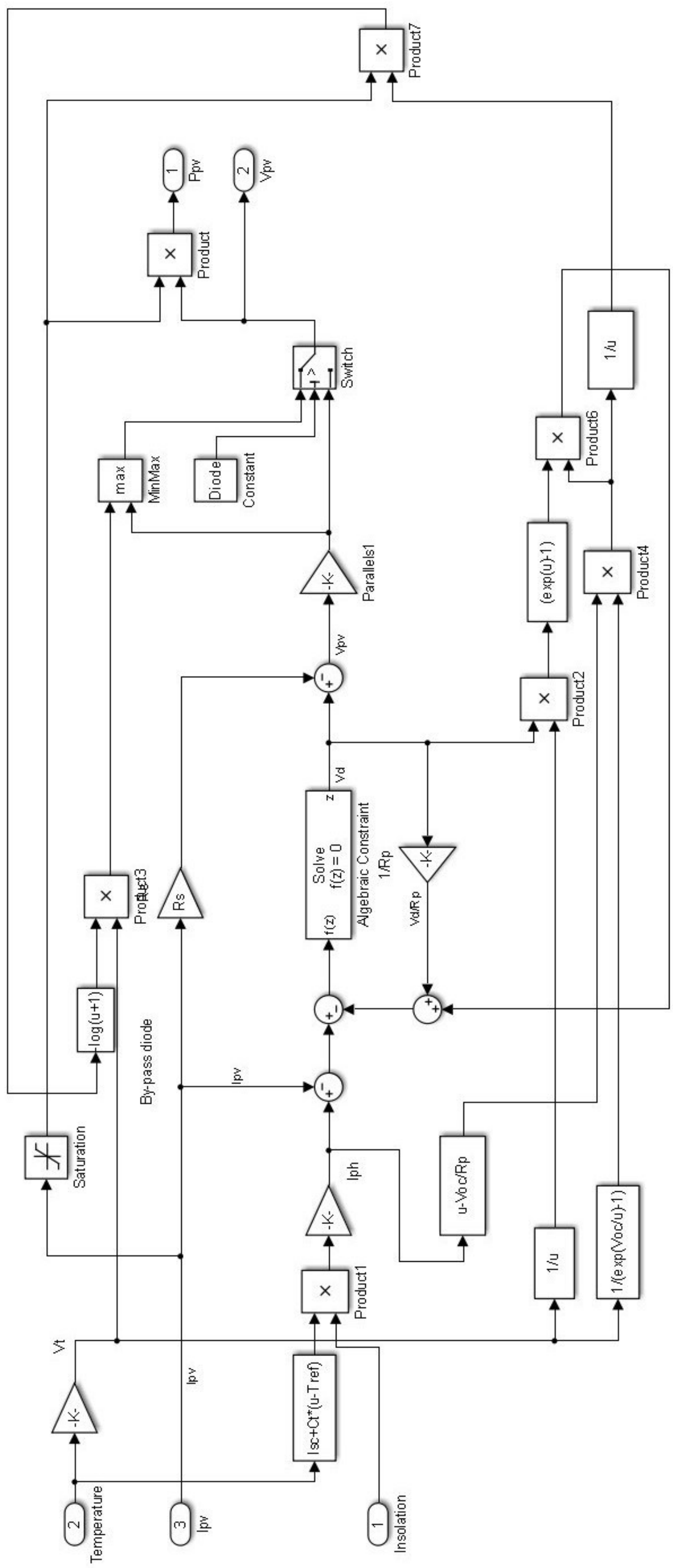

Figure II Look under mask of the simulation model of the PV module

3 Subroutine 3: Heat loss coefficient

1) Equations solution

```
global Eg Bo Ta Tsky Ep Fpg Ap Ag hga Tp
TA=csvread('TA.csv');
WIND=csvread('WIND.csv');
UT=zeros(365,24);
for m=1:365
    for n=1:24
        v=WIND(m,n);
        hga=5.62+3.9*v;
        Ta=TA(m,n)+273.15;
        X=fsolve('loss',[5,8,300,1.5],optimset('Display','off'));
        Ut=X(4)
        UT(m,n)=Ut;
    end
end
csvwrite('UT.csv',UT)
```

2) Equations establishment

```
function Z=loss(X)
global Eg Bo Ta Tsky Ep Fpg Ap Ag hga Tp
hrga=X(1);
hrpg=X(2);
Tg=X(3);
Ut=X(4);
Z(1)=hrga-Eg*Bo*(Tg^4-Tsky^4)/(Tg-Ta);
Z(2)=hrpg-(2*(Bo*(Tp^4-Tg^4)/(Tp-Tg)))/((1-Ep)/Ep+1/Fpg+(1-Eg)*2*Ap/(Eg*Ag));
Z(3)=Ut-(1/hrpg+1/(hga+hrga))^-1;
Z(4)=Ut*(Tp-Ta)-hrpg*(Tp-Tg);
```

4 Subroutine 4: Operation strategies for energy supply

1) Integrated electric power supply

```
%--------------------------Calculate P_FC----------------------------------
PL=csvread('PL.csv');
Pl=PL(n);
for n=1:8760*60
    if Pr==0
        P_FC(n)=0;
        Q_GAS(n)=0;
        QR(n)=0;
    else
        if Pl<Pr
            P_fc=Pl;
        else
            P_fc=Pr;
        end
        plf=P_fc/Pr;
        eta_e=(P1(1)*plf^4+P1(2)*plf^3+P1(3)*plf^2+P1(4)*plf+P1(5))/100;
        eta_h=(P2(1)*plf+P2(2))/100;
        Q_gas=P_fc/eta_e;
        Qr=Q_gas*eta_h;
        P_FC(n)=P_fc;
        Q_GAS(n)=Q_gas;
        QR(n)=Qr;
    end
end
csvwrite('QR.csv',QR)
%--------------------------Calculate P_PVDU P_PVEX P_PP---------------------
P_MAX=csvread('P_MAX.csv');
P_PV=P_MAX*Nmo;
```

```
for n=1:8760*60
    if P_FC(n)==PL(n)
        P_PVDU(n)=0;
        P_PVEX(n)=P_PV(n);
        P_PP(n)=0;
    elseif P_FC(n)+P_PV(n)>= PL(n)
            P_PVDU(n)=PL(n)-P_FC(n);
            P_PVEX(n)=P_PV(n)-(PL(n)-P_FC(n));
            P_PP(n)=0;
    else
            P_PVDU(n)=P_PV(n);
            P_PVEX(n)=0;
            P_PP(n)=PL(n)-(P_FC(n)+P_PV(n));
    end
end
```

2) Integrated hot water supply

```
UT=csvread('UT.csv');
IS=xlsread('IS.xls');
MVU=xlsread('MVU.xls');
TA=csvread('TA.csv');
TR=csvread('TR.csv');
TU=xlsread('TU.xls');
TW=csvread('TW.csv');
QR=csvread('QR.csv');
%--------------------------Calculate FR-----------------------------------
UL=Ut+Ub;
mass=(UL/(k*delta))^0.5;
F=tanh(mass*(W-D)/2)/(mass*(W-D)/2);
Fa=1./(W*(1./(D+(W-D)*F)+UL./(pi*D*he)));
Nm=Ntu*hc*Ac/(mv*Cp);
```

```
Nc=Ntu*Fa*UL*Ap/(mv*Cp);
F1=(1-exp(-Nm/Ntu))/(Nc/Ntu);
G=1-(Nc/Ntu)*(F1/(1+F1));
FR=Fa*(1-G^Ntu)/Nc;
%---------------------------Calculate taoalpha1 UL1-------------------------
taoalpha1=tao*alpha/(1+Ud*Ao/(mv*Cp));
UL1=UL*(1-Ud*Ai/(mv*Cp)+Ud*(Ai+Ao)/(Ntu*Ap*FR*UL))/(1+Ud*Ao/(mv*Cp));
%---------------------------Calculate Ti LSswh LSsofc LSsb-------------------
for n=1:8760*60
    if n==1
        TIswh(n)=Tw;
        TIsofc(n)=Tw;
    else
        TIswh(n)=0;
        TIsofc(n)=0;
    end
    Tiswh=TIswh(n);
    Tisofc=TIsofc(n);
    if Qu>0
         Qu=Ntu*Ap*FR*(Is*taoalpha1-UL1*(Tiswh-Ta));
    else
         Qu=0;
    end
    LSL(n)=Cp*mvu*(Tu-Tw);
    LsL=LSL(n);
    if n~=8760*60
        if Tisofc>=Tu
                TIswh(n+1)=Tiswh+dt*(Qu-Utankswh*Atankswh*(Tiswh-Tr))/(mtank
                swh*Cp);
                TIsofc(n+1)=Tisofc+dt*(Qr-LsL-Utanksofc*Atanksofc*(Tisofc-Tr))/(mt
                anksofc*Cp);
```

```
            LSswh(n+1)=0;
            LSsofc(n+1)=LsL;
            LSsb(n+1)=0;
    elseif Tiswh>=Tu
             TIswh(n+1)=Tiswh+dt*(Qu-LsL-Utankswh*Atankswh*(Tiswh-Tr))/(m
             tankswh*Cp);
             TIsofc(n+1)=Tisofc+dt*(Qr-Utanksofc*Atanksofc*(Tisofc-Tr))/(mtanks
             ofc*Cp);
            LSswh(n+1)=LsL;
            LSsofc(n+1)=0;
            LSsb(n+1)=0;
    elseif Tisofc>=Tiswh
             TIswh(n+1)=Tiswh+dt*(Qu-Utankswh*Atankswh*(Tiswh-Tr))/(mtank
             swh*Cp);
             TIsofc(n+1)=Tisofc+dt*(Qr-mvu*Cp*(Tisofc-Tw)-Utanksofc*Atanksofc*
             (Tisofc-Tr))/(mtanksofc*Cp);
            LSswh(n+1)=0;
            LSsofc(n+1)=mvu*Cp*(Tisofc-Tw);
            LSsb(n+1)=mvu*Cp*(Tu-Tisofc);
    else
             TIswh(n+1)=Tiswh+dt*(Qu-mvu*Cp*(Tiswh-Tw)-Utankswh*Atankswh
             *(Tiswh-Tr))/(mtankswh*Cp);
             TIsofc(n+1)=Tisofc+dt*(Qr-Utanksofc*Atanksofc*(Tisofc-Tr))/(mtanks
             ofc*Cp);
            LSswh(n+1)=mvu*Cp*(Tiswh-Tw);
            LSsofc(n+1)=0;
            LSsb(n+1)=mvu*Cp*(Tu-Tiswh);
    end
    if TIswh(n+1)>100
        TIswh(n+1)=100;
    end
```

```
        if TIsofc(n+1)>70
            TIsofc(n+1)=70;
        end
    end
    Qu(n)=Qu;
end
LSswh(isnan(LSswh))=0;
LSsofc(isnan(LSsofc))=0;
LSsb=LSL-LSswh-LSsofc;
```